Bachelor's thesis

NTNU
Norwegian University of Science and Technology
Faculty of Engineering
Department of Energy and Process Engineering

Hanna Marie Blakstvedt Svelander
Mia Hagen Sydskjør
Ebba Schjoll Polhammer

Investigation of Degradation Mechanisms in Lithium-ion Batteries

Testing and characterization of batteries with Revolve

Bachelor's thesis in Renewable Energy
Supervisor: Odne Stokke Burheim
Co-supervisor: Ejikeme Raphael Ezeigwe
May 2024

NTNU
Norwegian University of
Science and Technology

Hanna Marie Blakstvedt Svelander
Mia Hagen Sydskjør
Ebba Schjoll Polhammer

Investigation of Degradation Mechanisms in Lithium-ion Batteries

Testing and characterization of batteries with Revolve

Bachelor's thesis in Renewable Energy
Supervisor: Odne Stokke Burheim
Co-supervisor: Ejikeme Raphael Ezeigwe
May 2024

Norwegian University of Science and Technology
Faculty of Engineering
Department of Energy and Process Engineering

NTNU
Norwegian University of
Science and Technology

NTNU

Institutt for energi- og prosessteknikk

Bacheloroppgave

Oppgavens tittel: Testing og karakterisering av batterier med Revolve **Project title (ENG):** Testing and characterization of batteries with Revolve	**Gitt dato:** 20.11.2023 **Innleveringsdato:** 22.05.2024 **Antall sider rapport/sider vedlagt:** 80/12
Gruppedeltakere: Hanna Marie Blakstvedt Svelander Mia Hagen Sydskjør Ebba Schjoll Polhammer	**Veiledere:** Odne Stokke Burheim Ejikeme Raphael Ezeigwe **Prosjektnummer:** BIFOREN24-19
Oppdragsgiver: Revolve NTNU	**Kontaktperson hos oppdragsgiver:** Wilhelm Herrem

Fritt tilgjengelig: ☒

Tilgjengelig etter avtale med oppdragsgiver: ☐

Rapporten frigitt etter:

Gruppedeltakernes signatur:

Hanna Svelander

Mia Hagen Sydskjør

Ebba Polhammer

Preface

This bachelor's thesis is the concluding assignment within the engineering study of Renewable Energy at the Norwegian University of Science and Technology. The thesis is a collaborative effort involving three students, three supervisors, and the student organization Revolve NTNU. The students have specialization in the fields of energy storage and efficient energy consumption.

The purpose of this thesis is to conduct comprehensive testing and characterization of two types of lithium-ion batteries in order to identify the impact of temperature on their degradation and to find the option that offers optimal performance and durability.

Artificial intelligence has served as a valuable tool for paraphrasing, translations, and language refinement throughout this thesis, and to improve the coding during data processing.

The students would like to thank the two internal supervisors, Odne Stokke Burheim and Ejikeme Raphael Ezeigwe, as well as Wilhelm Herrem, the external supervisor from Revolve NTNU.

Hanna Marie B. Svelander | Mia Hagen Sydskjør | Ebba Schjoll Polhammer

Trondheim, 22.05.2024

Abstract

Battery degradation is one of the most critical problems to be managed in battery research, as it limits the energy capacity over a battery's lifespan. Understanding the degradation behavior is essential for optimizing the design of battery systems and enhancing sustainability. This thesis analyses the influence of various temperatures on battery degradation for two different types of batteries: an lithium cobalt oxide (LCO) pouch cell, produced by Melasta, and a lithium nickel manganese cobalt oxide (NMC) pouch cell by Grepow. This is done in collaboration with Revolve NTNU to find the most optimal solution for their race car.

The main goal is to investigate how the different temperatures of 25, 35, and 45 °C affect the degradation of the two selected batteries. Given the significance of LIBs in nearly all secondary battery applications, including electric vehicles (EVs), fully understanding the impact of temperature is crucial for identifying options that offer minimal degradation.

In the first part of the thesis, the complex structure of lithium-ion batteries (LIBs) is explained, highlighting the key components and their roles in battery operation. Following this, the most relevant battery performance metrics for this thesis are explained. The main degradation causes and mechanisms in LIBs are also presented as a part of the theory.

The test methodology is then introduced, detailing the degradation cycles and setup, and explaining the characterization techniques used. Comprehensive testing and characterization of different LIBs were conducted, employing methods such as constant current - constant voltage (CCCV) and hybrid pulse power characterization (HPPC).

The results and discussion section analyses the change in state of health (SOH), while also examining Arrhenius behaviour, internal resistance and conducting an incremental capacity analysis (ICA) to explore correlations with degradation. The results show that temperature influences the degradation most for the Melasta batteries. The results for these aligned with expectations based on the theory, showing that the decrease in SOH values increased with higher temperature, which is a typical degradation pattern. Conversely, the results for Grepow exhibited some atypical behavior, with the most significant decrease in SOH values occurring in the battery tested at 25 °C, while the batteries tested at 35 and 45 °C showed almost no changes in SOH values. However, testing the batteries for a longer period would have been optimal to better understand how temperature affects degradation over time, and to investigate other factors impacting degradation, such as C-rates.

Sammendrag

Degradering av batterier utgjør en av de mest kritiske utfordringene innen batteriforskning, ettersom det begrenser energikapasiteten over batteriets levetid. Å forstå aldringsegenskapene er av avgjørende betydning for å optimalisere designet av batterisystemer, og styrke bærekraften. Denne oppgaven undersøker hvordan ulike temperaturer påvirker batteridegradering for to forskjellige typer batterier: en litium koboltoksid (LCO) posecelle produsert av Melasta og en litiumnikkelmangan koboltoksid (NMC) posecelle produsert av Grepow. Dette gjøres som et samarbeid med Revolve NTNU for å finne den mest optimale løsningen for deres racerbil.

I den første delen av oppgaven blir den komplekse strukturen til litium-ion-batterier (LIBer) forklart, med fokus på deres hovedkomponenter og roller i batteridrift. Deretter følger en gjennomgang av ulike mål for batteriytelse som er relevante for denne oppgaven. Hovedårsakene og mekanismene til degradering i LIBer blir også presentert i teoridelen.

Videre presenteres testmetodologien, inkludert detaljer om ladesykluser og oppsett, og en forklaring av de anvendte karakteriseringsteknikkene. Det ble gjennomført omfattende testing og karakterisering av ulike LIB ved hjelp av metoder som konstant strøm - konstant spenning (CCCV) og karakterisering av hybrid pulskraft (HPPC).

Hovedmålet med oppgaven er å undersøke hvordan ulike temperaturer på 25, 35 og 45 °C påvirker batteridegraderingen for de to valgte batteriene. Med tanke på LIBer sin betydning i nesten alle sekundærbatteri applikasjoner, inkludert elektriske kjøretøy (EV), er det avgjørende å forstå temperaturens innvirkning for å kunne identifisere muligheter for å minimere degradering.

I resultat- og diskusjonsdelen analyseres endringen i helsetilstanden (SOH), samtidig som Arrhenius-adferd, indre motstand og en inkrementell kapasitetsanalyse (ICA) utføres for å utforske sammenhenger med degradering. Resultatene indikerer at temperatur har størst påvirkning på degraderingen av Melasta-batteriene. Disse resultatene samsvarer godt med teorien og viser en økende nedgang i SOH-verdier med stigende temperaturer, noe som er et typisk degraderingsmønster. Samtidig viser resultatene for Grepow noe uvanlig oppførsel, med den største nedgangen i SOH for batteriet testet ved 25 °C, mens batteriene testet ved 35 og 45 °C nesten ikke viser noe endringer i SOH-verdier. Testing av batterier over en lengre tidsperiode ville ha vært mer optimalt for å forstå hvordan temperaturer påvirker degradering over tid, og for å undersøke andre faktorer som påvirker degraderingen, for eksempel ulike C-rater.

List of terms

CC	Constant Current
CCCV	Constant Current-Constant Voltage
CV	Constant Voltage
DMC	Dimethyl Carbonate
DV	Diferential Voltage
EC	Ethylene Carbonate
EPT	Department of Energy and Process Engineering
EV	Electrical Vehicle
FS	Formula Student
GHG	Greenhouse Gas
HPPC	Hybrid Pulse Power Characterization
IC	Incremental Capacity
LAM	Loss of Active Material
LCO	Lithium Cobalt Oxide
LIB	Lithium-ion Battery
LLI	Loss of Lithium Inventory
LiPB	Lithium–ion Polymer Battery
NMC	Lithium Nickel Manganese Cobalt Oxide
NTNU	Norwegian University of Science and Technology
OCV	Open Circuit Voltage
PC	Propylene Carbonate
SEI	Solid Electrolyte Interphase
SOC	State of Charge
SOH	State of Health

Contents

List of Figures

List of Tables

1 Introduction

In a world that is increasingly electrified, battery technology is a significant part of the future, especially for electric vehicles (EVs). This thesis aims to collaborate with the student organization Revolve NTNU to evaluate and enhance the sustainability of their race car, through the characterization and testing of the batteries utilized in the car.

1.1 Motivation

The battery demand has significantly increased over the last decades due to several factors, including the increase of portable electronic devices, the rise of EVs, and the growing demand for renewable energy storage solutions [36]. Figure 1.1 shows projected global battery demand from 2020 to 2030. As the figure illustrates, the demand is expected to continue increasing substantially in the future. This significant increase is primarily attributed to the electrification of transportation, which is projected to dominate battery demand by 2030 in terms of total energy storage capacity. These factors necessitate advancements in battery technology, such as improved energy density, longer lifespan, faster charging capabilities, and reduced costs. [18]

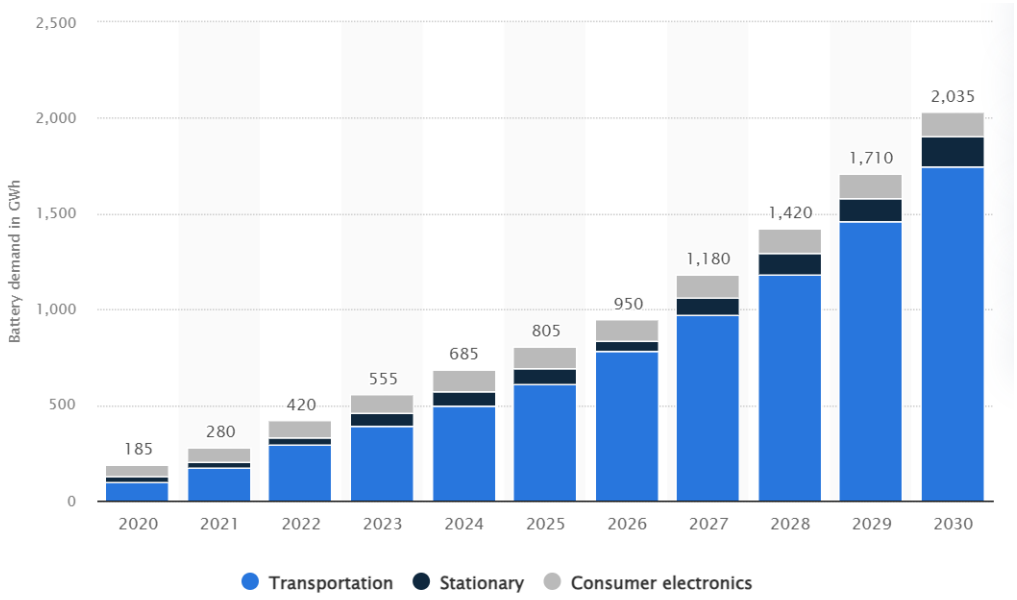

Figure 1.1: Projected global battery demand from 2020 to 2030 [18]

As an organization dedicated to innovation in sustainable race cars, Revolve NTNU seeks to continuously improve the environmental impact of their vehicle while maintaining competitive performance standards. The selection of suitable batteries plays a crucial role in achieving these objectives, as they serve as the primary energy source for the car. This project offers an

opportunity to contribute insights into battery technology selection for Revolve NTNU's car, utilizing both experimental and theoretical approaches. [50]

1.2 Background

Over the past thirty years since the first commercial lithium-ion battery (LIB) was introduced in Japan in 1991, the market for LIBs has grown rapidly. They have been instrumental in the development of portable electronic products, such as cell phones and laptops, and equally importantly, in the emergence of EVs. LIBs continue to prove themselves as the premier battery option for EVs, and are utilized by Revolve NTNU in their race cars. [68]

1.2.1 Brief History of Lithium-ion Batteries

The concept of a battery in which lithium-ions could move reversibly between the positive and negative electrodes was initially developed in the late 1970s, during the peak of the energy crisis when there was a significant emphasis on seeking alternatives to fossil fuels. In the initial trial, titanium disulfide and lithium metal were used as the electrodes, yet their combination presented numerous challenges, including significant safety risks. [12]

During the 1980s, John B. Goodenough conducted experiments substituting lithium cobalt oxide for titanium disulfide as the cathode. This proved successful, resulting in a doubling of the battery's energy capacity. [12]

However, the true inventor of the LIB is considered to be Akira Yoshino, when he made another swap in the battery. Instead of utilizing reactive lithium metal as the anode, he experimented with lower temperature carbons, such as petroleum coke. This groundbreaking research revealed that not only was the new battery considerably safer without lithium metal, but its performance was also more stable, ultimately resulting in the creation of the first prototype of the LIB. Yoshino's battery patent was commercialized by Sony in 1991, marking the onset of mass production of LIBs and starting a new era for communication and mobility. [12] [68]

1.2.2 Revolve NTNU

Revolve NTNU is an organization at the Norwegian University of Science and Technology (NTNU) that competes in Formula Student (FS), the student variant of Formula leagues. FS is organized by the Institution of Mechanical Engineers and is the world's largest engineering competition for students in motor sport. [50]

Revolve NTNU is an interdisciplinary team of students collaborating to construct an optimal

electric race car. The team includes mechanics, electricians, data and software engineers, marketers, drivers, ergonomists, and more. Since 2012, Revolve NTNU has annually designed and developed a new race car, and the team continuously works to enhance the car's performance for participation in FS. Figure 1.2 shows this years race car. [50]

Figure 1.2: Revolve NTNU´s race car for the 2024 season

Revolve NTNU's ongoing process of selecting new batteries for their car, is the background for this bachelor's thesis. The assignment is to conduct testing of these batteries. By closely examining the various degradation factors affecting the batteries, the new knowledge will then be utilized in the development of the race car model for 2025.

1.3 Sustainable Development

The push towards renewable energy and the subsequent rise in demand for efficient energy storage solutions have led to significant advancements in battery technology, particularly with the widespread adoption of LIBs. However, ensuring the longevity and optimal performance of these batteries is crucial to maximizing their effectiveness and minimizing costs over their operational lifetimes. By investigating degradation factors such as temperature, this bachelor's thesis aims to further enhance battery performance, thereby contributing to advancing sustainable solutions within the context of both motor sport and the entire transportation sector. [14]

Furthermore, addressing the environmental aspect aligns with the broader concept of sustainability, which emphasizes the importance of minimizing negative impacts on the environment, while meeting the needs of the present generation, without compromising the

ability of future generations to meet their own needs. Revolve NTNU focuses on sustainability through the "UN Sustainable Development Goals", where they have placed primary emphasis on the following objectives: [50]

- Goal 4: Quality Education
- Goal 7: Affordable and clean energy
- Goal 9: Industry, innovation and infrastructure

Goal 9, the most relevant for this thesis, invest in research and innovation in sustainable production, material recycling, and advanced manufacturing technologies to reduce the environmental impact of industry. Improving the lifespan of batteries trough testing and characterization to define degradation factors, can contribute to this goal. By extending the operational life of batteries, fewer resources are required for manufacturing replacements, leading to fewer discarded batteries entering the waste stream and resulting in reduced environmental impact. This facilitates the implementation of efficient recycling systems, enabling the recovery of valuable materials and reducing the demand for new resources. [40]

1.4 Problem Formulation

The objective of this thesis is to examine how various factors contribute to the degradation of two chosen batteries. By conducting comprehensive testing and characterization of different LIBs, the aim is to identify the option that offer optimal performance, durability, and environmental sustainability for Revolve NTNU. Temperature was singled out for particular attention due to its dominant influence on battery degradation. By undertaking this research, valuable insights can be gained to inform future decisions regarding technology adoption and contribute to the broader goal of promoting sustainable practices within the automobile industry.

2 Theory

The theory part of this thesis explores the intricate structure of LIBs, highlighting the key components and their roles in battery operation, followed by examination of battery performance metrics and the parameters used to quantify battery performance. Finally an overview of the causes and mechanisms of degradation, vital for advancing battery technology and optimizing usage, will be provided.

2.1 The Structure of a Lithium-ion Battery

The LIBs have emerged as a dominant energy storage technology across various sectors, due to its high energy and power density, efficient energy conversion, long shelf life, low self-discharge rate and compatibility with existing electric infrastructure [35].

LIBs are assembled through the integration of some primary components. The two electrodes, where the anode is made of graphite and the cathode consists of a lithium metal oxide, serve as main components in a slurry mix that is coated onto their respective current collectors. LIBs also include an electrolyte containing solvent molecules and a separator. Figure 2.1 illustrates the structure of the battery. [52]

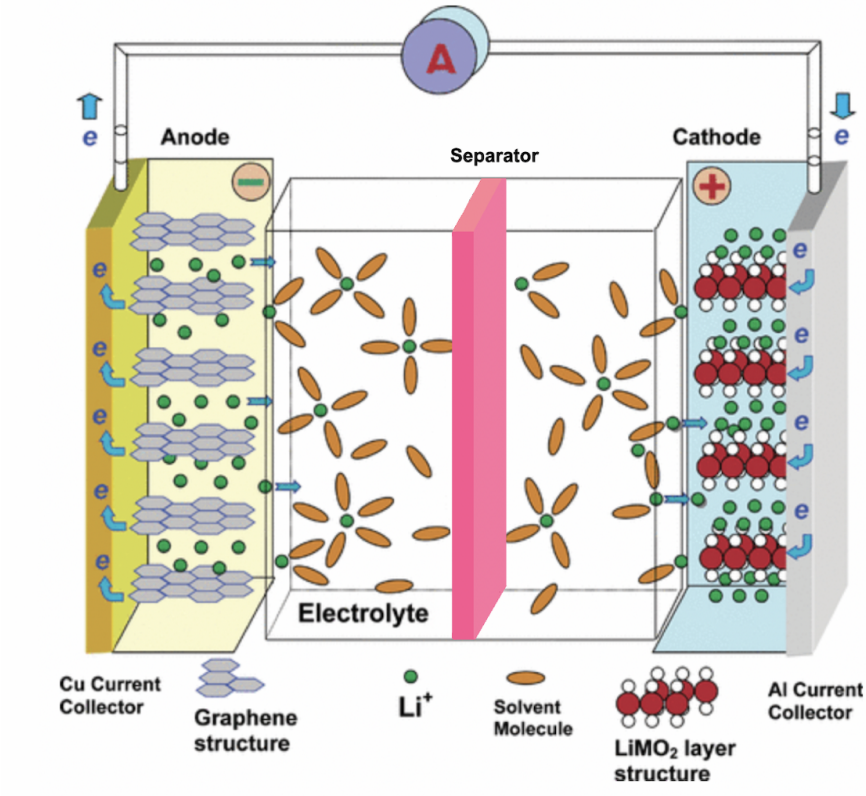

Figure 2.1: The structure of a LIB with inspiration from ACS publications [48]

The LIB operates through redox reactions, wherein the oxidation of lithium occurs at the anode during discharge. The positively charged lithium ion migrates through the electrolyte and solvent molecules before reaching the cathode. The electron liberated from lithium at the anode is captured by the current collector on the anode side and is conducted through the external circuit before reaching the current collector on the cathode side. At the cathode, the lithium metal oxide undergoes a reduction reaction. [9]

2.1.1 Cathode Material

For this thesis lithium cobalt oxide (LCO) and lithium nickel manganese cobalt oxide (NMC) are used as the cathode materials in the two batteries to be analyzed.

Lithium Cobalt Oxide

LCO, with formula $LiCoO_2$, exhibits a layered structure, where lithium, cobalt, and oxygen atoms are arranged in a regular pattern, shown in Figure 2.2. Lithium-ions are intercalated into the structure of the material, meaning they are inserted between the layers of cobalt oxide. This process contributes to the high ion conductivity observed in the material, enabled by the diffusion of lithium-ions along the two-dimensional plane. [30]

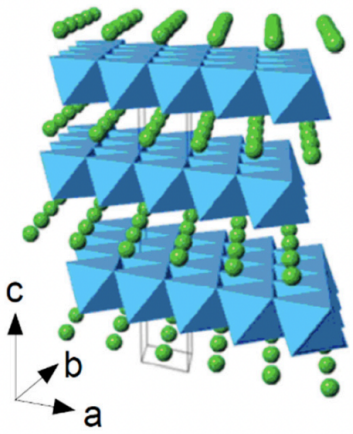

Figure 2.2: Layered structure of the LCO and NMC cathode material [30]

LCO is characterized by a high operating potential and stable electrochemical characteristics, making it a versatile and widely utilized cathode material in LIB technology. Due to its relatively high theoretical specific capacity, high theoretical volumetric capacity, low self-discharge rate, high discharge voltage, and good cycling performance, LCO is an attractive cathode material. [30]

The anode and cathode reactions used for the LCO cell are expressed in Equation 2.1 and 2.2, respectively. The overall reaction is represented by Equation 2.3, where the discharge reaction proceeds from left to right, and the charging reaction proceeds from right to left. [9]

$$anode : Li_xC_6 \rightarrow C_6 + xLi^+ + xe^- \tag{2.1}$$

$$cathode : Li_{1-x}CoO_2 + xLi^+ + xe^- \rightarrow LiCoO_2 \tag{2.2}$$

$$total : Li_xC_6 + Li_{1-x}CoO_2 \rightarrow C_6 + LiCoO_2 \tag{2.3}$$

Nickel Manganese Cobalt Oxide

The NMC material, with formula $LiNiMnCoO_2$, is similar to the LCO in terms of behavior and structure, also illustrated in Figure 2.2. Like the LCO, NMC displays a layered structure where lithium, nickel, cobalt, manganese, and oxygen ions are arranged in a regular pattern, facilitating the reversible intercalation and deintercalation of lithium-ions during charge and discharge cycles. The NMC cathode material has high electrochemical performance with high operating voltages and high reversible capacity. [17]

For the NMC 811 cell, utilized in this thesis, the anode and cathode reactions are stated in Equation 2.4 and 2.5. In the anode reaction, lithium-ions are released from the carbon host material while in the cathode reaction, lithium-ions are intercalated into the cathode material. These results in the formation of a mixed metal oxide $LiNi_{1-x-y}Mn_xCo_yO_2$, where $0 \leq y+x \leq 1$, shown in Equation 2.6. [9]

$$anode : Li_xC_6 \rightarrow C_6 + xLi^+ + xe^- \tag{2.4}$$

$$cathode : Li_{1-x}Ni_{0.8}Mn_{0.1}Co_{0.1}O_2 + xLi + e^- \rightarrow LiNi_{0.8}Mn_{0.1}Co_{0.1}O_2 \tag{2.5}$$

$$total : Li_xC_6 + Li_{1-x}Ni_{0.8}Mn_{0.1}Co_{0.1}O_2 \rightarrow C_6 + LiNi_{0.8}Mn_{0.1}Co_{0.1}O_2 \tag{2.6}$$

A Comparison of LCO and NMC

Figure 2.3 illustrates a comparison of the qualities of the LCO and NMC cathode materials. The two materials are similar in specific capacity, cost and performance, but NMC is possessing the best overall characteristics. NMC batteries also have higher thermal stability than LCO batteries, making them safer overall. [16]

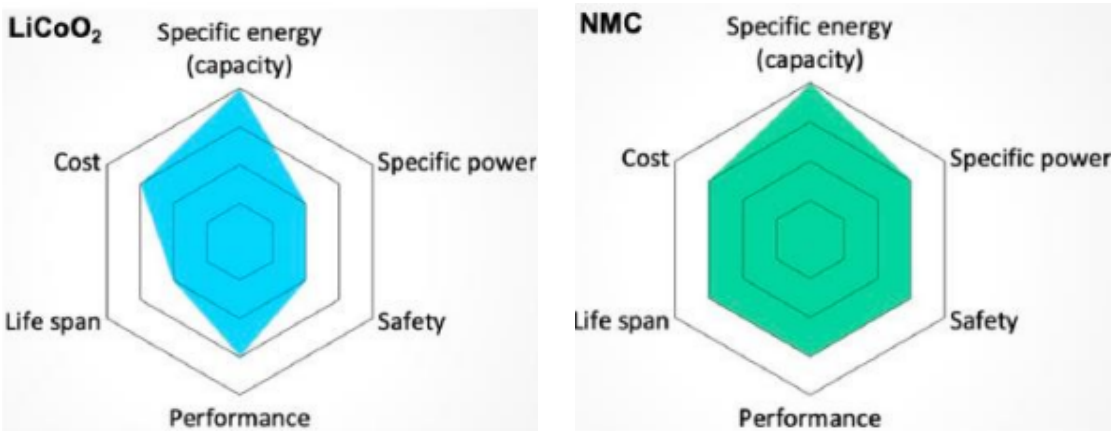

Figure 2.3: The qualities of LCO (left) compared to NMC (right) [16]

Figure 2.4 illustrates a more in-depth display of the specific capacity compared to the potential of different cathode materials during discharge. The figure illustrates the discharge behavior of LCO (green), showing a high initial potential, followed by a gradual decrease in potential while increasing in specific capacity. Finally, LCO experiences a significant drop in potential as the battery discharges further. The curve displaying the discharge behavior of NMC (yellow) follows a similar discharge pattern to LCO, but initiates discharge with an even higher potential. Furthermore, its potential declines at a steadier rate compared to LCO as the battery discharges. Notably, around 80 mAh/g specific capacity, the NMC curve experiences a drop to a lower potential than that of the LCO. However, after this point, LCO's potential decreases more rapidly than NMC's, highlighting the difference in performance under higher discharge levels. [42]

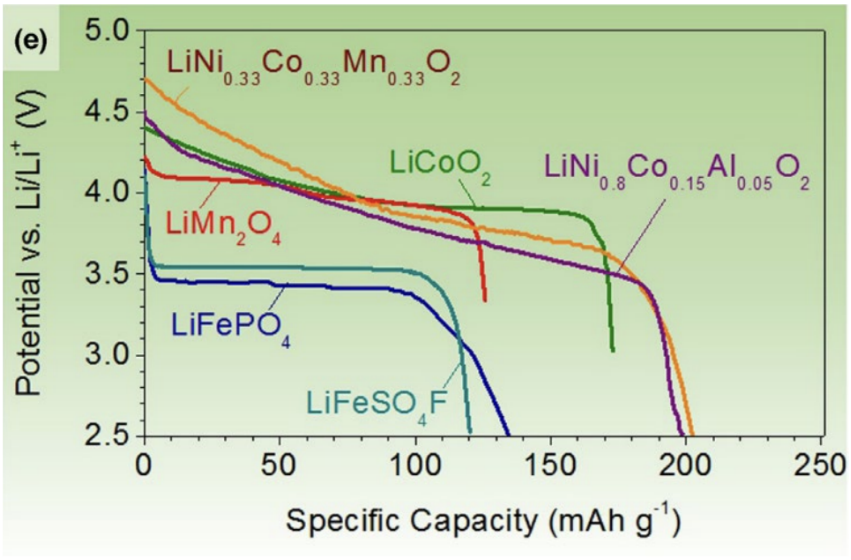

Figure 2.4: Discharge profiles of different LIB cathode materials [42]

2.1.2 Anode Material

Anode materials in LIBs are commonly classified into three categories based on their performance and reaction mechanisms: intercalation anodes, alloy anodes, and conversion anodes. Intercalation anodes, primarily carbon-based, are widely used in commercial batteries, due to their favorable characteristics. Carbon, being inexpensive and easily available, exhibits low delithiation potential versus Li/Li^+, high lithium diffusivity, excellent electrical conductivity, and minimal volume changes during lithiation and delithiation processes. [44]

Within the realm of carbon anode materials, two main types are prevalent: hard carbons and graphitic carbons. Figure 2.5 shows the structure of hard carbon compared to graphite.

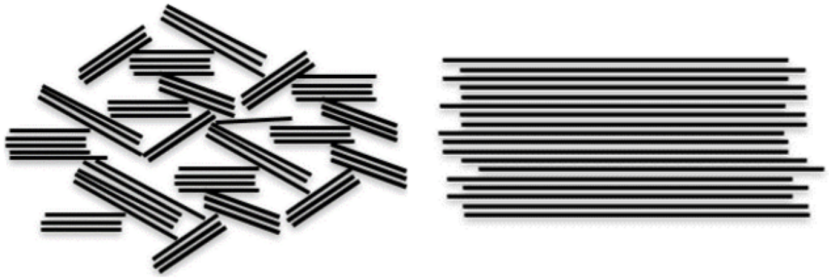

Figure 2.5: The structure of both hard carbon (left) and graphite (right) [56]

Graphite, a well-known example of a graphitic carbon, possesses a three-dimensional ordered crystal structure with large graphite grains and a density of approximately 2.26 g/cm^3. It serves as a stable form of carbon, with lithium-ions intercalating between the graphite layers during battery operation to form an intercalation compound, typically LiC_6. Although the basal plane of graphite is the most exposed surface to the electrolyte, lithium-ions predominantly intercalate into the graphene layers through the edge planes perpendicular to the graphene layers. This intercalation process results in uniaxial strain along the edge planes of the graphitic particles. [44]

2.1.3 Separator

The separator in a battery cell serves a central role in preventing internal short circuits by physically separating the positive and negative electrodes, while still allowing the passage of lithium-ions during charge and discharge cycles. The separator barrier is crucial for ensuring that the electrodes do not come in direct contact. This could lead to short circuits and potential safety hazards. The separator usually consists of microporous layers of either polymer membranes or non-woven fabric. [5]

2.1.4 Electrolyte

The electrolyte infiltrates almost the entire cell as it saturates the porous electrodes and separators. It supports both the stability of the electrolyte and the ion movement, establishing a conductive path for flow between the electrodes.

The electrolyte consists of two primary components: a solvent and a salt. The two parts play a crucial role in determining the capacity, efficiency, and calendar life, as further explained in Chapter 2.2.4, of LIBs. The salt gives the electrolyte its ability to conduct ions, whereas the solvent, although not directly involved in chemical reactions, dissolves the salt and assists in the migration of ions.

Lithium hexafluorophosphate ($LiPF_6$) stands out as the primary salt utilized, alongside other commonly employed salts such as lithium tetrafluoroborate ($LiBF_4$) and lithium perchlorate ($LiClO_4$). The most frequently utilized solvents in electrolytes consist of combinations of cyclic carbonates, like ethylene carbonate (EC) and propylene carbonate (PC), along with linear carbonates, such as dimethyl carbonate (DMC). [41] [47]

2.1.5 Current Collectors

The battery also contains two current collectors: one on the anode side made of copper, and one on the cathode side made of aluminum. These materials are chosen, due to their electrical conductivity and stability. The current collectors serve as links that collect electrical current generated at the electrodes, establishing connections with external circuits. [71]

The current collectors must remain electrochemically stable under operating conditions. To achieve high potential in a cell, graphite anodes need low potentials (0.01–0.25V vs. Li/Li+), while cathodes, like $LiCoO_2$, require higher potentials (∼4V vs. Li/Li+). Copper is treated to become electrochemically stable at low potentials, making it the preferred material for the anode, while aluminium, stable at higher potentials, is suitable for cathodic current collectors. However, exposure to these potentials can trigger undesirable reactions with the electrolyte. Despite benefits, maintaining stability in current collectors poses challenges, with undesired reactions causing capacity degradation and reduced lifetime. [71]

The design of current collectors is tailored to maximize electrical conductivity while minimizing resistance and weight. They are often thin and lightweight to minimize added mass to the battery system, especially in applications where weight is a critical factor, such as in EVs. [71]

2.1.6 Construction of a Cell

The batteries tested for Revolve NTNUs race car are pouch cells. The completed pouch cell incorporates all the previously mentioned components, assembled together. As illustrated in Figure 2.6, the cell comprises several stacks of electrode pairs placed on top of one another, with a small part of the electrode extended welding the current collectors. It is normal to have an uneven amount of electrodes inside the cell, with anode being the predominant, as the current collectors possess electrode material on both surfaces. Consequently, each side of the cell possesses a single electrode. The unit cells are enclosed within a casing, that consists of an aluminum foil coated with a non-conductive material. [54] [19]

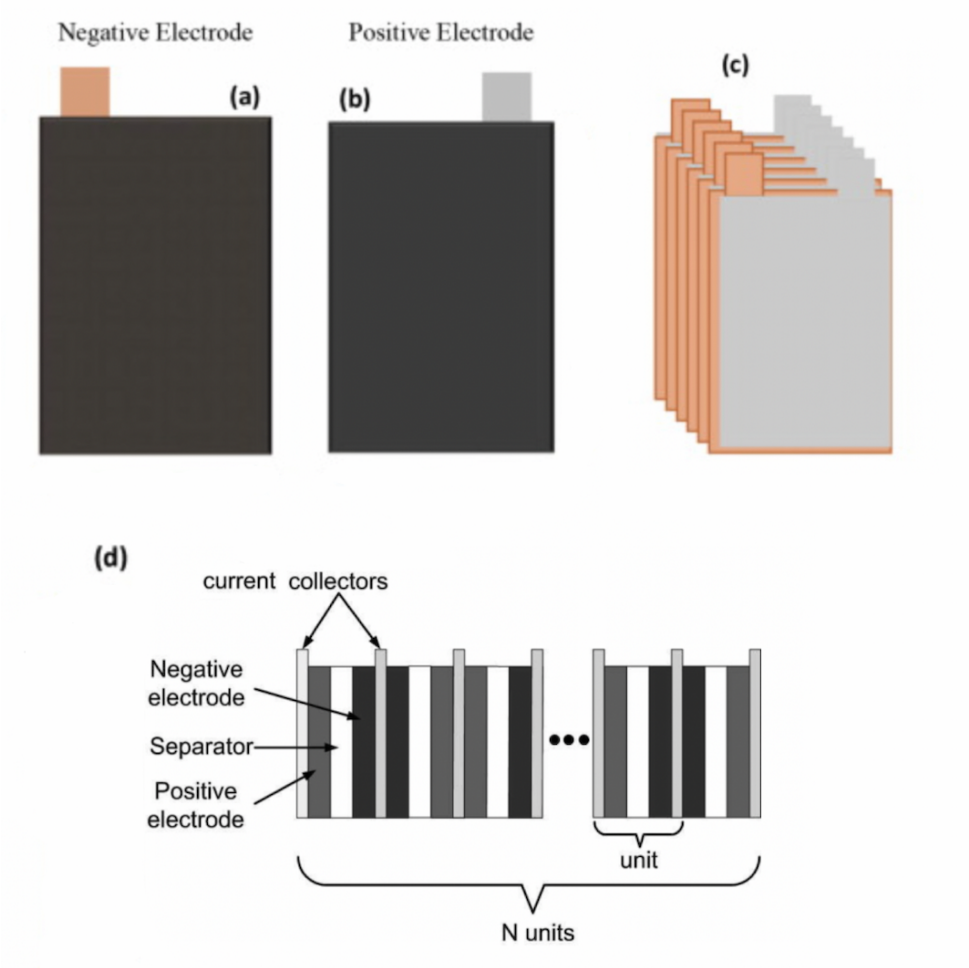

Figure 2.6: The battery cell consists of several units stacked on top of each other [61] [38]

The separators, current collectors and electrodes are typically manufactured to be as thin as possible. Traditional high-energy cells typically feature electrodes with a thickness ranging from approximately 50 to 60 µm. As the electrode thickness increases, the limitations on lithium-ion transport within the electrolyte phase and the impedance for electron movement in the solid phase of the electrode, become more pronounced. This results in reduced cell capacity due to higher overpotentials during charging and discharging within fixed voltage limits. Simultaneously, when electrodes are thicker, the geometric current density within the separator increases at a given C-rate compared to thinner electrodes. This can cause extra overpotential and, during charging, it might result in lithium plating on nearby graphite particles near the separator. This will be further explained in Chapter 2.3.4. [54]

2.2 Battery Performance Metrics

This section explains various performance metrics used to assess the function and reliability of batteries. Understanding these metrics is important for evaluating the battery's durability.

2.2.1 C-rate

The charge and discharge current is often expressed using a C-rate to standardize the current, relative to the battery's capacity. It indicates the rate at which a battery is charged and discharged compared to its maximum capacity. A 1C-rate means that the charge or discharge current will fill or deplete the entire battery in one hour, which is a full cycle. For a battery with 2C-rate, the charge or discharge current will fill or deplete the battery twice as fast, meaning in thirty minuets. [60]

2.2.2 State of Charge

State of charge (SOC) for a battery is defined as the ratio between current capacity (Q(t)) and nominal capacity (Q$_n$). The manufacturer specifies the nominal capacity, which represents the maximum amount of charge the battery can store. SOC can be described in Equation 2.7. [13]

$$SOC(t) = \frac{Q(t)}{Q_n} \cdot 100\% \tag{2.7}$$

In the realm of battery management systems, which will be further explained in Chapter 2.2.5, SOC holds a crucial role, indicating the remaining energy within a battery to power an EV. Accurately estimating the state of the battery, not only offers a glimpse into present and expected performance, but also ensures a reliable and safe operation. Nevertheless, the estimation of a battery's SOC stands out as a challenge for the successful operation of EVs. Factors like degradation, temperature fluctuations and charge/discharge cycles significantly impacts the SOC. [23]

2.2.3 State of Health

The battery's ability to store energy, and the assessment of its condition influenced by its history, is referred to as state of health (SOH). Battery performance, such as available capacity, available energy, and available power, typically diminishes as the battery degrades. [22]

The SOH of a battery can be determined by the ratio of its measured capacity (C_m) at a specific point, to its rated capacity (C_N), given by the manufacturer at nominal operating conditions. This essentially describes the condition of the cell, compared to its condition as brand new. The SOH can be expressed by Equation 2.8. [51]

$$SOH = \frac{C_m}{C_N} \cdot 100\% \tag{2.8}$$

A SOH of 100% indicates that the measured capacity matches the rated capacity, while a SOH below 100% indicates degradation relative to the rated capacity. By definition, a battery is typically considered to have reached the end of its lifespan when its SOH drops to 80%. After that its degradation progresses at an accelerated pace, which is illustrated in Figure 2.7. The four cells shown in the figure are of the same model and tested at 25 °C with a discharge/charge rate of 1C/0.5C. The difference between them are due to inaccuracies in the manufacturing. [51] [62]

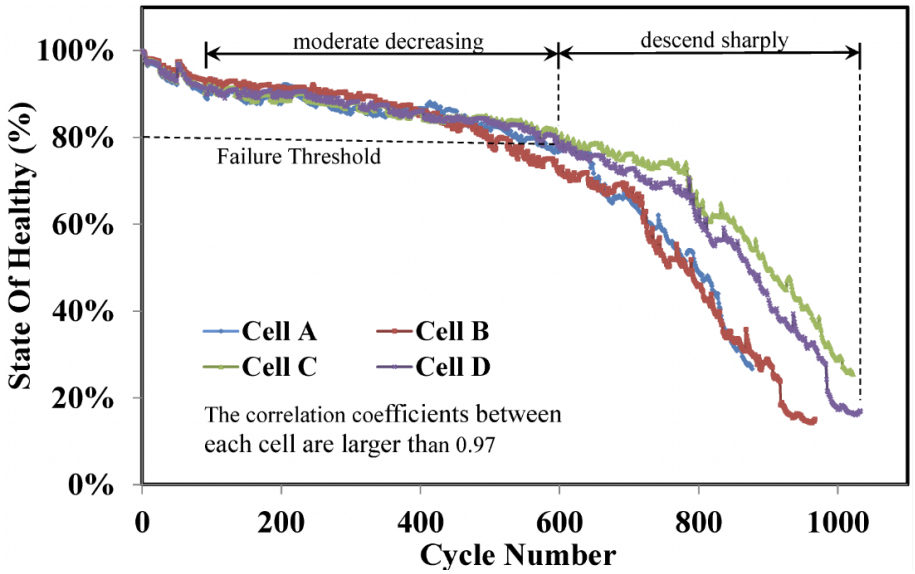

Figure 2.7: Accelerated decrease in SOH for four batteries after reaching 80% SOH [62]

Numerous variables can impact the SOH of a battery, such as high operating temperatures, the solid electrolyte interphase (SEI), lithium plating, and charging and discharging, especially fast charging. These aspects will be further elaborated upon in Chapter 2.3.

2.2.4 The Lifespan of a Battery

In general, battery lifespan can be divided into two main components: calendar life and cycle life. Calendar life relates to how long a battery can maintain its capacity and performance while in storage, without undergoing charge or discharge cycles. Factors affecting calendar life include temperature, SOC during storage, and overall chemical degradation over time. [20]

Cycle life, on the other hand, refers to the number of charge and discharge cycles a battery can go through before experiencing significant capacity degradation. Factors impacting cycle life include the extent of charging and discharging, rates of charging and discharging, and operational conditions. [20] [22]

2.2.5 Battery Management Systems

The Battery Management System (BMS) has emerged as a fundamental element within automotive technology. The BMS plays a critical role in overseeing and controlling the battery's performance, guaranteeing its safety, durability, and efficient functioning. Its primary functions include monitoring various parameters like battery cell voltages and temperatures within the battery module, as well as overseeing battery voltage and current. Additionally, the BMS performs tasks such as balancing cell voltages and assessing the SOC of the battery. By implementing these measures, the stress on the battery cells is reduced, thereby preventing overcharging or overdischarging, both of which can accelerate degradation. [67]

2.3 Degradation

There are several significant factors that contributes to battery degradation, and understanding these factors is essential for minimizing degradation and improving battery performance and longevity. These factors impact various mechanisms, which in turn influence different modes of degradation and their effects.

An overview of the relationship between operational stress factors, corresponding degradation mechanisms, degradation modes, and their impact on the battery degradation, is illustrated in Figure 2.8. Several of these topics, along with other explored ones, will be further discussed in the upcoming chapters.

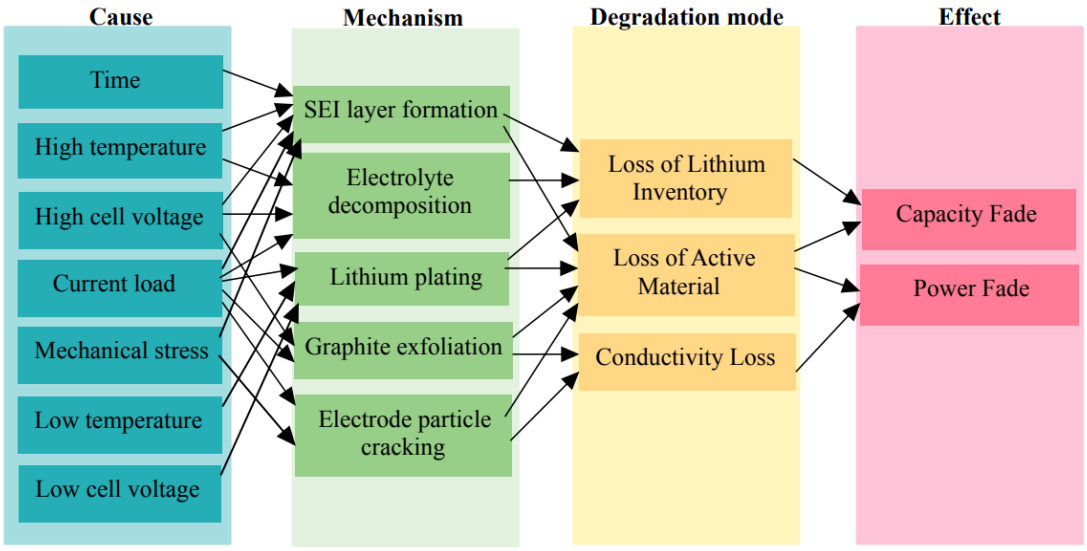

Figure 2.8: The relationship between different degradation factors, inspired by [63] and [11]

2.3.1 Temperature Influence

One of the main factors that contributes to degradation within a battery is the temperature. Elevated temperatures accelerate the chemical reactions within a battery, including unwanted side reactions. High temperatures can cause the electrolyte to decompose and contribute to the formation of SEI layers on the electrodes, which will be further described in Chapter 2.3.3. The SEI layer can grow thicker and less uniform at higher temperatures, which increases the internal resistance of the battery. The higher internal resistance can result in reduced efficiency and power output. [64] [31]

On the other hand, at lower temperatures, the ionic conductivity of electrolytes is reduced, resulting in increased charge transfer resistance. This can lead to high polarization of the graphite anode [31]. As a result, lithium plating, further explained in Chapter 2.3.4, can occur.

Thermal degradation forms the foundation for analysis with Arrhenius. The Arrhenius Equation 2.9 describes the temperature dependence of reaction rates in chemical reactions.

$$k = Aexp(\frac{E_a}{RT}) \tag{2.9}$$

k is the rate of degradation, E_a the activation energy of the reaction, A is the pre-exponential factor or frequency factor, R is the universal gas constant (8.314 J/(mol·K)), and T is the absolute temperature in Kelvin. [15]

2.3.2 C-rate Influence

The C-rate is the charging or discharging rate that correlates with the speed of lithiation or delithiation of the electrode material. Generally, higher C-rates results in increased capacity fade due to mechanically-induced damage to active particles. Higher C-rates also effectively increases the strain rate for the lithiation of $LiCoO_2$, resulting in intercalation-induced stresses that lead can to microcrack formation, defect generation, and ultimately particle fracture. [55]

Fast Charging

Fast charging is a big challenge for the extensive adoption of EVs compared with the rapid refueling of traditional engine vehicles. Standard LIBs can not efficiently handle rapid charging without compromising performance and safety. Fast charging leads to faster performance degradation and a significant increase in the temperature, driven by various physical and chemical processes within the battery. [69]

Physically, the high currents during fast charging generate Joule heat, rapidly increasing the battery's temperature. This rise in temperature aggravates unwanted reactions between the electrodes and electrolyte. [69]

Chemically, fast charging leads to a decrease in Coulombic efficiency, meaning not all of the charge put into the battery is effectively stored. This process also results in an increase in impedance and the overall volume of the battery, as well as depletion of the electrolyte. Ultimately, the loss of cyclable lithium-ions and the subsequent increase in battery impedance are the primary reasons for performance degradation. [69]

2.3.3 Growth in the Solid Electrolyte Interphase Layer

During the initial charging cycle of the battery, a layer naturally forms on the negative electrode, known as the SEI. This layer consists of lithium-ions that have reacted with decomposed electrolyte materials, creating a protective barrier between the anode and the electrolyte, as illustrated in Figure 2.9. The formation of the SEI layer is crucial as it provides electrical insulation while facilitating the movement of lithium-ions, protecting the negative electrode from potential corrosion, as well as preventing reductions in the electrolyte. [8]

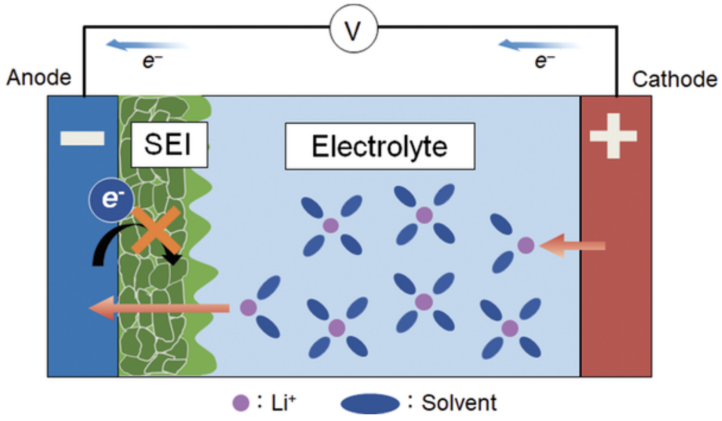

Figure 2.9: The creation of the SEI layer in a LIB [59]

However, with further charging cycles, the SEI layer continues to grow, leading to the loss of continuous lithium-ions. This occurs as lithium-ions in the electrolyte are absorbed and incorporated into the SEI layer, making them unavailable for lithium-ion transport during charging and discharging. The loss of continuous lithium-ions contributes to a decrease in battery capacity. Additionally, the increasing thickness of the SEI layer raises mass transfer resistance, thereby increasing electrical resistance. This makes the development of the SEI layer one of the main degradation factors on the graphite electrode with time, constituting a significant portion of the battery's overall degradation. [8] [26]

The formation of the SEI layer on the carbon anode is influenced by various properties of the graphite material. Factors such as the degree of crystallinity, basal-to-edge-plane ratio, particle and pore size, and surface chemical composition, play crucial roles in determining the characteristics of the SEI layer. In graphite, a high degree of crystallinity is generally preferred for achieving high energy density in the anode. However, the strain exerted on the SEI during lithium intercalation in graphitic particles can lead to SEI damage and a reduction in the cell's cycle life. [2] [57]

At extreme temperatures above 60 °C, volume changes, resulting in the intercalation or deintercalation of lithium-ions during cycling. This can create mechanical stress on the electrodes, which can further lead to cracks in the SEI, allowing new reactions to occur. This cycle of cracking and repair causes the SEI to continue growing, which leads to additional loss of lithium inventory (LLI) and loss of active material (LAM). These processes are further explained in Chapter 2.3.6. [63]

2.3.4 Lithium Plating

Along with the development of the SEI layer, lithium plating is a main degradation factor on the graphite electrode with time. Lithium plating occurs when metallic lithium gathers on the surface of the battery's anode during the charging process. This is caused by low-temperature charging, or when the current is too high at a high SOC. However, deficient capacity balance can also lead to the deposition of metallic lithium at higher temperatures. The buildup of metallic lithium can result in the creation of dendrites or needle-like structures. These have the potential to pierce through the separator, triggering short circuits, as shown in Figure 2.10. This can again lead to serious safety risks, including thermal runaway or fire. [45]

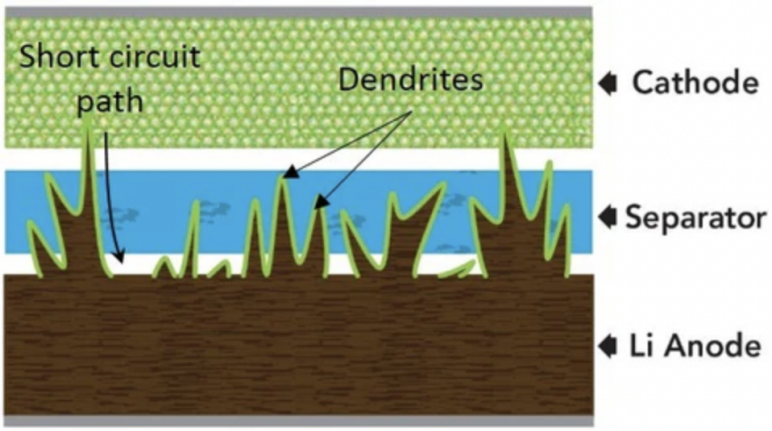

Figure 2.10: The creation of dendrite in lithium batteries can lead to failure [58]

The SEI layer plays a crucial role in preventing lithium plating, because it acts as a protective barrier, preventing additional electrolyte decomposition. Yet, if the SEI layer suffers damage or is insufficient, it can worsen lithium plating. If the SEI layer is compromised, it can lead to increased electrolyte decomposition, which can promote the formation of lithium dendrites, aggravating lithium plating. [45]

At elevated temperatures, the SEI layer may dissolve, forming lithium salts that are less permeable to lithium-ions, thereby increasing the negative electrode impedance. This is illustrated in Figure 2.11. In contrast, low temperatures result in reduced lithium diffusion within the SEI layer and the graphite, which can overlay the electrode with lithium plating. [8]

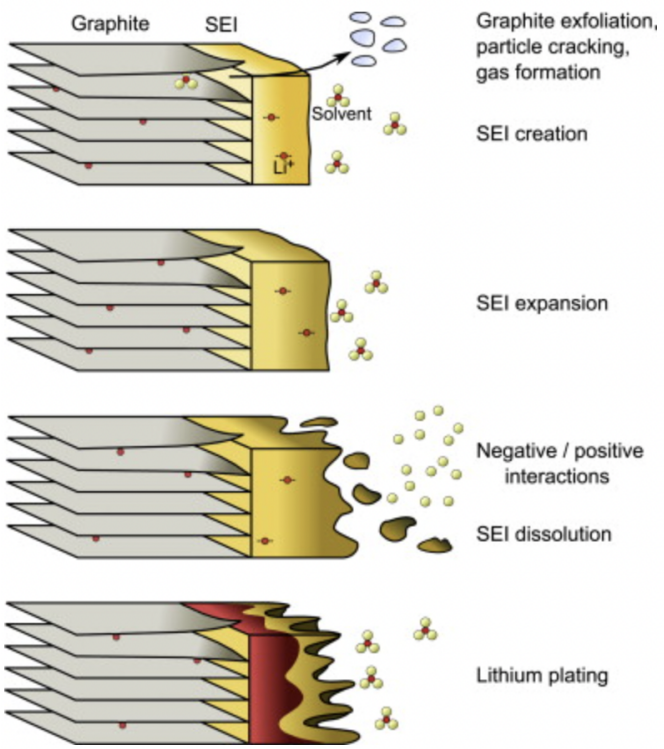

Figure 2.11: The process through which lithium plating can emerge from a damaged SEI layer [8]

2.3.5 Increase in Internal Resistance

Internal resistance is a critical factor for analyzing battery degradation and overall performance, reflecting the total opposition to the flow of current within a battery. This parameter significantly influences how a battery operates under different conditions.

The term internal resistance includes several components, which affects battery behavior. This includes ohmic resistances, which is specifically related to resistances following Ohm's law, stating that the current passing through a conductor is directly proportional to the voltage across it [1]. This resistance primarily arises from the materials used in the battery such as the electrolyte, separator, and electrodes [65].

Additionally, internal resistance includes non-ohmic resistances, which lead to a non-linear relationship between current and voltage. One key component of non-ohmic resistance is the charge transfer resistance, which occurs at the interface between the electrodes and the electrolyte. This type of resistance is crucial as it affects the movement of ions, such as lithium-ions, during the battery's charge and discharge cycles. [25]

Another important aspect of non-ohmic resistance is mass transport resistance, which is influenced by electro-migration and diffusion. These are the primary mechanisms for ion movement within the electrolyte. Electro-migration involves ions moving under the influence of an electric field gradient in addition to concentration gradients, while diffusion occurs as ions move from areas of higher to lower concentration. [32]

During cycling, and as the battery degrades, the internal resistance typically increases, which will lower battery discharge voltage, shorten discharge time, limit spesific power and contribute to capacity loss [65]. The relationship between SOC and internal resistance in batteries is complex and often non-linear. Typically, the internal resistance increases during the discharge of a battery, because as the battery discharges, chemical reactions take place inside the cell, causing alterations in both the electrodes and the electrolyte's composition and structure. This can lead to increased resistance to the flow of electrons within the battery, consequently increasing its internal resistance. During charge, the internal resistance tends to decrease. This is because the process that took place during the discharge is reversed, leading to a reduction in the resistance within the battery, and a decrease in internal resistance. However, the exact behaviour of the internal resistance based on the SOC can vary depending on varoius factors, such as the battery chemistry, temperature and operating conditions. [29]

2.3.6 Loss of Active Material and Loss of Lithium Inventory

In the context of battery degradation, LAM and LLI refer to specific degradation mechanisms that can affect the performance and lifespan of a battery.

LAM refers to the loss or structural degradation of available anode or cathode material. Possible causes for this include the growth of surface layers on the electrodes, due to the consumption of lithium-ions, or cycling-induced cracks and exfoliation. LAM can lead to both power and capacity fade, and can cause a decrease in the height and area of peaks in the battery's incremental capacity (IC) curves, particularly in lower SOC. [21] [53] [63]

LLI is a degradation process in which active lithium-ions become unavailable for cycling within the battery. This can occur due to the formation of the SEI layer, lithium plating, or other

side reactions that consume lithium. LLI can also be caused by irreversible reactions involving lithium. These factors collectively contribute to the reduction in available lithium-ions, leading to capacity fade. [53] [63]

Figure 2.12 illustrates the differences in IC curves and differential voltage (DV) curves when comparing high C-rate and low C-rate charge/discharge cycles. The IC curves typically highlight the LAM, which can be observed as changes in the peak intensity and shape of the curves. This indicates degradation in the battery's ability to hold a charge due to the reduction in active electrode material. Meanwhile, the DV curves typically reveal the LLI, which is assessed through shifts or changes in the end-of-curve points, but LLI can also be observed in the IC curves. These shifts indicate a decrease in the available lithium-ions within the cell. [53]

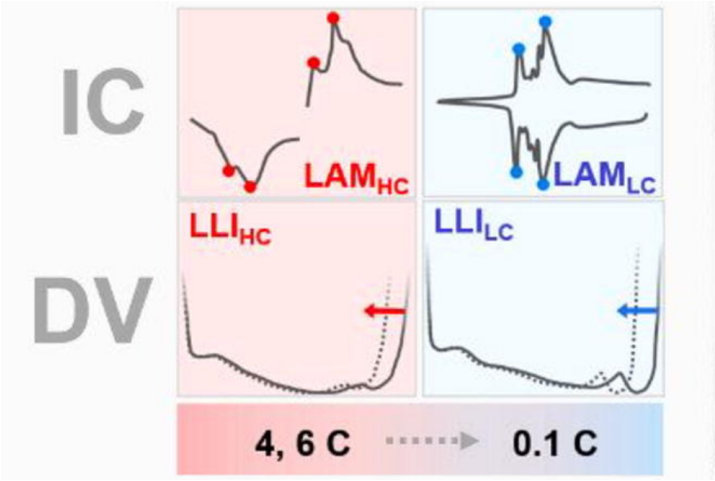

Figure 2.12: IC and DV curves at high and low C-rates, illustrating LAM and LLI [53]

Both LAM and LLI are crucial factors that influence battery lifespan and efficiency. Detecting these issues through IC and DV curve analysis is essential for evaluating battery health and identifying potential problems.

2.4 Environmental and Economic Aspects

LIBs are fundamentally environmentally sustainable. Due to their superior cell voltage, good life-cycle and enhanced energy density, LIBs have become increasingly more important in industrial applications and are now the most preferred batteries for commercial use. [37]

However, the production of LIBs are not entirely emission-free. Figure 2.13 illustrates the greenhouse gas (GHG) emissions associated with the material and production phases of various LIBs. These are gases which contribute to global warming by trapping heat in the atmosphere. GHGs include gases like carbon dioxide (CO_2), methane (CH_4), and nitrous oxide (N_2O). [6]

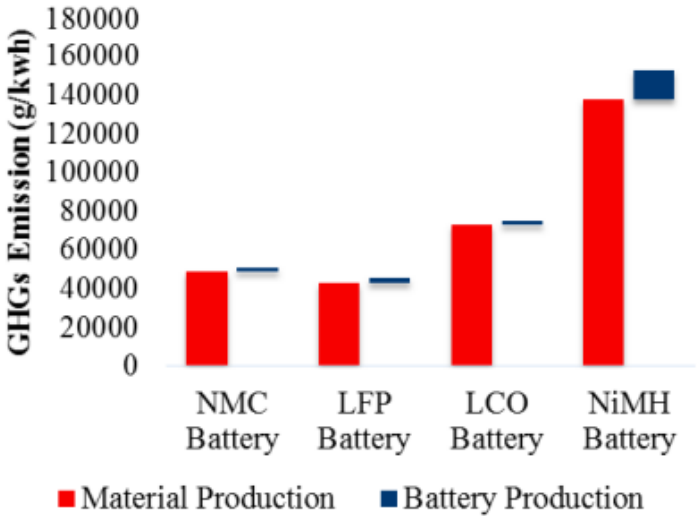

Figure 2.13: GHG emissions of the material production and battery production process for NMC (left) and LCO (second from the right) [6]

As the figure shows, emissions from LCO batteries are slightly higher than those from NMC batteries. It is also evident that the majority of emissions are related to the production of materials. GHG emissions are higher for LCO batteries than for NMC batteries, because LCO has higher total energy consumption during the extraction of raw materials. This data were derived from a Life Cycle Assessment (LCA) about the effectiveness of the LIB technology. [6]

The prices of LIBs have increased due to the expansion in EV production in recent years. An overview of the overall cost breakdown of a LIB is presented in Figure 2.14.

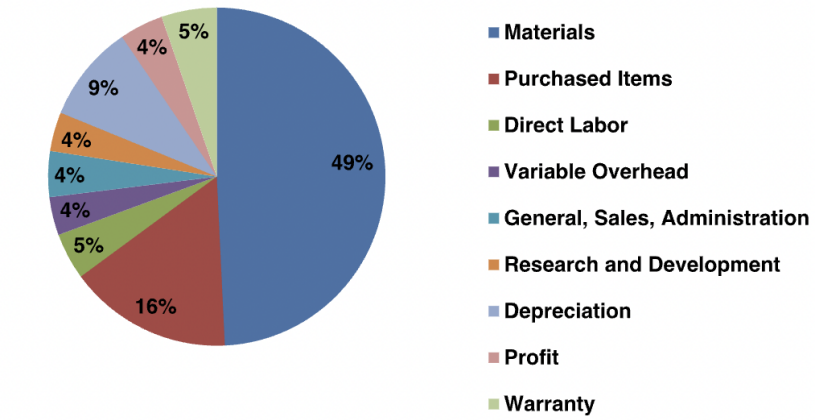

Figure 2.14: Breakdown of the overall expenses associated with LIB manufacturing [49]

Cobalt-based batteries, such as LCO, offer higher specific energy and energy density, but are also more expensive compared to manganese-based LIBs, such as NMC batteries. The cost disparity is significant, as cobalt is rarer and more challenging to ethically source than manganese. This makes cobalt-based batteries not only pricier, but also more contentious from a sourcing perspective. [37]

3 Test Methodology

In this thesis, all the battery tests were carried out in the laboratory at the Department of Energy and Process Engineering (EPT). The institute supplied the necessary testing equipment for evaluating the battery cells, utilized by Revolve NTNU in their racing vehicle. Two types of battery cells have been tested: an LCO pouch cell, produced by Melasta, and an NMC pouch cell by Grepow. In this section, an overview will be provided regarding the instruments utilized, along with an explanation of their setup and the different analysis methods.

3.1 Selected Batteries and Specifications

Table 3.1 displays the battery specifications found in the data sheets from Melasta and Grepow, extracted from Appendix B and Appendix C.

Table 3.1: Specifications for Melasta and Grepow

Manufacturer	Cathode	Anode	Nominal Capacity	Nominal Voltage	Study Type
Melasta	LCO	graphite	6.55 Ah	3.7 V	cycling
Grepow	NMC	graphite	10.50 Ah	3.8 V	cycling

The pouch cells used in this bachelor's thesis are illustrated in Figure 3.1. The cells are constructed with layers of aluminum foil, which is the current collector on the cathode, a cathode, electrolyte, an anode, and copper foil, which is the current collector on the anode, all stacked in parallel. There is a positive and a negative tab serving as the contact points between all the positive and negative layers of the cell. Outermost, the cell is covered with a thin aluminum pouch to protect it against shocks and impacts. [19]

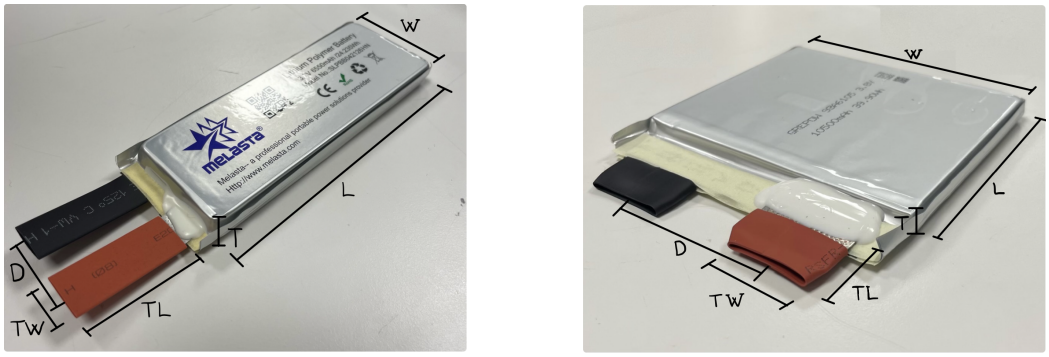

(a) Melasta, model: SLPBB042126HN *(b) Grepow, model: GRP93A6105*

Figure 3.1: Figure illustrating the LCO cell from Melasta and the NMC cell from Grepow

The dimensions for both the Melasta battery and the Grepow battery are found in their data sheets, and listed in Table 3.2.

Table 3.2: Dimensions for Melasta and Grepow

Dimensions	Melasta	Grepow
Thickness, T	10.7 ± 0.3 mm	≤ 9.3 mm
Width, W	42 ± 0.5 mm	≤ 106.5 mm
Length, L	127.5 ± 0.5 mm	≤ 106.5 mm
Distance between 2 tabs, D	21 ± 1 mm	55.0 ± 1.5mm
Tab Width, TW	12 mm	30 ± 0.2mm
Tab Thickness	0.2 mm	0.2 mm
Tab Length, TL	30 ± 1.5 mm	20.0 ± 1.5 mm
Weight	128.5 ± 3.0 g	≤ 195.0 g

3.2 Test Setup

During testing the batteries are inserted into a temperature chamber to provide controlled environmental conditions and ensure precise regulation of temperature. The cells are connected to the measuring instrument inside the chamber through the tabs. The two tabs on each cell establish an external terminal connection, perfect for cell testing purposes, by linking to the electrodes through the current collectors. The tabs are comprised of a conductive material, typically coated with a durable metal layer to inhibit corrosion. A red and thick power cable, along with a white thin voltage meter, are attached to the tab on the positive electrode side, while a black power cable and a green voltage meter are connected to the negative tab, as illustrated in Figure 3.2. The power cables conducts electricity and measures the amount of current moving in and out of the battery, while the voltage meters is used to measure the individual cell voltages during testing. To measure the real time temperature of the battery cell, an external temperature sensor is affixed to the surface of the battery cell using insulating tape.

Figure 3.2: How the batteries are connected with cables to the chamber

3.2.1 Arbin Instrument

Data acquisition systems are used to collect and record data from the measuring instruments during the test. This system include software for data analysis and visualization, as well as hardware for connecting and interfacing with the measuring tools.

During testing, Arbin instruments are utilized to monitor the performance of the batteries. The model utilized is the Laboratory Battery Test Series (LBT21), shown in Figure 3.3. In this particular thesis, cycling testers are utilized to execute repeated charge/discharge cycles on batteries, assessing their performance, lifetime, and degradation mechanisms. Arbin's cycling testers are equipped with advanced features for precise control of cycling parameters and automated data collection. Battery analyzers are used to evaluate battery performance and health, measuring parameters such as capacity, internal resistance, voltage profiles, and more. Arbin's battery analyzers are also designed to deliver accurate and reliable data for quality control, research, and development purposes. [4]

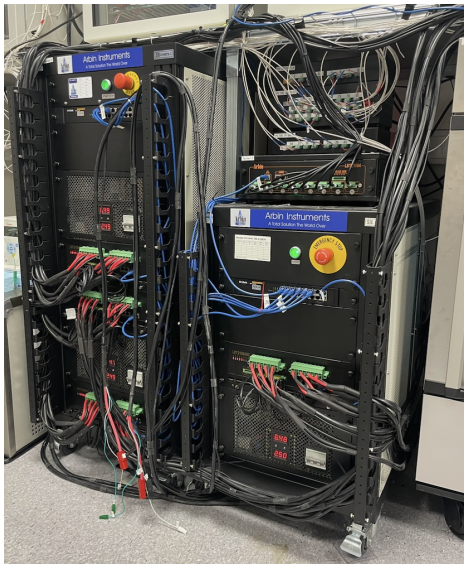

Figure 3.3: Arbin LBT21

Additionally, Arbin offers auxiliary modules to address further testing requirements. In the context of this thesis, temperature measurements are necessary for accurately assessing battery performance and degradation, under various temperature conditions. Arbin's auxiliary modules provide temperature monitoring, and control features that can be integrated into battery test systems to monitor the temperature of batteries during testing. Moreover, they offer temperature control modules, allowing users to regulate the temperature within the test environment. These are crucial characteristics, essential for achieving the desired results from testing. [3]

3.3 Testing and Analysis Methods

This section aims to describe the testing methods that have been used. It includes an explanation of the charge and discharge cycles and setup, as well as details on which characterizations were conducted.

3.3.1 Constant Current-Constant Voltage and Constant Current Charging

The constant current-constant voltage (CCCV) protocol is a standard fast charging method for LIBs, consisting of two stages. Firstly, the battery undergoes constant current (CC) charging until the voltage reaches a predetermined cut-off limit, found in Table 3.7. Following that, it enters constant voltage (CV) charging, where the voltage is maintained at the same level until the current drops to a predetermined minimum value as shown in Figure 3.4. This stage ensures that the battery reaches its full charge capacity while minimizing the risk of overcharging. By maintaining a CV, the charger prevents the battery from exceeding its maximum voltage limit. Additionally, the CV stage helps decrease impedance, minimizing polarization losses and the risk of excessive temperatures within the cell. Overall, this two-stage process optimizes charging efficiency while minimizing the risk of overcharging and associated detrimental effects. [39]

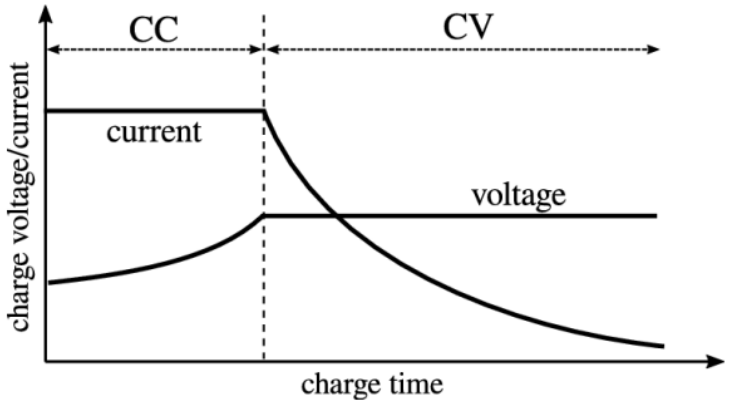

Figure 3.4: Current and voltage profile of a CCCV charge [34]

3.3.2 Open Circuit Voltage Method

There is a significant relationship between the SOC and the open circuit voltage (OCV) for batteries [43]. This relationship gives rise to the OCV method. The OCV refers to the voltage between the terminals of a battery when no external load is connected. The relationship between the SOC and the OCV is usually approximately linear, but this correlation varies among different battery types, depending on the battery's capacity and material. The LIB does not have a linear relationship between the OCV and SOC. [23]

Figure 3.5 illustrates the OCV versus the SOC for a lithium–ion polymer battery (LiPB). A SOC of 100% represents a fully charged battery and 0% SOC is a fully discharged battery. The OCV of a LiPB cell exhibits a consistently rising pattern as its SOC increases.

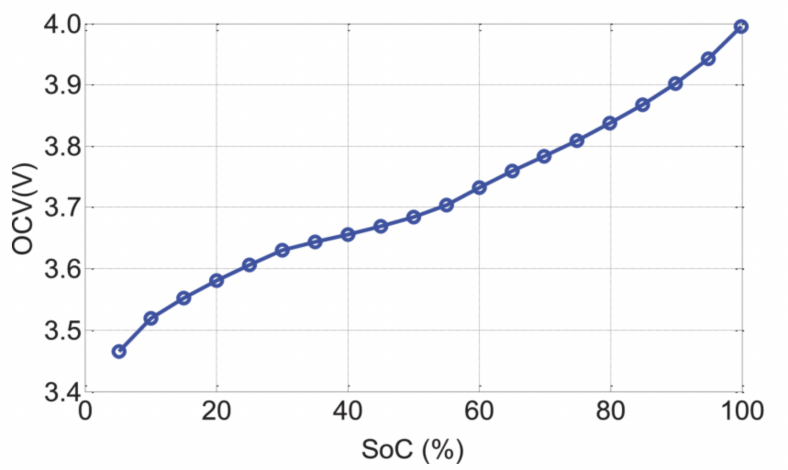

Figure 3.5: A rendition of a typical OCV curve for a LiPB cell [66]

Quasi-OCV

A quasi-OCV test is a method designed to evaluate the battery's voltage under conditions that mimic an open circuit, although not necessarily completely free of current. This could imply the presence of either a minimal load or an extremely high impedance linked to the battery. The purpose of a quasi-OCV test is often to simulate the actual operating situation of the battery more accurately than a pure OCV test. This can be useful for assessing the battery's performance under realistic conditions. [46]

The curve for the quasi-OCV versus the SOC will resemble that in Figure 3.5, especially if the dynamic conditions in the quasi-OCV curve are minimal, but it may exhibit fluctuations or irregularities, depending on the specific testing conditions.

During the testing of the batteries, they go through a quasi-OCV test with C/20 discharge and hybrid pulse power characterization (HPPC) current pulses every fifteenth cycle. The assessment of the quasi-OCV versus SOC begins by completely charging the cells until they reach the end-of-charge voltage. This voltage is specified by the manufacturer and can be found in Table 3.7. Afterwards, the cells undergo discharge at a C/20 current rate, until they reach the end-of-discharge voltage. This voltage is also listed within Table 3.7. The utilised rate needs to be small enough for the measured voltage to be considered a quasi-OCV. Following this stage, the cell continues to be subjected to charging and discharging at the normal C-rates.

3.3.3 Hybrid Pulse Power Characterization Method

HPPC is a test method used to evaluate the dynamic performance and behavior of LIBs under various operating conditions. This test is particularly important for identifying overpotentials

and assessing battery performance in hybrid and EV applications, where batteries are subjected to dynamic and high-power demand scenarios. [10]

For this thesis, the HPPC method is used to investigate the change in internal resistance for the different battery cells. The HPPC utilizes the voltage reaction to a current alteration, called the current step response, to determine the internal resistance. The voltage and current for a charge and discharge pulse are illustrated in Figure 3.6.

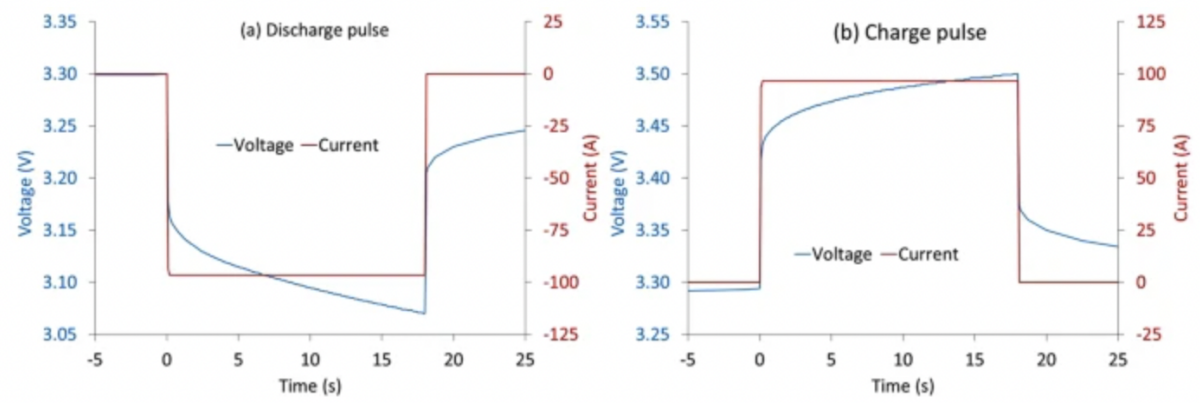

Figure 3.6: Example of a voltage response to 18 second charge and discharge pulse [7]

To measure the internal resistance a current charge pulse is applied to the battery resulting in a voltage change. By analyzing this relationship, the internal resistance of the battery can be calculated using Ohm's law, in Equation 3.1.

$$R_i = \frac{U_1 - U_2}{I_2 - I_1} \tag{3.1}$$

For the HPPC current pulses, the two batteries will be tested at a C/20 discharge. Other conditions, such as temperature, remains consistent with those of the CCCV testing. The current pulses last for two seconds, and every fifth millisecond data points are collected to be utilized for calculations in the results.

3.3.4 Incremental Capacity Analysis

Incremental capacity analysis (ICA) is a technique used in battery management and characterization to assess the health and performance of LIBs. An IC curve is a plot that represents the derivative of the capacity with respect to the voltage (dQ/dV) as a function of the OCV of a battery. [70]

A typical ICA graph is shown in Figure 3.7. Each battery chemistry typically exhibits its own unique IC curve, characterized by specific patterns of peaks and dips. These features are

indicative of the underlying electrochemical processes occurring within the battery [33]. The peaks in the IC curve are mainly defined by the electrodes, with decreasing peaks potentially indicating changes in the other electrode. The variation in changes between the peaks holds more significance than the changes in the peaks themselves when comprehending battery behavior. [27]

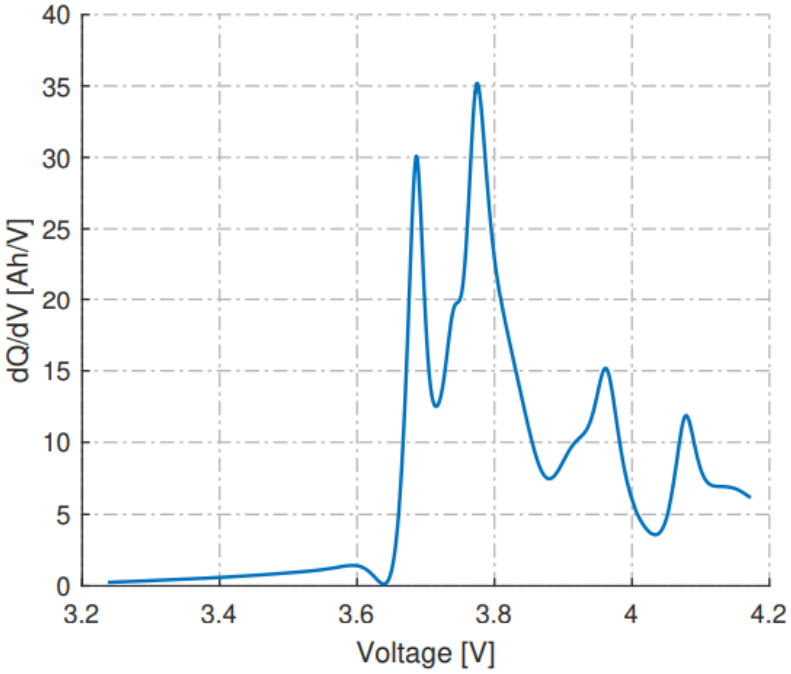

Figure 3.7: IC of a Melasta cell at 100 SOH [33]

The IC for this thesis were acquired through a C/20 cycle, collecting data every other second. A more frequent data collection would result in an unmanageable amount of data.

As a full cell is discharged, the voltage of the cathode decreases as it is lithiated, while the voltage of the anode increases as it is delithiated. The occurrence of degradation modes such as LAM and LLI can be determined, qualified, and quantified through the analysis of IC curves. These modes reflect different aspects of battery degradation and can help in predicting battery lifespan. [70]

When using CV at higher charge states, unevenness or peaks in charging may occur. This happens because the current delivered to the battery varies depending on the battery's SOC and charging conditions, which can lead to imprecise or uneven charging peaks. One way to manage these inconsistencies is to use the discharge peak as a reference in analysis. This means evaluating the battery's condition and performance based on how it discharges and when the battery loses power, rather than focusing solely on the charging process. [28]

3.3.5 Visual Inspection

To monitor potential visible changes inside the LIBs, inspections were conducted on one battery from each set after the cycling process was completed.

Before the batteries can be opened, they must be fully discharged to have a SOC of 0%. This is for safety reasons, to prevent, for example, sudden ignition. Subsequently, they are placed inside a LABmaster pro ECO glovebox with an internal Argon atmosphere, as shown in Figure 3.8 [24]. Here, the battery is carefully opened, and the electrodes are separated layer by layer to be inspected for any signs of degradation.

Figure 3.8: The LABmaster pro ECO glovebox utilized for visual inspection

3.4 Implementation

Table 3.3 illustrates the planned procedure for the CCCV testing. As the table indicates, the plan was to test the batteries at various temperatures and C-rate levels. The table represents the implementation plan for one of the two battery types, implying that this process will be carried out for each battery. The full setup for all the tested cells is shown in Appendix A.

Table 3.3: Initial plan for CCCV testing

Temp/C-rate	2C/2C	2C/1C	1C/1C	1C/0.5C
25			2	1
35	1	1	2	1
45		1	1	
55		1	2	

This test plan was intended to be the most optimal. When testing batteries at different C-rates and temperatures, it is important to focus on the outer points to obtain the most comprehensive analysis. By examining these values, one can estimate the likely outcomes for the intermediate values, ensuring a more thorough understanding of the battery's performance across the entire range.

Due to insufficient time and significantly less space in the temperature chambers than originally intended, the battery testing was not carried out entirely according to plan. To maximize the amount of material for comparison, it was decided to somewhat overlook the C-rate and instead focus primarily on the different temperatures. Charging was set at 2C throughout, as it is less time consuming and plays a less significant role in degradation as discharging. Discharging was either at 0.5C or 1C, but the difference between the two C-rates was almost negligible. Therefore, the results section focuses only on the batteries discharged at 1C. Unfortunately, testing at 55 °C was also discontinued, as the internal temperature in the batteries turned out to exceed the limit set in the battery data sheets, shown in Table 3.7. Finally, the new test plan, as illustrated in the Table 3.4, was implemented.

Table 3.4: Modified plan for CCCV testing

Temp/C-rate	0.5C/2C	1C/2C
25		2
35	1	2
45	1	2

Table 3.5 provides a schedule indicating the duration of each test. This is just an assumption used to schedule the duration required for testing the cells for approximately 200 cycles.

Table 3.5: Schedule for the test duration

C-rate	n (cycles)	Total time (h)	Total time (days)
0.5C/2C	200	873.48	36
1C/2C	200	673.48	28

3.5 State of Charge Window

When testing the batteries, they were all intended to stay within the 10-90% SOC window. In the real-world application for Revolve NTNU's race cars, batteries are typically used within this SOC range. Therefore, testing batteries within this interval provides insights that are directly applicable to practical usage scenarios. While testing the batteries within this SOC window may

not push them to their limits, it still provides valuable information about their performance and potential degradation over time.

However, due to a lot of irregularities in the initial data, there was a suspicion that there might be an issue with the test window. A retest was conducted to accurately determine the actual SOC window. The subsequent analysis revealed that the real SOC window was 9.25% to 90% for Melasta and 7.94% to 90% for Grepow. Table 3.6 presents the intended SOC window compared to the actual SOC window.

Table 3.6: Deviation in SOC from intended values

	Limits	**Melasta**		**Grepow**	
		Voltage [V]	**SOC [%]**	**Voltage [V]**	**SOC [%]**
Inteded	Lower	3.12	10	2.91	10
	Higher	4.08	90	4.19	90
	SOC Window		*80*		*80*
Actutal	Lower	3.1259	9.2456	2.9167	7.9357
	Higher	4.0800	90	4.1898	90
	SOC Window		*80.75*		*82.06*

3.6 Test Schedule

The final test setup for the utilized batteries is illustrated in Figure 3.9. The degradation stage is depicted in the green box, while characterization is represented by the yellow box. This setup is used for all tested batteries, which are analyzed in the results and discussion sections in Chapter 4.

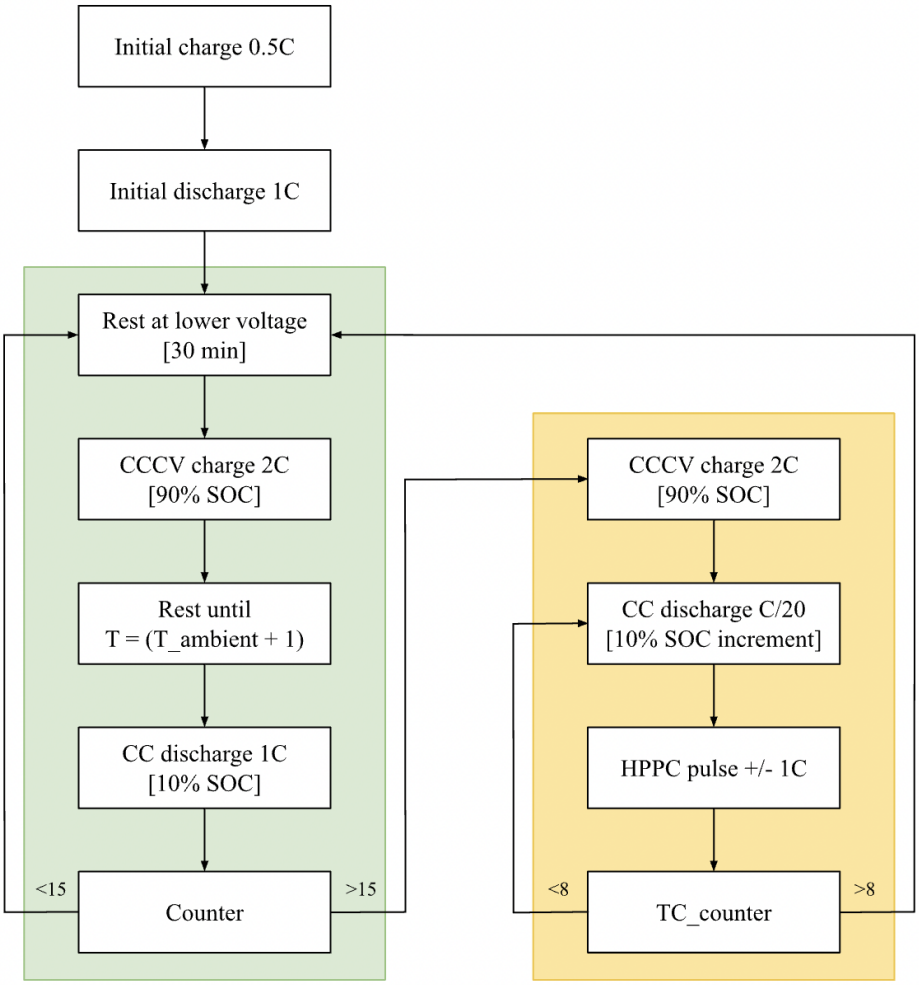

Figure 3.9: Test schedule for the batteries

3.7 Safety Restrictions

Safety is essential when conducting experiments in the battery lab. With the potential risks associated with handling hazardous materials and operating high-energy systems, ensuring a safe working environment is crucial to the success of battery research.

Prior to accessing the lab, it was required to complete both a safety course and a guided tour of the facility. This ensures compliance with safety regulations and guidelines established by the institution, reducing the risk of accidents, injuries, and regulatory violations.

During the testing process, several considerations had to be taken into account to maintain the safety protocols. For example, the tabs of the batteries had to be securely taped with insulating tape at all times. Taping helps prevent accidental short circuits by ensuring that the positive and negative terminals of the battery do not come in contact with each other or any other conducting material. Inadequate taping could potentially lead to the batteries igniting or catching fire.

Additionally, it was crucial to uphold a clean and organized workspace to minimize the likelihood of accidents. One must also maintain a cautious approach while working in the lab. The presence of various equipment posed potential risks, underscoring the importance of attentiveness.

3.7.1 Battery Constraints

Table 3.7 present the constraints for the batteries, found in Appendix B and Appendix C, which include factors such as voltage, current and temperature constraints. These limitations are crucial for ensuring the safe and efficient operation of the batteries within the specified parameters of the system.

Table 3.7: Constraints for the batteries

		Melasta	**Grepow**
Charge condition	**Max continuous current**	13.1 A	-
	Max peak current	54 A ($\leq$ 1sec)	-
	Cut-off voltage	4.2 V $\pm$ 0.03 V	-
	Operating temp.	0 ℃ $\sim$ 60 ℃	5 ℃ $\sim$ 65 ℃
Discharge condition	**Max continuous current**	65.5 A	240 A
	Max peak current	98.25 A ($\leq$ 3sec)	315 A ($\leq$ 3sec)
	Cut-off voltage	3.0 V	-
	Operating temp.	-20 ℃ $\sim$ 70 ℃	-20 ℃ $\sim$ 60 ℃

The datasheet for Grepow is missing some information about the battery, hence, some values are unknown in the table.

4 Results and Discussion

This section focuses on investigating the degradation of the tested LIBs, drawing from the diverse methodologies employed to assess the batteries in the laboratory. By conducting systematic tests, including SOH and Arrhenius behaviour evaluations, and assessments of internal resistance and ICA, the objective is to understand the extent of the degradation. The examination not only reveals the results, but also investigates potential sources of error and external influences impacting testing precision.

To examine results and execute necessary calculations, MATLAB is utilized. After testing, the finished data sets were retrieved and downloaded from the Arbin software, and plotted for processing and analyzing in MATLAB.

The results presents the Melasta and Grepow batteries individually in each section across the different testing temperatures, before they are later compared. Melasta plots are represented using a blue color palette, while Grepow plots are represented by a pink color palette. Due to time limitations the cells tested with a 0.5C discharge rate and a 2C charge rate was not analyzed. Therefore, all the battery cells examined in the results section were tested with a 1C discharge rate and a 2C charge rate. The objective was to test each cell for approximately 200 cycles, but due to time constraints, some cells have undergone a shorter cycling period.

4.1 State of Health Analysis

This chapter will analyze and discuss the difference in the SOH graphs at the chosen temperatures, first for the Melasta batteries followed by the Grepow batteries.

4.1.1 Melasta

Figure 4.1 shows the evolution of SOH as a function of cycles for the Melasta cell at temperatures of 25, 35, and 45 °C. For the cell at 25 °C, the SOH decreased from 88.1% to 87%, which is a relatively small decline. However, this small decrease is expected given the moderate temperature and the fact that the battery underwent only 200 cycles. For the cell at 35 °C, the SOH decreased from 90.2% to 88.5%, which is also a small decline, but slightly more significant than the decline at 25 °C. For the cell at 45 °C, the SOH decreased from 92.2% to 90.7%. Although this cell underwent fewer cycles, the degradation is more pronounced.

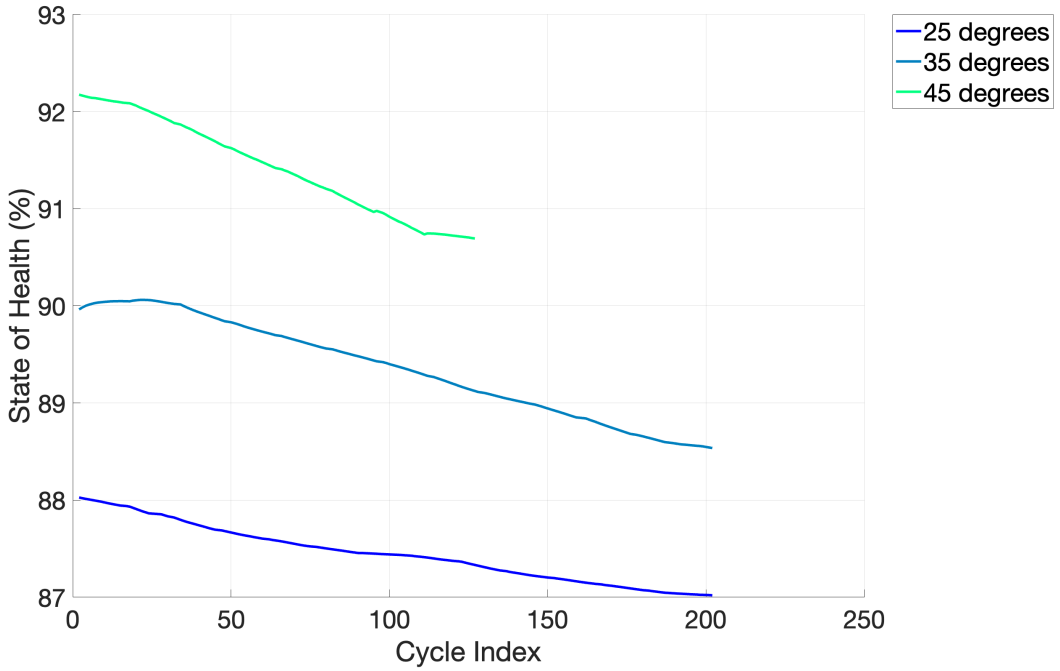

Figure 4.1: SOH as a function of cycles for the different temperatures for Melasta

To determine the degradation rate more accurately for the temperatures, a linear regression analysis was performed in the interval where the SOH is most stable, spanning from cycle 40 to cycle 90. This analysis, along with a regression equation for each temperature, is presented in Figure 4.2.

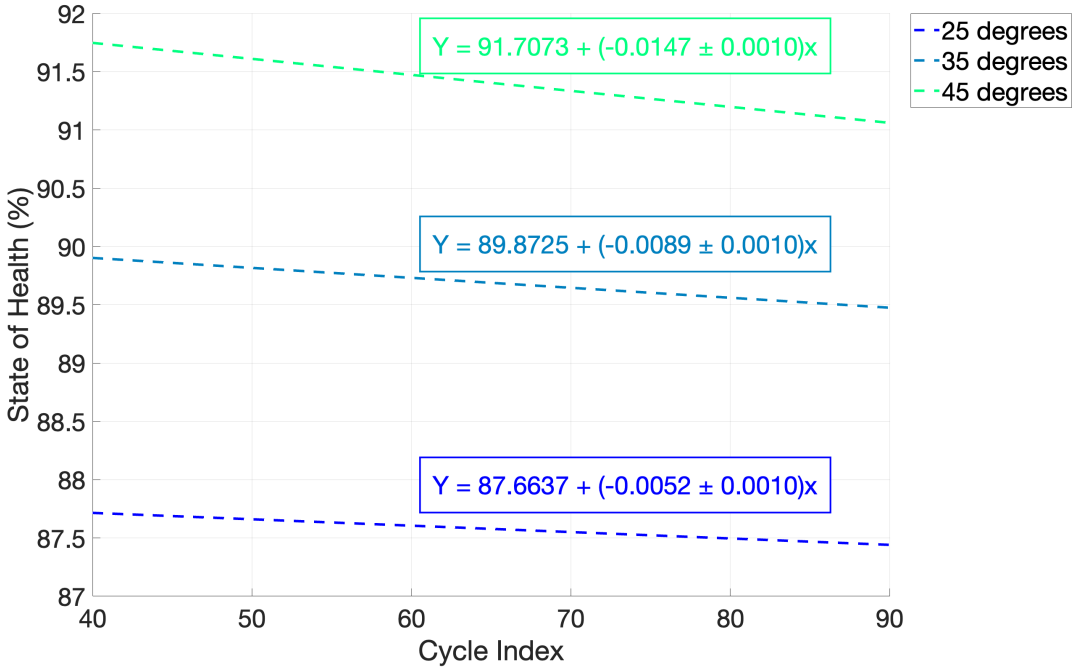

Figure 4.2: Linear regression of SOH from cycle 40 to 90 for Melasta

Table 4.1 presents the degradation rate from the slope values in the regression equations at the chosen temperatures. As shown in the table, the rate increases with rising temperatures. This indicates that the battery degrades faster at higher temperatures, a common observation that confirms a well-established understanding within battery technology. The elevated temperatures can accelerate chemical reactions within the battery, such as growth of SEI layer, contributing to a shorter battery lifespan and increased degradation. The SEI layer can grow thicker and less uniform at higher temperatures, which can increase the internal resistance of the battery. While higher temperatures may in some cases enhance immediate performance metrics such as power output, they come at the expense of the extended reliability and durability.

Table 4.1: Degradation rate for the Melasta batteries at 25, 35 and 45 °C

Degrees (°C)	25	35	45
Degradation rate (%)	0.0052	0.0089	0.0147

Assuming that the battery continues to degrade linearly according to these degradation rates, they can be used to estimate the number of cycles the battery can undergo before it is effectively dead. Calculations indicate that the Melasta battery at 25 °C will reach a SOH of 0% after 16 858 cycles, at 35 °C it can last for 10 098 cycles, and the one at 45 °C will reach a SOH of 0% after only 6 239 cycles. However, this is not a completely realistic approach, as it is well-known in theory that the degradation rate of the batteries is likely to accelerate more significantly once they reach a SOH of 80%, as shown in Figure 2.7. Therefore, in reality, the batteries are likely to undergo even fewer cycles than estimated here. The cell at 25 °C will by calculations reach a SOH of 80% after 1 473 cycles, the one at 35 °C does so after 1 109 cycles, and finally, 45 °C reaches a SOH of 80% after 796 cycles, if they follow the same degradation rate as the first cycles.

The SOH graphs clearly show that the three batteries tested did not start cycling with the same SOH value. This is not entirely uncommon and may result from the impact on the batteries' calendar life. As mentioned in Chapter 2.2.4, a battery that remains unused for an extended period will experience some capacity reductions. Notably, the Melasta battery had been stored and unused for three years before the commencement of testing, so calendar aging could be a key factor in the degradation of these batteries. The difference in initial SOH might also be attributed to minor variations within the individual cells.

Since none of the temperatures appeared to have a significant impact on the SOH of the batteries from Melasta, it speaks volumes about the quality of the cells. The batteries are evidently of

high quality, at least initially during the first cycles. However, with only around 200 cycles completed, it is challenging to predict their degradation over a longer period.

A deeper understanding of the variations in the graphs at the different temperatures and their degradation will be provided when discussing the internal resistance and the ICA in Chapter 4.3 and 4.4.

4.1.2 Grepow

Figure 4.3 illustrates the development of SOH as a function of cycles for the three Grepow cells, at 25, 35, and 45 °C. The SOH values for the batteries at 35 and 45 °C have decreased minimally and remain stable at around 91% and 93% SOH, respectively. However, the battery tested at 25 °C seems to have undergone a huge degradation compared to the other cells. This indicates that there is likely something wrong with this particular battery, as it does not align with the theory that the battery tested at 25 °C should degrade more than those tested at 35 and 45 °C. Additionally, the battery degrades from approximately 86.9% to 75% according to the graph, which seems somewhat high considering that the test temperature is stable at only 25 °C and the C-rate is also at a reasonable level with a 1C discharge rate and 2C charge rate. However, the behaviour of this battery aligns well with the theory mentioned in Chapter 2.2.3, which states that the SOH graph drops sharply after reaching an SOH of 80%. The error analysis for this battery will be further discussed in Chapter 4.7.2.

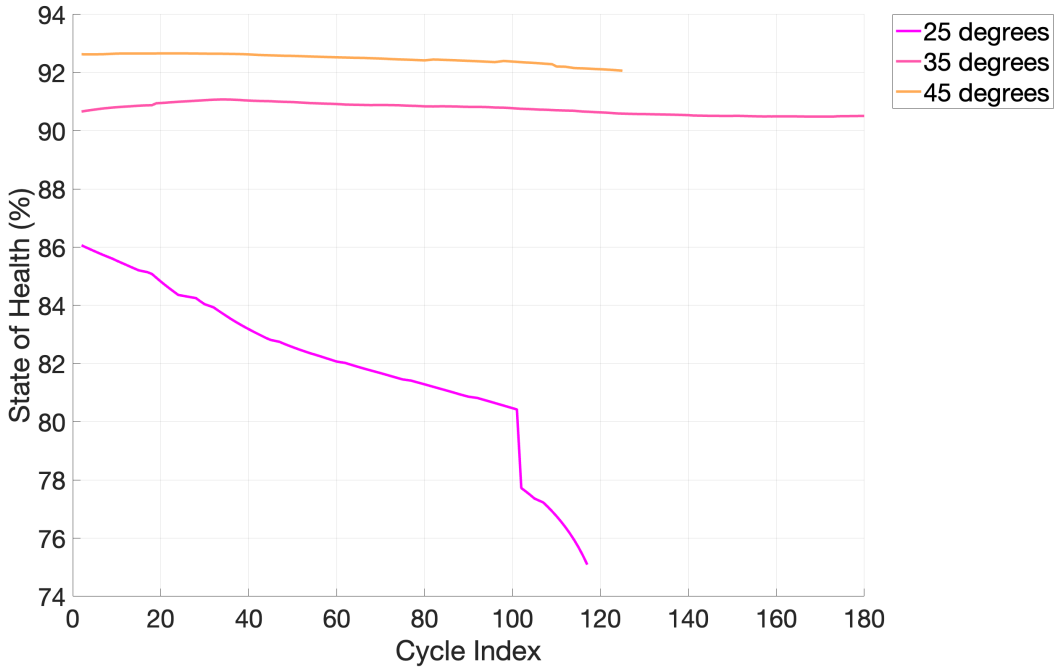

Figure 4.3: SOH as a function of cycles for the different temperatures for Grepow

A regression analysis was also carried out for the Grepow batteries to simplify the calculation of degradation rates at various temperatures within a stable SOH interval. This, along with the regression equation and standard deviation, is shown in Figure 4.4. The interval was selected from cycle 20 to 80.

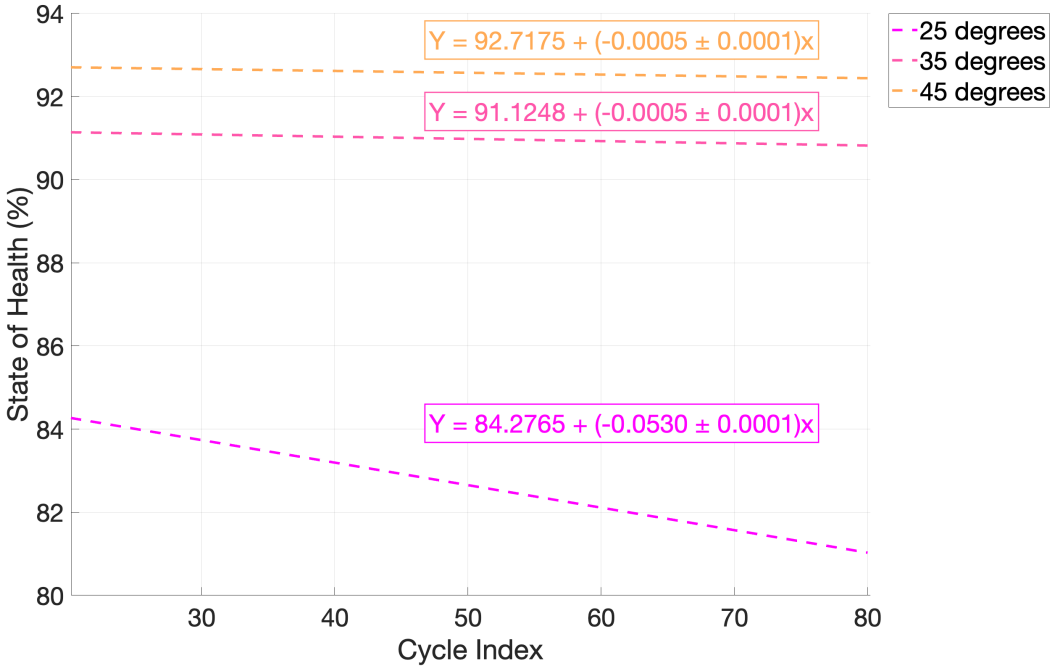

Figure 4.4: Linear regression of SOH from cycle 20 to 80 for Grepow

Table 4.2 presents the degradation rate at the chosen temperatures. It is worth noting that the batteries tested at 35 and 45 °C showed similar negligible degradation, but this could be because the batteries have not been tested for a long enough period to observe noticeable changes in degradation. The battery at 45 °C was also cycled for only approximately 120 cycles, while the one at 35 °C underwent over 180 cycles. Hence, it is possible that at 45 °C, the battery would have experienced a higher degradation rate if it had been cycled for the same number of cycles as the one at 35 °C. Ideally, the batteries should be tested over a much larger cycle number to observe more substantial changes.

Table 4.2: Degradation rate for the Grepow batteries at 25, 35 and 45 °C

Degrees (°C)	25	35	45
Degradation rate (%)	0.0530	0.0005	0.0005

Assuming linear degradation, the degradation rates for Grepow also provide estimates for the number of cycles until the battery is considered unusable. Calculations suggest that the Grepow

battery at 25°C will reach 0% SOH after 1 583 cycles, while the 35°C and 45°C batteries can last for 182 249 and 185 435 cycles, respectively. However, these big number does not seem realistic, but as mentioned, real-world degradation may accelerate after 80% SOH, potentially reducing the actual cycle life. By calculations, the cell at 25 °C reaches 80% SOH after only 113 cycles. This correlates strongly with the observations depicted in Figure 4.3, where a distinct decline in the graph is evident right after cycle number 100, coinciding with the battery reaching an SOH of approximately 80%. The cell tested at 35 °C reaches 80% SOH after 22 249 cycles, and finally, at 45 °C, it reaches 80% SOH after 25 435 cycles. This also represents high numbers of cycles, and in reality, degradation may occur at a faster rate, especially considering that the graphs for 35 and 45 °C exhibit very flat slopes.

It also becomes evident for the Grepow batteries that they start their cycling with different SOH values. This is likely due to individual differences between the batteries and their storage situation. These cells have remained in an unused state for approximately one year, which may have led to some degree of calendar aging.

Overall, the Grepow batteries also appear to be of high quality, considering the minimal degradation of the cells tested at 35 and 45 °C. However, it is crucial to remember that they have not undergone many cycles yet, so the trend could potentially change by extending the testing period. The battery tested at 25 °C has degraded unusually quickly, indicating a potential issue.

4.2 State of Health and Temperature

Arrhenius behavior is essential in understanding the relationship between temperature and degradation, as mentioned in Chapter 2.3.1. This section will examine whether the batteries exhibit typical Arrhenius behavior.

4.2.1 Melasta

Figure 4.5 present the Arrhenius behavior for the Melasta batteries at 25, 35 and 45 °C, with ln(degr.rate) on the y-axis and the inverse temperature, 1000/T, on the x-axis. The graph is based on the degradation rate determined by the linear regressions in Figure 4.2, using the same data as the SOH regression, covering cycles from 40 to 90. There is a considerable spread of data points not utilized, as shown in the top right corner of the figure, which makes the it somewhat less presentable.

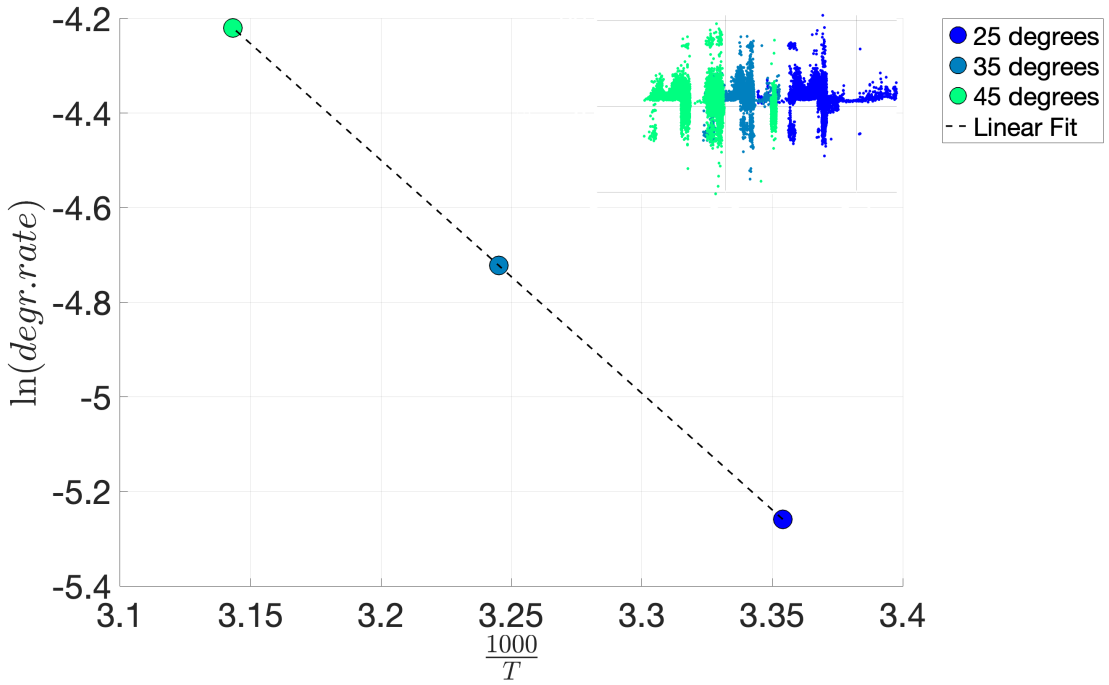

Figure 4.5: Arrhenius behavior for Melasta based on linear regression

However, the linear regression exhibits typical Arrhenius behavior, where the rates of chemical reactions generally accelerate as the temperature increases. This is evidenced by the higher ln(degr.rate) value at 45 °C, indicating that chemical reactions occur more instantly at this temperature. This interpretation is consistent with the Arrhenius equation, which predicts that reaction rates increase with temperature due to higher active energy leading to more frequent and effective collisions among reacting molecules.

4.2.2 Grepow

Figure 4.6 illustrates the Arrhenius behavior for the Grepow batteries at the chosen temperatures, plotting ln(degr.rate) on the y-axis against 1000/T on the x-axis. The line in the graph is based on the linear regression that covers cycles from 20 to 80 in Figure 4.4, derived from the same data used in the SOH regression. Due to the spread of data points, as shown in the top right corner, the line represents a simplified version of the actual data.

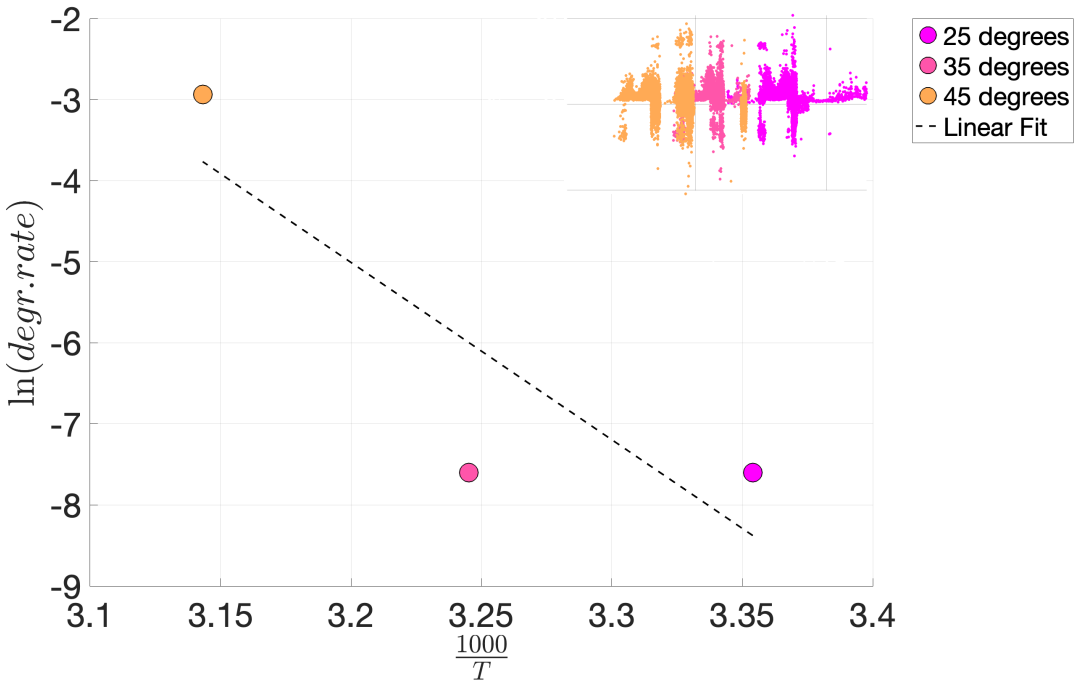

Figure 4.6: Arrhenius behavior for Grepow based on linear regression

As observed in the graph, the ln(degr.rate) value for 25 °C is lower than for 45 °C. The linear fit through these points shows a negative slope, which is consistent with Arrhenius behavior. This behavior indicates that an increase in temperature leads to an acceleration of the chemical reactions that contribute to faster battery degradation. However, this was not the case if considering the results from Chapter 4.1.2.

If the battery were tested for a longer period, it would likely result in more consistent data points and a reduction in data variability, leading to more accurate results.

4.3 Internal Resistance

The graphs for internal resistance are created by locating the HPPC current pulses over the C/20 cycles as explained in Chapter 3.3.3. Further, the internal resistance is calculated for each pulse, using Equation 3.1 and plotted against the SOC. During the calculations of internal resistance the SOC window only ranges from 10% to 80% for most batteries, which does not align with Table 3.6, but this will be further explored in Chapter 4.7.3.

4.3.1 Melasta

Figure 4.7 presents the change in internal resistance for Melasta at 25 °C. Dark blue colors in the plot represent internal resistance at a high SOH, while lighter blues represent the internal resistance as the battery degrades.

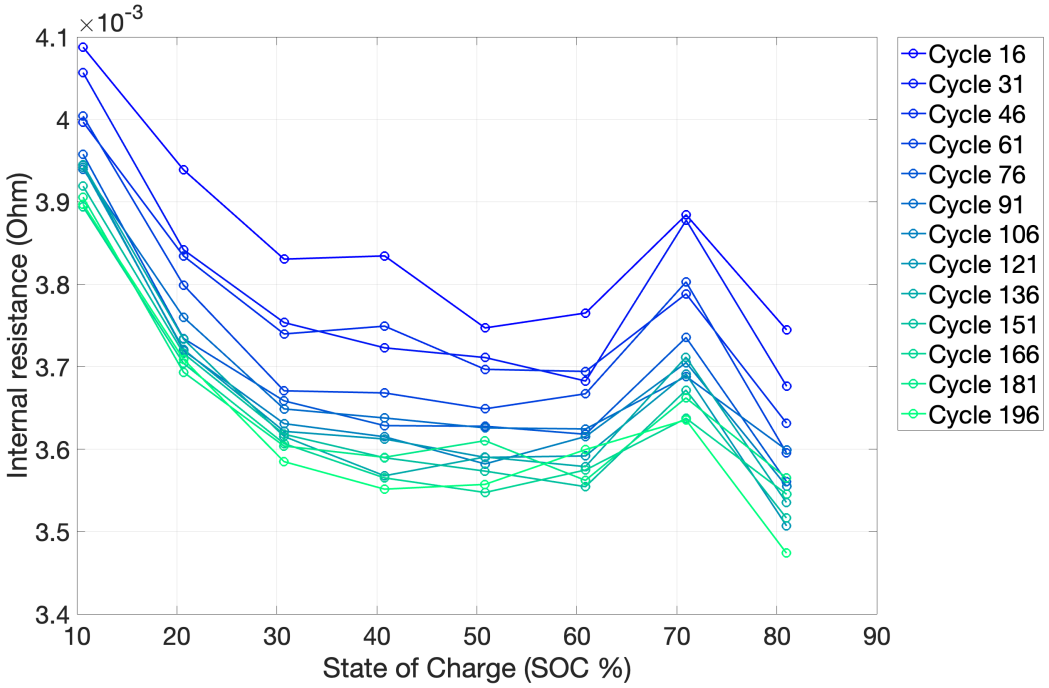

Figure 4.7: Internal resistance for Melasta, 25 °C

Table 4.3 presents SOH values for different cycle counts. As the number of cycles increases, the SOH decreases, indicating that the battery's performance gradually degrades over time. Given the minimal changes in SOH, using cycle numbers for the graph and a table to represent the different SOH values, provides a clearer overview.

Table 4.3: SOH values for the different cycle count for Melasta, 25 °C

Cycles	16	31	46	61	76	91	106	121	136	151	166	181	196
SOH (%)	87.97	87.80	87.71	87.59	87.54	87.47	87.39	87.39	87.28	87.22	87.16	87.08	87.02

As shown in Figure 4.7, the internal resistance decreases more sharply at the beginning of the SOC window, which is typical for a LIB. In the beginning, the battery has a lower concentration of lithium, leading to higher internal resistance, which then decreases rapidly as the battery begins to charge. This reduction in internal resistance can be attributed to various factors, including changes in electrolyte composition, lithium distribution in the electrodes, or other chemical reactions occurring in the battery. As the lithium concentration increases in the battery, the internal resistance tends to stabilize.

As stated in Chapter 2.3.5, the internal resistance generally decreases with increasing SOC. In the case of the 25 °C Melasta cell, the graph's trend aligns with theoretical expectations. As the battery's SOC increases, there is a general decline in the internal resistance. The resistance is reduced by about 9% as the SOC is raised from approximately 10% to 50% across nearly every

cycle. However, after this, the cell goes through a slight increase in internal resistance until it reaches a SOC of 70%. This increase could be due to the fact that the battery's electrodes may experience increased stress or degradation at this rate, which can lead to an increase in internal resistance. For the final part from 70% to 80%, the internal resistance continues to decrease.

At the same time, there is also an overall decrease in internal resistance at about 6% from the first cycle to the last, thus the internal resistance decreases as the SOH decreases. This does not fully align with the theory stated in Chapter 2.3.5, which decleares that internal resistance should actually increase over time. While this tendency may seem unusual, the 6% change is almost negligible, and therefore may not necessarily have significant implications. It could possibly be as minor a factor as the particle contact between the clamp on the cable and the tab, may have improved over time, for example, by the clamp settling better into the material. Thus, it might not necessarily be due to anything happening inside the battery. It is believable that due to the battery's minimal change in SOH, only about 1% degradation, the impact on internal resistance may not be substantial within the duration of the testing period. One can attempt to identify the reasons for the slight decline, but in reality, it represents a very little portion, making it difficult to pinpoint the exact cause. The outcome is simply that the Melasta battery performs adequately at 25 °C, aligning with the minor change in SOH.

The graph for internal resistance as a function of SOC for Melasta at 35 °C is presented in Figure 4.8.

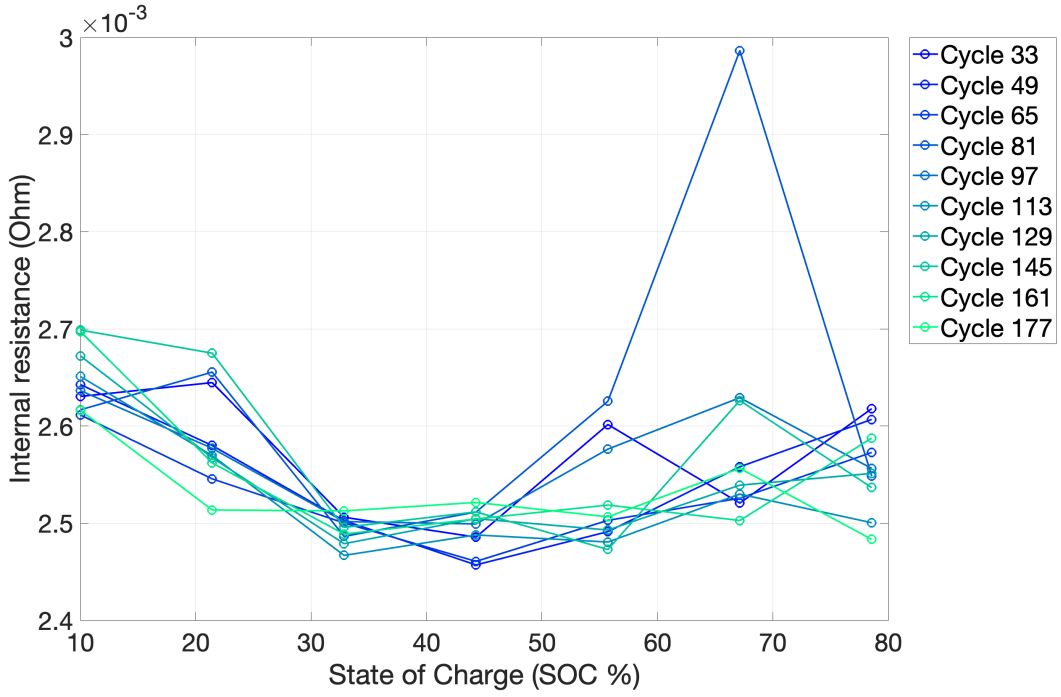

Figure 4.8: Internal resistance for Melasta, 35 °C

Table 4.4 displays SOH values across various cycle counts, for a more concise presentation. With an increase in cycle count, there is a decrease in SOH.

Table 4.4: SOH values for the different cycle count for Melasta, 35 °C

Cycles	33	49	65	81	97	113	129	145	161	177
SOH (%)	89.95	89.76	89.63	89.49	89.34	89.16	89.02	88.86	88.69	88.58

Although this graph shares some similarities with the one for 25 °C, it is evident that it does not align with the theoretical expectations. Most of the irregularities in the graph arise because the HPPC current pulses for this battery were not square shaped, as depicted in Figure 3.6, but triangular, due to errors in data collection. Consequently, calculating the internal resistance became more challenging, which this will be further explained in Chapter 4.7.3.

The typical decrease in internal resistance at the start of the SOC window is also evident here, and the graph follows the same shape as the one for 25 °C, with a decrease in approximately 6% from a SOC from 10% to around 40% for each cycle. This is followed by an increase, but the incline of this increase is very different from cycle to cycle. Cycle 81 has a significant incline, while some of the first cycles actually experiences a further decline during this interval. It appears there may be an issue with the calculations, likely due to the error in the collection of the data of the pulses. The overall values for the internal resistance are somewhat lower for the Melasta at 35 °C than for the one tested at 25 °C.

Determining the changes in internal resistance relative to the SOH of the battery during cycling is somewhat more difficult to ascertain from this graph. There is not a clear trend for the increasing cycle number, as the internal resistance both increases and decreases throughout the testing. This could be due to calculation errors, but also simply because the internal resistance has not changed significantly during the testing period.

Figure 4.9 illustrates the change in internal resistance as a function of SOC for the Melasta tested at 45 °C.

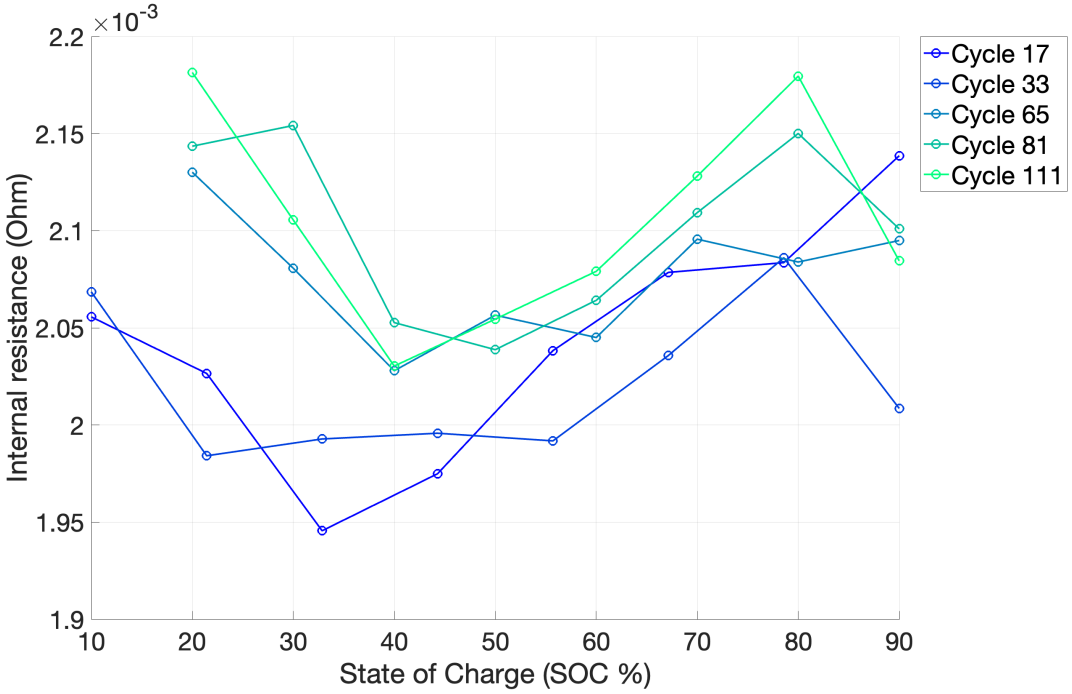

Figure 4.9: Internal resistance for Melasta, 45 °C

Table 4.5 provides a concise overview of the SOH values at different cycle counts. This cell was not cycled for as long as the two at lower temperatures, but also here, a consistent degradation trend is observed with increasing cycle number.

Table 4.5: SOH values for the different cycle count for Melasta, 45 °C

Cycles	17	33	65	81	111
SOH (%)	92.11	91.94	91.43	91.30	90.61

The graph for Melasta at 45 °C also exhibits some irregularities. Similar to the battery at 35 °C, the initial HPPC current pulses for this cell were of a triangular shape. However, this issue was identified and corrected, so starting from cycle 65, the pulses are of a normal square shape. This likely contributes to the not ideal appearance of the graph, with a noticable distinction between the internal resistance calculated from the triangular pulses and the internal resistance calculated from square pulses. The cycles that experienced the triangle shaped pulses had a lower internal resistance overall, while the cycles from cycle 65 onwards exhibit a slightly higher internal resistance. Nevertheless, it is still possible to extract some useful data from the graph.

The variations in internal resistance follow a similar pattern across the different cycles, with a slightly steeper decline at the start of approximately 5% between SOC levels of 10% and 40%, before curving upwards to a peak at around 80% SOC. Naturally, there are some fluctuations

among the different cycle numbers as well. For instance, cycle 17 appears to continue rising until it reaches 90% SOC. In other words, it is somewhat difficult to observe a definitive correlation between internal resistance and SOC. There is no noticeable decrease in the overall internal resistance with increasing SOC, but this is possibly due to the low degradation rate and the battery not being cycled for a sufficient duration to significantly affect internal resistance.

However, this is the first battery that demonstrates a correlation between SOH and internal resistance consistent with the theory mentioned in Chapter 2.3.5. The graph indicates that as the cycle number increases, and thus the SOH decreases, the internal resistance increases. From cycle 17 to cycle 111, the internal resistance increases by approximately 6% overall, but this increase may be attributed to the fact that the calculations were initially performed on triangular pulses and later on square pulses, which may not be sufficiently accurate to assess the difference in internal resistance as genuine.

4.3.2 Grepow

Figure 4.10 presents the change in internal resistance for Grepow at 25 °C. Pink colors in the plot represent internal resistance at high SOH, while the more yellow colors represent the internal resistance as the battery degrades.

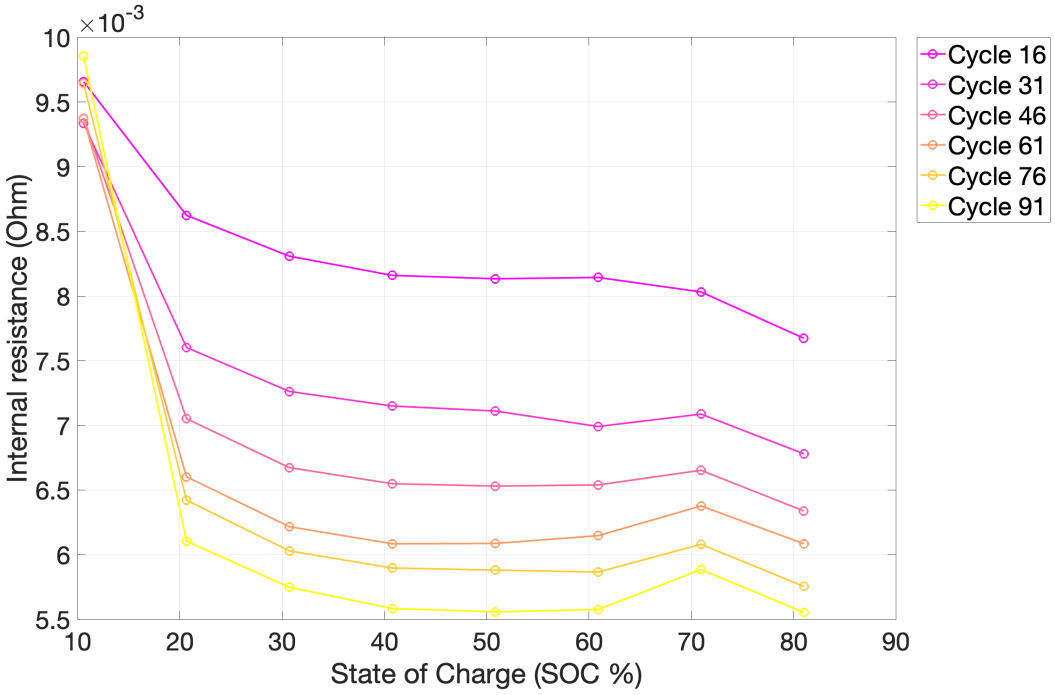

Figure 4.10: Internal resistance for Grepow, 25 °C

Table 4.6 presents SOH values for the different cycle counts. This cell was cycled for just over 100 cycles and experienced the highest degradation rate. It has only been chosen to analyze

the values of internal resistance up to cycle 91, because after that the battery experiences an extreme decline in SOH. It was decided to disregard this decline, as there was a desire for a consistent basis for analysis, similar to the other tested batteries.

Table 4.6: SOH values for the different cycle count for Grepow, 25 °C

Cycles	16	31	46	61	76	91
SOH (%)	85.10	83.64	82.70	81.97	81.37	80.82

Similar to Melasta batteries, the Grepow battery tested at 25 °C also exhibits a notably sharper decline in internal resistance at the beginning of the SOC window. In fact, the decrease is even more pronounced compared to the Melasta cells. The steep decline in internal resistance within the SOC from 10% to 20% constitutes approximately 25% on average across the cycles. This suggests a lower concentration of lithium, leading to higher internal resistance, also for this cell. Further as the SOC increases, there is an increase in lithium concentrations and the internal resistance stabilizes, as observed in the figure. From an SOC of 20% to 80%, the internal resistance decreases by only 10% overall.

In general, the internal resistance for this battery is much higher than for those analyzed previously, reaching values up to 10 milliohms. This may help explain why the degradation rate for the Grepow at 25 °C is significantly higher than expected. A higher internal resistance can, as mentioned in Chapter 2.3.5, contribute to lower battery discharge voltage, limit spesific power and contribute to capacity loss.

For this battery, the same trend as before is evident, with the internal resistance decreasing as the SOH decreases, rather than increasing as the theory suggests. From cycle 16 to cycle 91, the decline in internal resistance is approximately 30%. This is a much larger decrease than what has been observed for the other batteries tested, further raising suspicions that something might be wrong with this particular cell.

The internal resistance for the Grepow battery at 35 °C is presented in Figure 4.11.

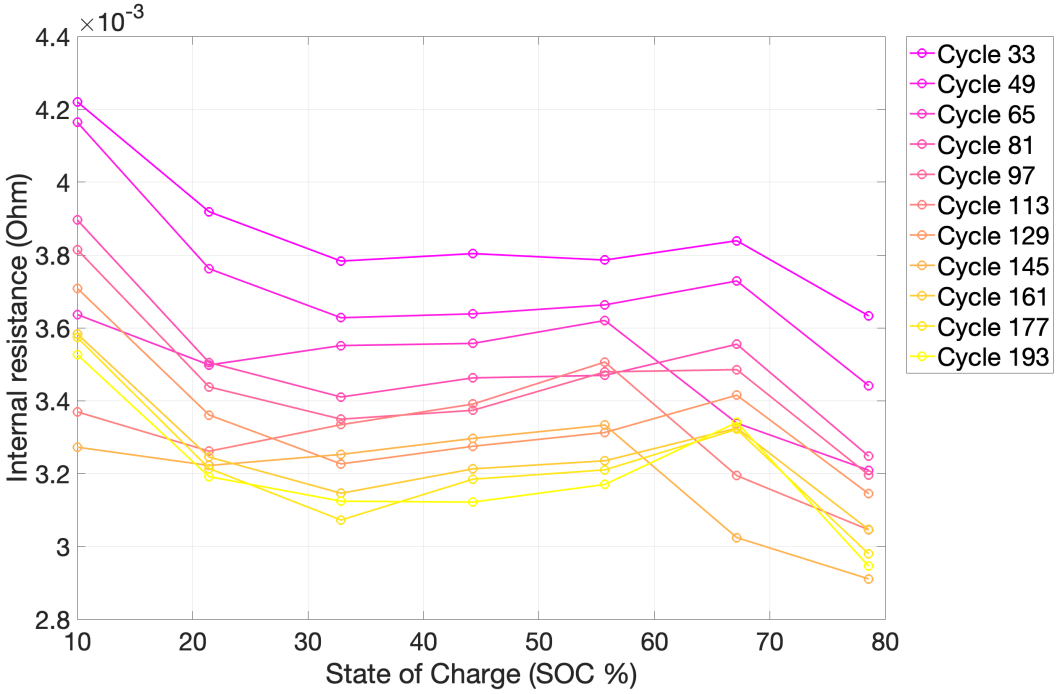

Figure 4.11: Internal resistance for Grepow, 35 °C

The SOH values corresponding to the cycle numbers depicted in this graph are presented in Table 4.7. This is one of the cells that underwent the most cycles, with nearly 200 cycles completed, yet the degradation rate, however, was minimal.

Table 4.7: SOH values for the different cycle count for Grepow, 35 °C

Cycles	33	49	65	81	97	113	129	145	161	177	193
SOH (%)	91.15	91.03	90.90	90.86	90.81	90.65	90.56	90.57	90.44	90.63	90.29

Similar to the Melasta battery tested at 35 °C, this battery also experienced errors during the calculation of internal resistance because the HPPC curves were recorded as triangular instead of square shaped. How this issue was resolved is elaborated upon in Chapter 4.7.3. Despite this, the graph follows a fairly clear trend that can be analyzed.

This battery also experiences a decrease in internal resistance at the beginning of the cycles, but this decline is not as steep as for the other batteries. Instead, the decrease is rather consistent, at approximately 15%, across the almost entire SOC window from an SOC at 10% to 80%. There is only a slightly steeper decline right at the beginning and at the very end. The fact that the internal resistance decreases with increasing SOC generally aligns with the theory, mentioned in Chapter 2.3.5.

Also in this case, the internal resistance decreases as the SOH declines, which contradicts

theoretical expectations. The internal resistance decreases by approximately 15% from the first cycle to the last cycle for Grepow at 35 °C. This is not a very significant decrease, and thus may have the same explanation as for Melasta at 25 °C. The cause might not necessarily be internal to the battery, but rather due to the minimal change in SOH. As a result the effect on the internal resistance may not be significant within the duration of the battery testing period.

The last battery to be analyzed is the Grepow battery tested at 45 °C. Figure 4.12 presents the battery's internal resistance as a function of SOC.

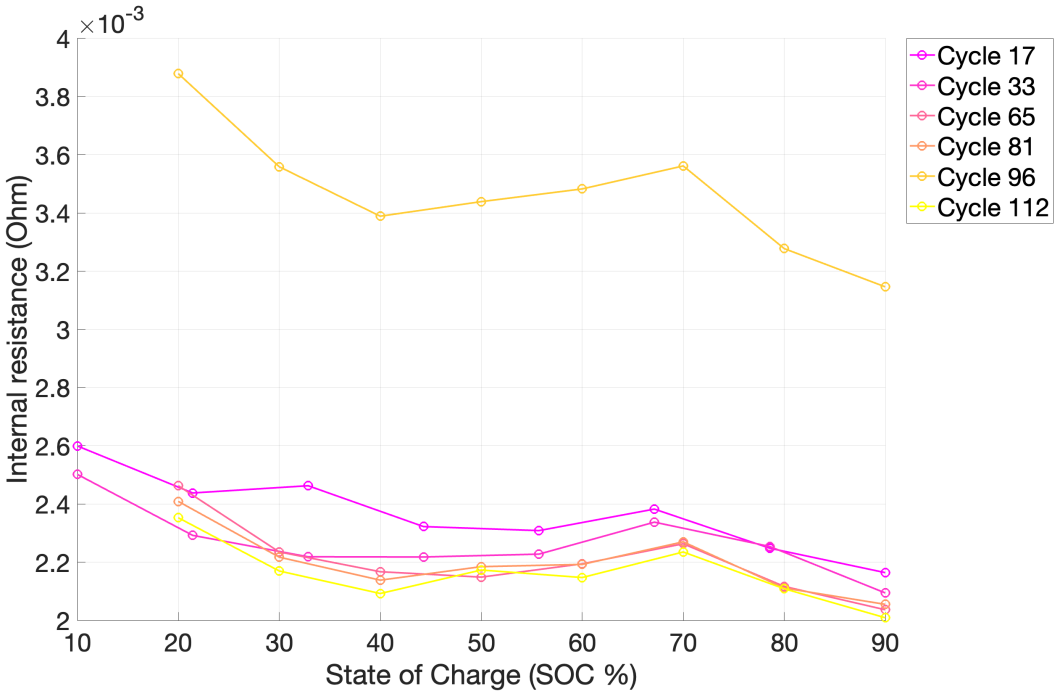

Figure 4.12: Internal resistance for Grepow, 45 °C

The SOH values corresponding to cycle numbers are presented in Table 4.8. Grepow at 45 °C was cycled for just over 100 cycles and the degradation of this battery was very minimal. In fact, cycles 96 and 112 in the table indicate that the SOH has slightly increased compared to the earlier cycles.

Table 4.8: SOH values for the different cycle count for Grepow, 45 °C

Cycles	17	33	65	81	96	112
SOH (%)	92.64	92.66	92.52	92.47	93.42	93.63

This battery encountered a similar issue as the Melasta battery at 45 °C. Initially, the HPPC current pulses had a triangular shape for the first few cycles. However, after cycle 65, the pulses resumed their normal square shape once the error in data collection was corrected. This may

have contributed to the graph not being a completely accurate representation of the real internal resistance.

The internal resistance for cycle 17 and 33 remain relatively flat throughout the SOC window, experiencing only a decline of about 16% from SOC at 10% to 90%. However, these were the cycles where the internal resistance was calculated using triangular pulses, which may have impacted the final appearance of the graph. For cycle 81 and 112, there is a slightly larger decrease in internal resistance observed at the start from an SOH of 10% to 20%, but it is cycle 96 that stands out the most, with a significantly higher overall internal resistance. It also exhibits a much clearer steep decline at the start of the SOC window, similar to several other batteries. Overall, there is a decrease in internal resistance with increasing SOC for all the cycles.

Assessing the fluctuations in internal resistance relative to the battery's SOH during cycling proves somewhat challenging for this battery as well, as the cycles do not follow any clear trend. If excluding cycle 96, it appears that the internal resistance mainly has a small decrease as the SOH decreases, similar to most other cells tested. However, it is important to remember that miscalculations may have occurred because the initial HPPC pulses were triangular, while the later ones were square.

4.4 Incremental Capacity Analysis

When using CV at higher charging states, unevenness or peaks in charging may occur. This happens because the current delivered to the battery varies depending on the battery's SOC and charging conditions, which can lead to imprecise or uneven charging peaks. One way to manage these inconsistencies is to use the discharge peak as a reference in analysis. This means evaluating the battery's condition and performance based on how it discharges and when the battery loses power, rather than focusing solely on the charging process. The discharge process is represented as the inverted graph throughout the analysis.

4.4.1 Melasta

In this chapter, Melasta will be analyzed across all tested temperatures, starting with 25 °C, followed by 35 °C, then 45 °C.

Figure 4.13 shows the charge and discharge characteristics of the Melasta cell at 25 °C over an interval ranging from 5 to 180 cycles, resulting in a decrease of 1% in SOH. During charging, the small peaks occur at 3.78 V and 4.05 V, while the largest peak is at 3.89 V. During discharge,

the minor peaks occur at 3.65 V and 3.93 V, while the major peak is at 3.73 V.

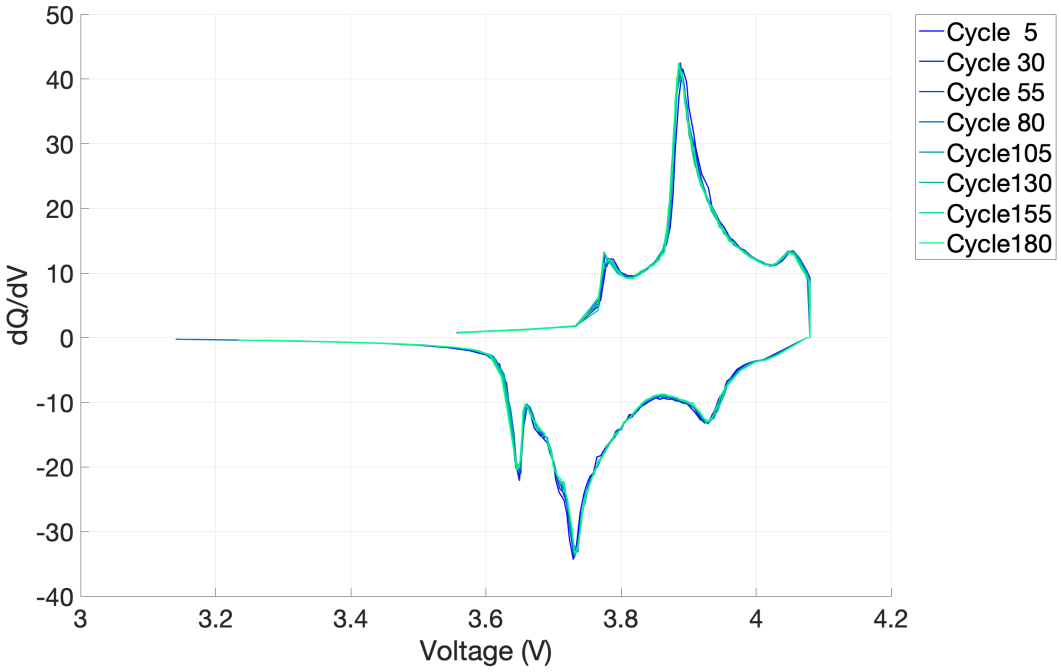

Figure 4.13: dQ/dV plot for Melasta, 25 °C

Table 4.9 displays SOH values for different cycle counts. Given the minimal changes in SOH, presenting the different SOH values in a table offers a more concise and clear overview.

Table 4.9: SOH values for the different cycle count for Melasta, 25 °C

Cycles	5	30	55	80	105	130	155	180
SOH (%)	88.08	87.80	87.63	87.51	87.39	87.28	87.18	87.08

As the battery degrades, the positions of the peaks remain unchanged, but their sizes decrease. The reduction in the peaks can indicate various types of battery degradation, including the decline of the structural integrity of the electrodes over time. This could possibly lead to increased mechanical stress within the electrode material, which again affects the pathways available for lithium-ions. Consequently, these disruptions can reduce the efficiency of lithium intercalation and deintercalation processes during charging and discharging cycles, resulting in the observed reduction of the peaks. This phenomena can happen for all the temperatures tested.

Other contributing factors to the reduction in the peaks observed in the ICA could be LAM and LLI, as explained in Chapter 2.3.6. LAM can be caused by several factors, including mechanical damage to the electrodes, deposition on the electrodes, or degradation of the electrodes due to

chemical reactions. When active material is lost, the electrodes' capacity to store and release charge is reduced.

LLI can occur due to various mechanisms, including the formation of the SEI, electrolyte leakage, or unwanted reactions of lithium with other materials. When lithium is lost, the battery's capacity to effectively perform cycles is reduced, which can result in lower peaks in the dQ/dV graphs.

The reduction in peak performance can also result from an increase in internal resistance. However, this is unlikely to be the cause here, given that no increase in internal resistance was observed for this battery, as discussed in Chapter 4.3.1. It is also unlikely that lithium plating has occurred, given the temperature at which the cell was tested.

Figure 4.14 shows a close-up view of the largest discharge peak for this battery at 3.73 V. As the number of cycles increases, the intensity of the peak gradually decreases, indicating potential battery performance degradation. The color shift, from blue to lighter blue as the battery degrades, suggests a decline in the battery's ability to effectively hold a charge at this voltage with increasing charge and discharge cycles.

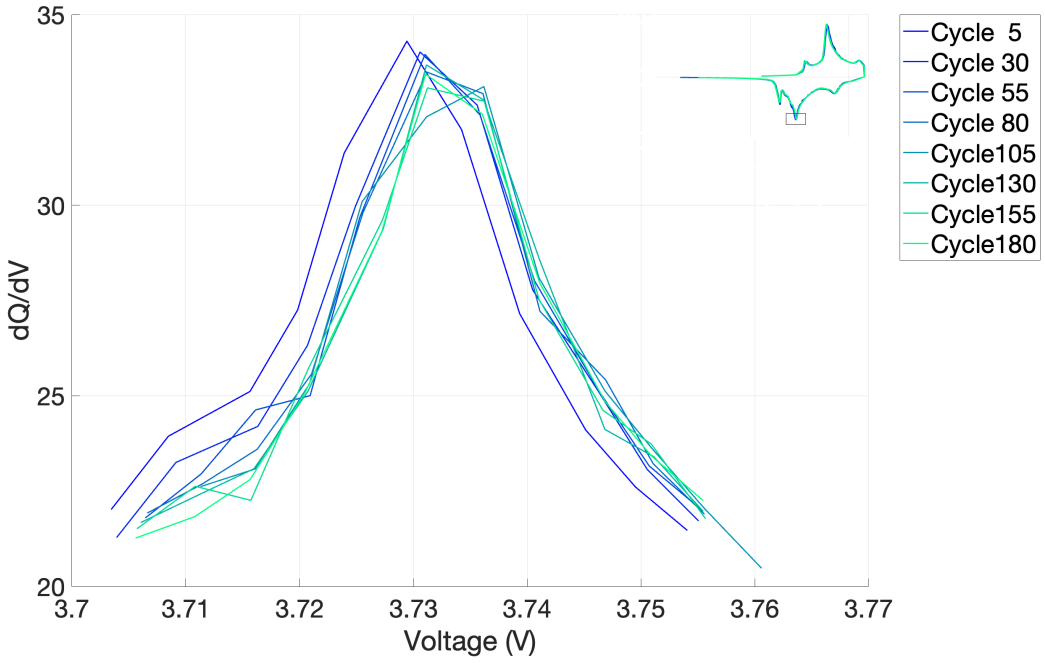

Figure 4.14: Close-up of dQ/dV discharge peak for Melasta, 25 °C

Figure 4.15 shows the development of the dQ/dV vaules as a function of cycles for the same peak. The graph reveals a decrease in maximum dQ/dV values from cycle 5 to cycle 180, at approximately 3%, confirming the decline in peak height as the battery degrades.

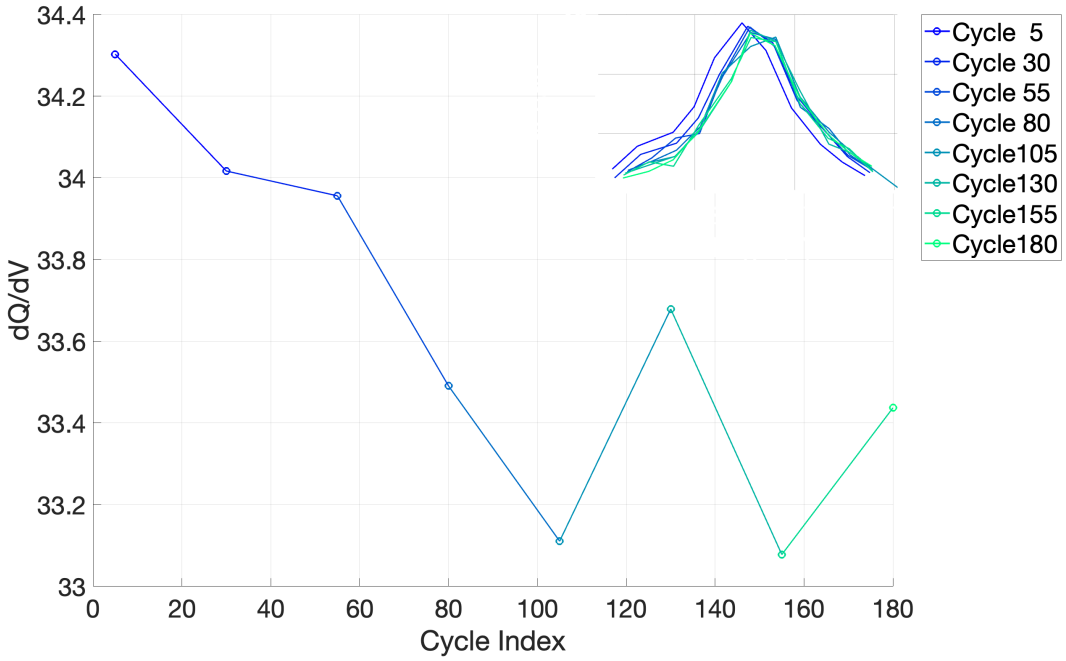

Figure 4.15: Development of the maximum dQ/dV vaules for Melasta, 25 °C

Figure 4.16 displays the charge and discharge characteristics for the Melasta cell at 35 °C over an interval ranging from 5 to 180 cycles, resulting in a decrease of 1.32% in SOH. During charging, the small peaks occur at 3.75 V and 4.05 V, while the large peak is located at 3.87 V. During discharging, the small peak is at 3.95 V, and the largest peaks are at 3.65 V and 3.74 V.

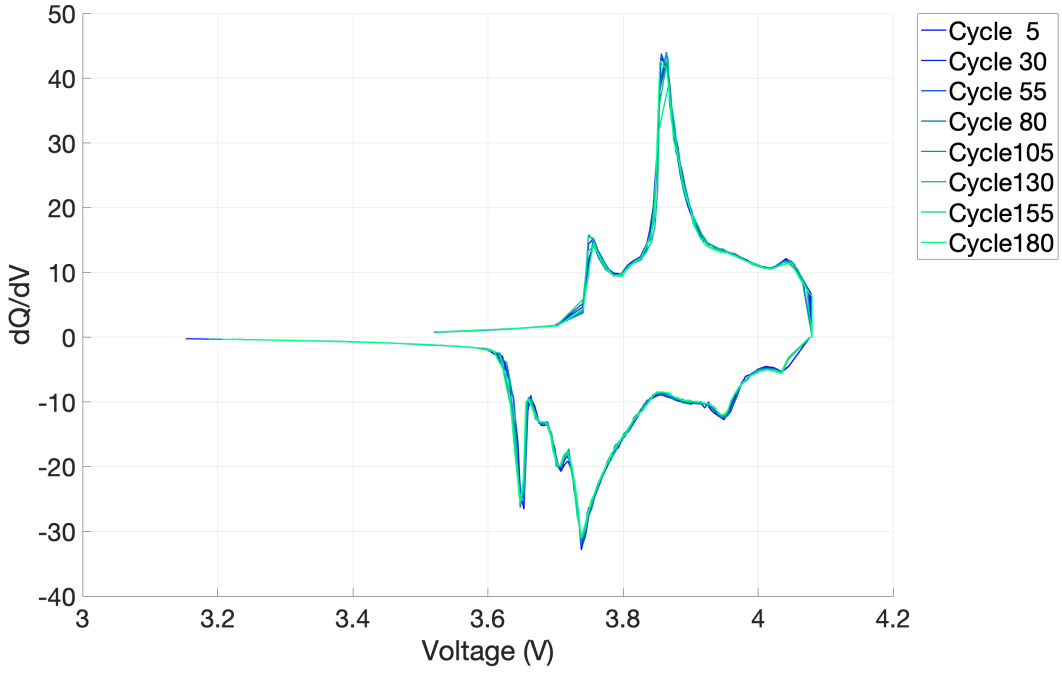

Figure 4.16: dQ/dV plot for Melasta, 35 °C

Table 4.10 displays SOH values for different cycle counts. Also here presenting the different SOH values in a table offers a more clear overview given the minimal changes in SOH.

Table 4.10: SOH values for the different cycle count for Melasta, 35 °C

Cycles	5	30	55	80	105	130	155	180
SOH (%)	89.95	90.08	89.78	89.56	89.38	89.02	88.95	88.63

Similar to the battery tested at 25 °C, there is a reduction in the peaks observed. This reduction could also be attributed to the degradation of the structural integrity of the electrodes over time, and other factors, such as LAM and LLI.

Figure 4.14 shows a close-up view of the largest discharge peak at 3.74 V. As the number of cycles increases, the intensity of the peak gradually decreases, indicating battery performance degradation that correlates with the degradation in SOH for the increasing cycle numbers.

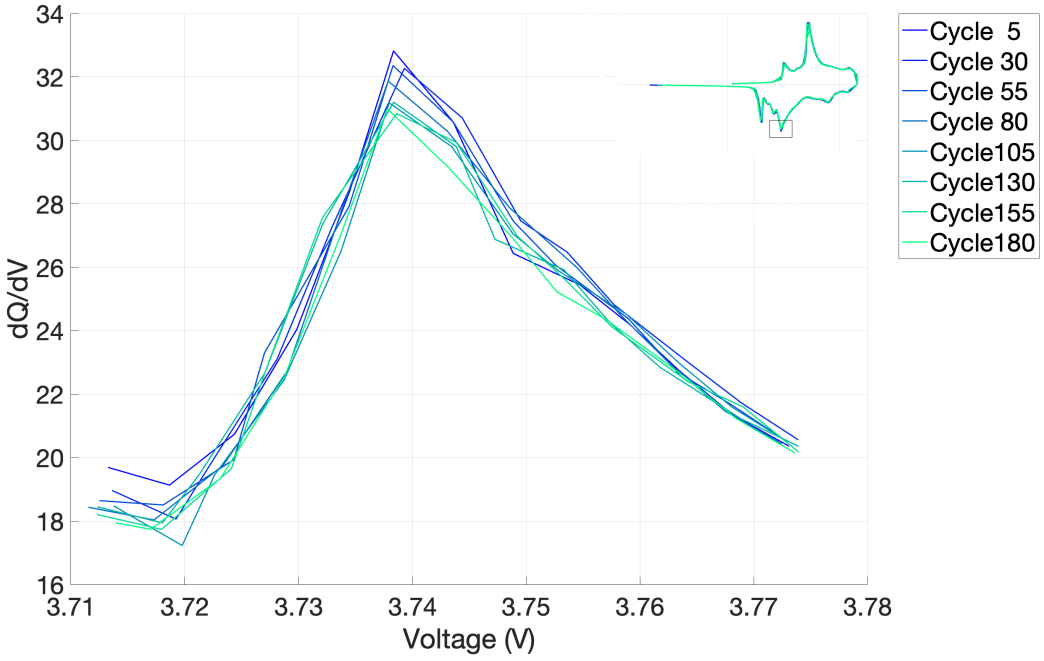

Figure 4.17: Close-up of dQ/dV discharge peak for Melasta, 35 °C

Figure 4.18 illustrates the evolution of the maximum dQ/dV values as a function of cycles for the battery cell at 35 °C. As depicted in the figure, the decrease in peaks is even more pronounced here, with a decline of about 5% from cycle 5 to cycle 180. This could be attributed to a larger reduction in SOH compared to the battery tested at 25 °C, as discussed in Chapter 4.1.1.

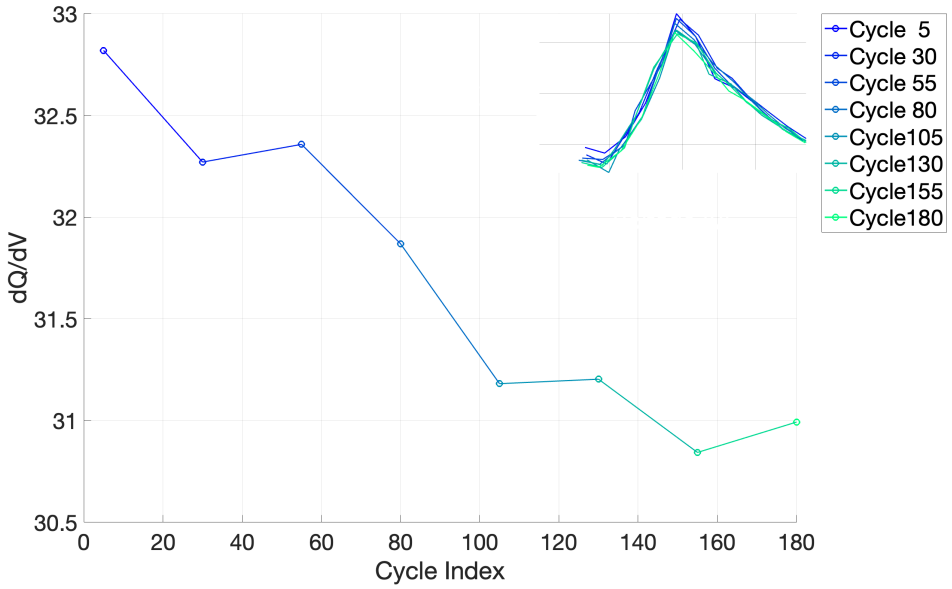

Figure 4.18: Development of the maximum dQ/dV vaules for Melasta, 35 °C

Figure 4.19 shows the charge and discharge characteristics for the Melasta cell at 45 °C over an interval ranging from 5 to 80 cycles, resulting in a decrease of 1.37% in SOH. During charging, the minor peaks occur at 3.74 V, while the large peak is located at 3.84 V. During discharging, the small peak is at 4.05 V, and the large peaks are at 3.65 V and 3.75 V.

Even though the peaks are located at approximately the same positions for all temperatures, there are slight differences among the various batteries. This could be due to individual variations in batteries and the fact that they have been tested at different temperatures.

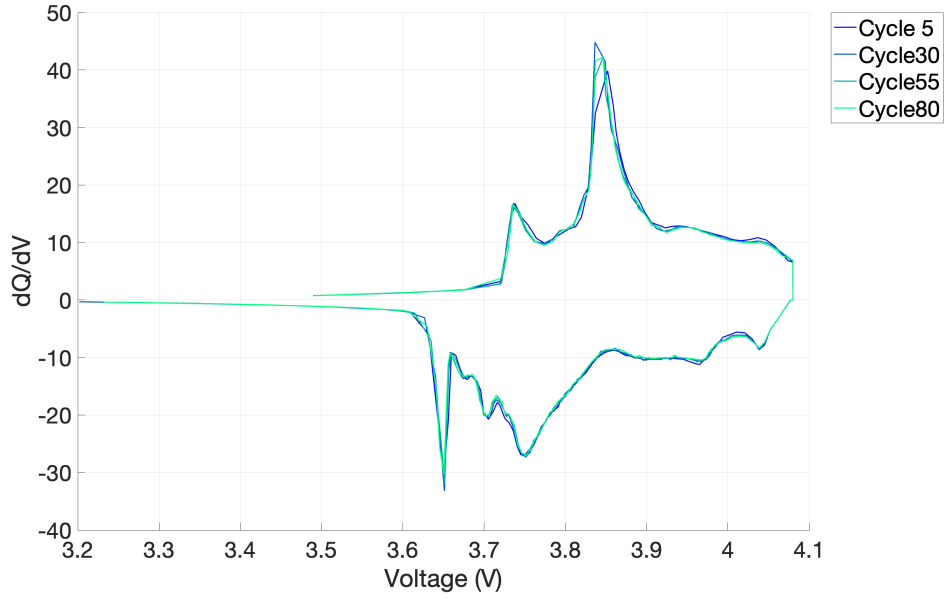

Figure 4.19: dQ/dV plot for Melasta, 45 °C

Table 4.11 displays SOH values for different cycle counts used for the figure.

Table 4.11: SOH values for the different cycle count for Melasta, 45 °C

Cycles	5	30	55	80
SOH (%)	92.18	91.96	91.52	91.30

Notable reductions in the peaks are also observed here. The previously discussed degradation of the electrodes' structural integrity, noted in the cell tested at 25 and 35 °C, similarly impacts the cell at 45 °C, but the elevated temperature tends to accelerate the chemical reactions within the battery. This can lead to a faster decline in the efficiency of the lithium intercalation and deintercalation processes, further influencing the performance and health of the battery. Therefore, while lithium intercalation and deintercalation processes are common at several temperatures, they tend to be more efficiently and safely sustained at the lower temperature of 25 °C.

For this battery, the internal resistance increased, which could be a typical reason for the decrease in the peaks. However, the changes in the internal resistance are very minimal, so this does not necessarily have a huge impact.

Since the degradation is not very significant and the battery has been tested at a relatively high temperature, the reduction in peaks is unlikely to be due to lithium plating, as lithium plating typically occurs at lower temperatures such as 25 °C or below. Instead, this reduction may be attributed to both LAM and LLI.

Figure 4.20 shows a close-up view of the discharge peak at 3.75 V. Also here the intensity of the peak gradually decreases as the number of cycles increase, indicating potential degradation.

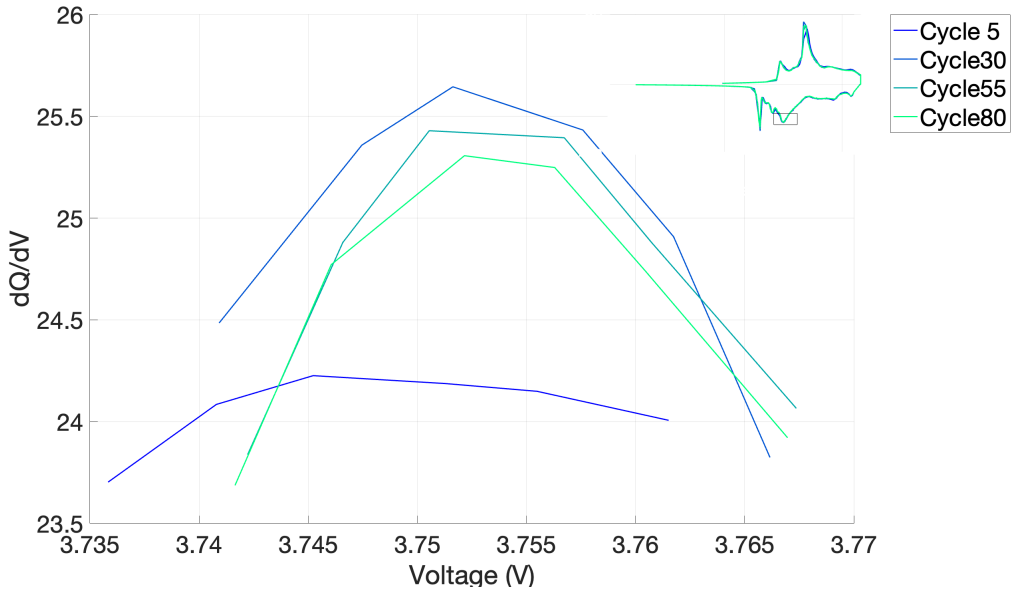

Figure 4.20: Close-up of dQ/dV discharge peak for Melasta, 45 °C

Figure 4.21 illustrates the evolution of the maximum values of the dQ/dV peaks. The graph depicts a sharp rise followed by a decline, primarily because for cycle number 5, the peak is smaller than in subsequent cycles. This unusual occurrence is likely due to an error, as a pattern emerges afterwards indicating that the peaks decrease in size as the number of cycles increases. If the decline after cycle 5 is calculated, it is approximately 2%, which is less than for both the Melasta tested at 25 °C and the Melasta tested at 35 °C. This is unexpected given that this battery has a greater reduction in SOH than the other two from Melasta, but it is anticipated that the peaks will decrease further with additional cycles.

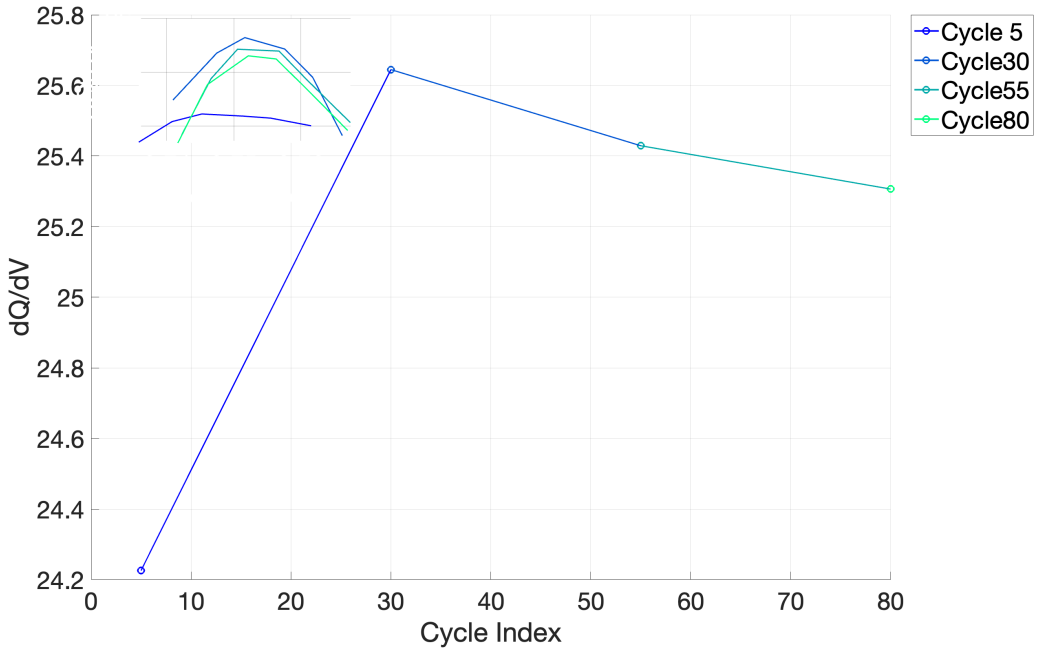

Figure 4.21: Development of the maximum dQ/dV vaules for Melasta, 45 °C

By comparing the three batteries from Melasta, it is evident that the ICA correlates with the values found during the analysis of SOH in Chapter 4.1.1 for 25 and 35 °C.

4.4.2 Grepow

In this chapter, Grepow will be analyzed across all tested temperatures, starting with 25 °C, followed by 35 °C, then 45 °C.

Figure 4.22 shows the charge and discharge characteristics of the Grepow cell at 25 °C over a range of 5 to 105 cycles, revealing the most significant decrease in SOH by 6.21%. The minor peak for the charging process occur at 4 V, while the major peak is situated at 3.8 V. For the discharge process, the minor peaks are at 3.65 V and 4 V, while the largest peak is located at 3.5 V.

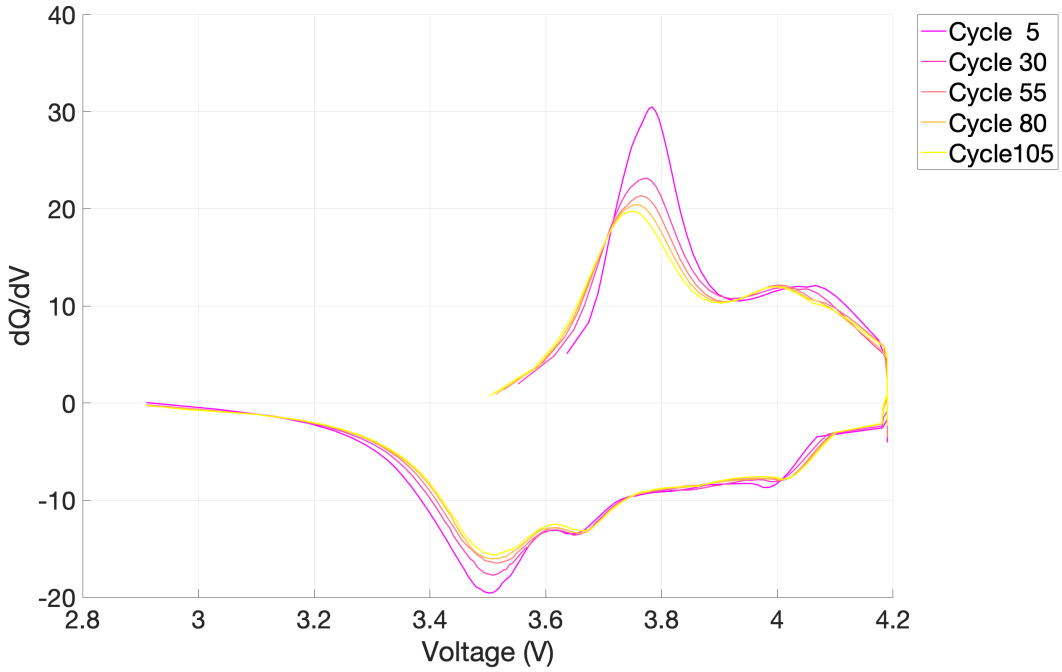

Figure 4.22: dQ/dV plot for Grepow, 25 °C

Table 4.12 presents the SOH values for the different cycles represented in the figure.

Table 4.12: SOH values for the different cycle count for Grepow, 25 °C

Cycles	5	30	55	80	105
SOH (%)	86.50	83.84	82.25	81.27	80.29

The discharge peak at 3.5 V diminishes as the number of cycles increases, indicating a loss of capacity and efficiency over the cycles. The primary reason for the significant changes in the peaks can be attributed to substantial changes in the SOH. The battery has undergone considerable degradation over just a few cycles. This degradation could also be due to factors such as LAM and LLI, similar to the Melasta cells, or because of the electrolyte composition. Over time, the electrolyte might degrade, leading to the formation of a resistive layer on the electrode surfaces, such as SEI, which could also contribute to changes in the dQ/dV profiles without an increase in the measured internal resistance.

Figure 4.23 shows a close-up view of a discharge peak at 3.5 V. As the battery degrades, the peak color changes from pink to lighter yellow.

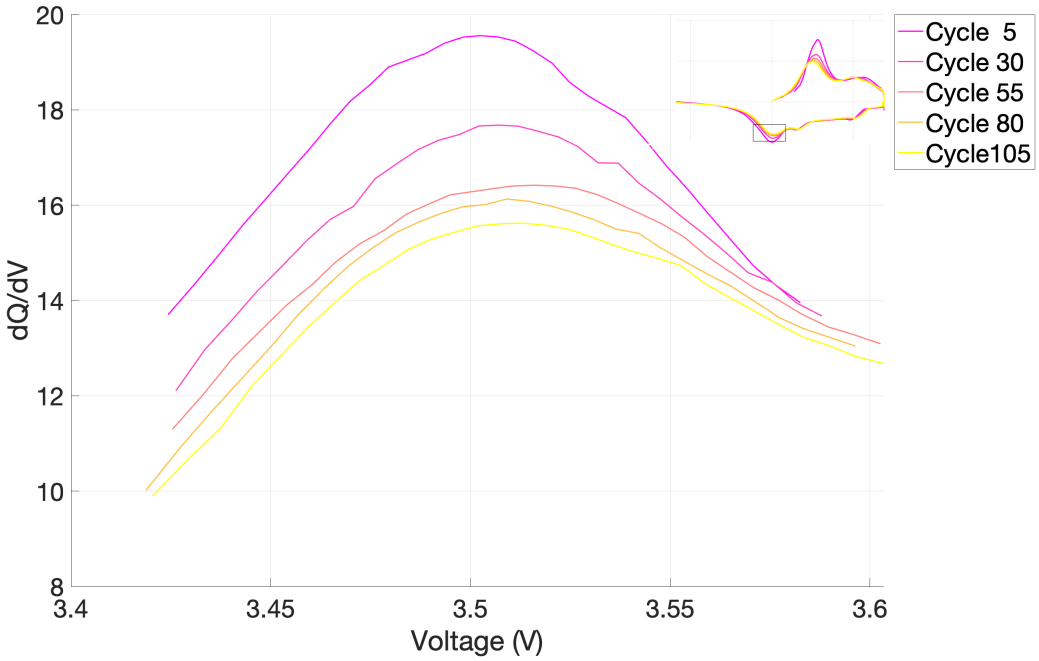

Figure 4.23: Close-up of dQ/dV discharge peak for Grepow, 25 °C

Figure 4.24 illustrates the evolution of the maximum values of the dQ/dV peaks. This figure clearly demonstrates that the peaks decrease more rapidly for this cell as the number of cycles increases. From cycle 5 to cycle 105 the decline in the peak is at approximately 15%. This is logical given that this is the battery with the highest degradation.

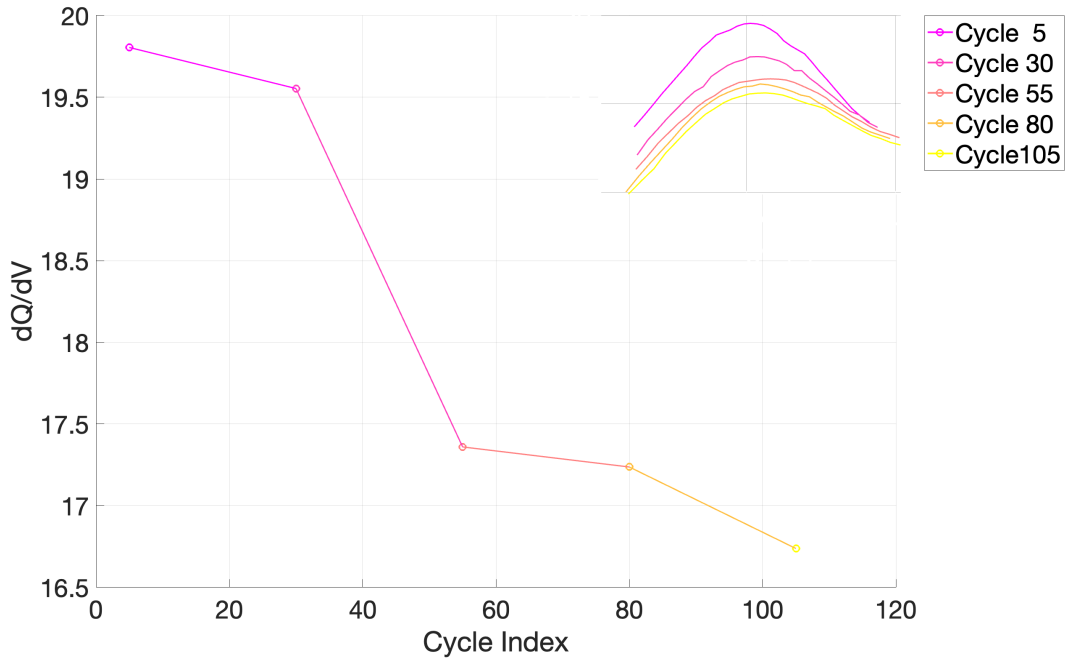

Figure 4.24: Development of the maximum dQ/dV vaules for, Grepow 25 °C

Figure 4.25 illustrates the charge and discharge characteristics of the Grepow cell at 35 °C, covering a range from 5 to 180 cycles, which corresponds to a almost negligible SOH decline of 0.36%. This battery has charge peaks at 3.7 V and 3.9 V, and the largest discharge peaks at 3.55 V and 3.72 V.

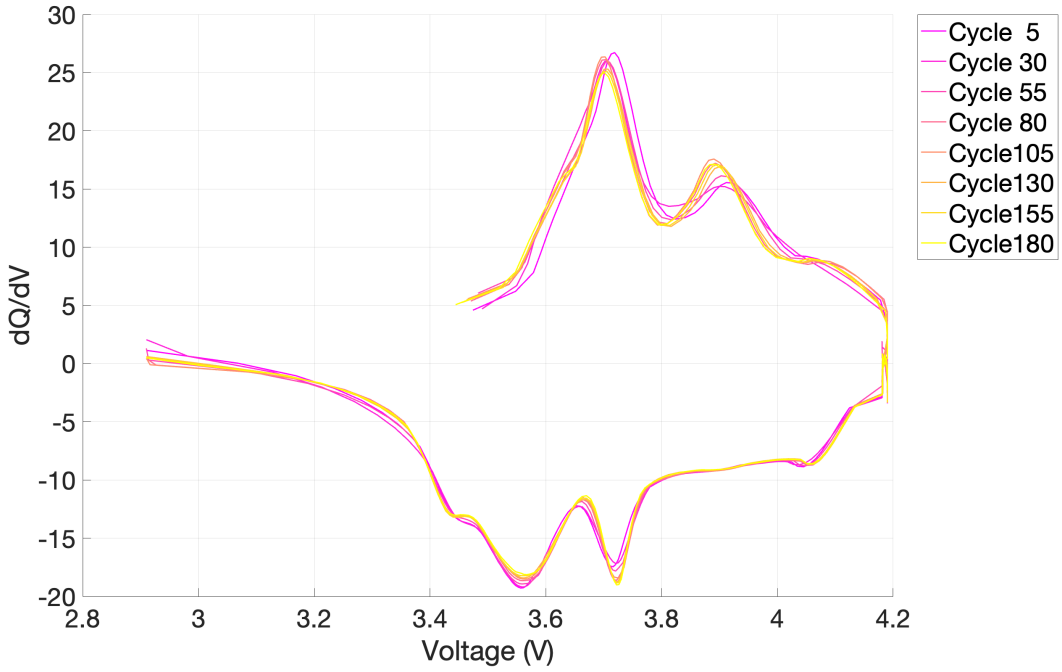

Figure 4.25: dQ/dV plot for Grepow, 35 °C

Table 4.13 displays SOH values for different cycle counts, to give a better overview.

Table 4.13: SOH values for the different cycle count for Grepow, 35 °C

Cycles	5	30	55	80	105	130	155	180
SOH (%)	90.74	91.08	90.83	90.86	90.83	90.49	90.47	90.38

Unlike the battery tested at 25°C, this cell exhibits almost no change in SOH. However, the dQ/dV curves still experiences some changes. This could be due to the non-uniform degradation of the cell, which can lead to different parts of the electrodes reaching varying OCVs at different times. This variation in OCV across the cell can lead to less distinct dQ/dV peaks because different parts of the electrode contribute differently to the overall capacity changes during cycling. This results in a broader and less pronounced peaks in the dQ/dV graph, reflecting the non-homogeneous behavior of the degradation of the cell.

Figure 4.26 provides a close-up view of the discharge peak at 3.55 V. The peak's intensity gradually decreases with increasing cycle numbers as seen for the other batteries.

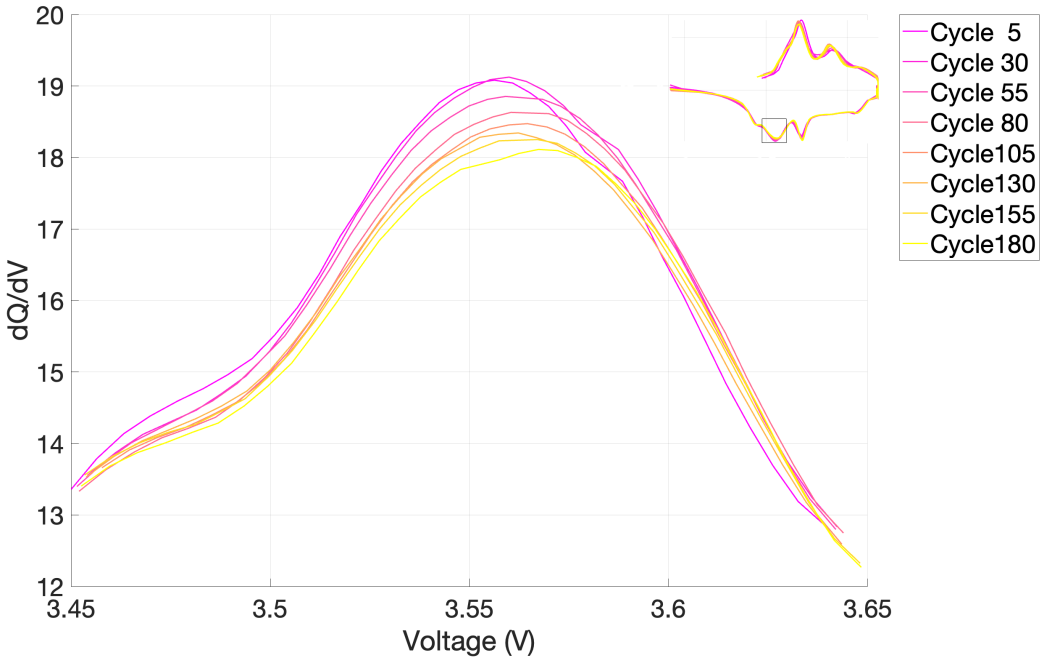

Figure 4.26: Close-up of dQ/dV discharge peak for Grepow, 35 °C

Figure 4.27 shows the changes in maximum dQ/dV values as a function of cycle count for the cell at 35 °C. The figure confirms that the peak values decrease as the number of cycles increases, but the decrease is not as evident as for the Grepow at 25 °C. The decline in the peaks from cycle 5 to cycle 180 only corresponds to about 5%.

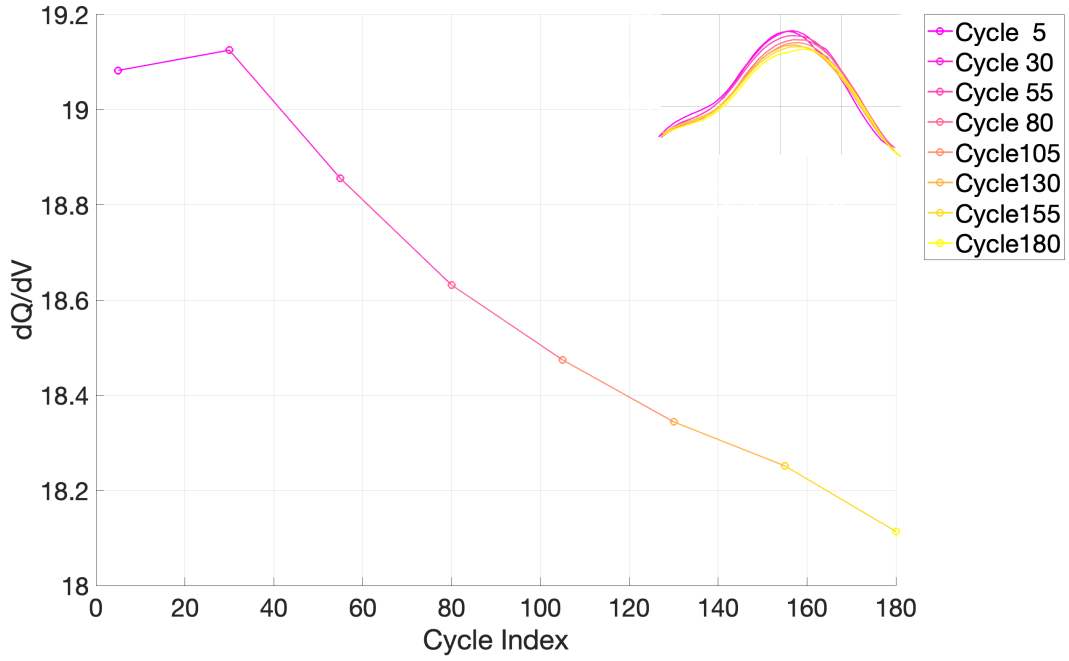

Figure 4.27: Development of the maximum dQ/dV vaules for Grepow, 35 °C

Figure 4.28 shows the charge and discharge characteristics for the Grepow cell at 45 °C over an interval ranging from 5 to 55 cycles, resulting in the minimal decrease of 0.03% in SOH. This battery exhibits only one distinct charge peak at 3.7 V. For the discharge process, there are two small peaks at 3.42 V and 3.75 V, while the largest peak is at 3.61 V.

Although the peaks occur at similar positions for all testing temperatures for Grepow, there are subtle differences among the batteries here as well, possibly because of individual variations between the batteries and the diverse testing temperatures.

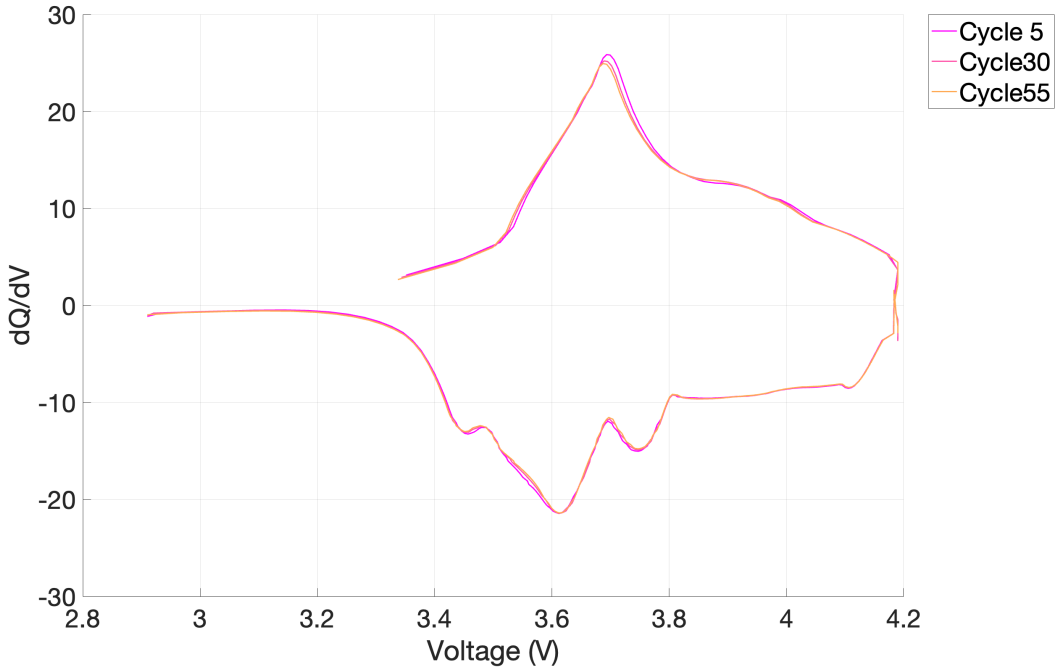

Figure 4.28: dQ/dV plot for Grepow, 45 °C

Table 4.14 displays SOH values for different cycle counts.

Table 4.14: SOH values for the different cycle count for Grepow, 45 °C

Cycles	5	30	55
SOH (%)	92.61	92.67	92.58

Similar to the battery tested at 35 °C, this battery exhibits almost no change in SOH. This stability is also evident in the dQ/dV curves, where the peaks change minimally compared to the battery tested at 25 and 35 °C.

Figure 4.29 provides a close-up view of the discharge peak at 3.61 V. As the figure shows, there is almost no change in the peaks. However, there are only peaks available for three cycles for comparison, which might explain the lack of significant changes and the difficulty in identifying

any trends. In this case as well, extending the testing period would have been beneficial to potentially uncover more pronounced changes and trends.

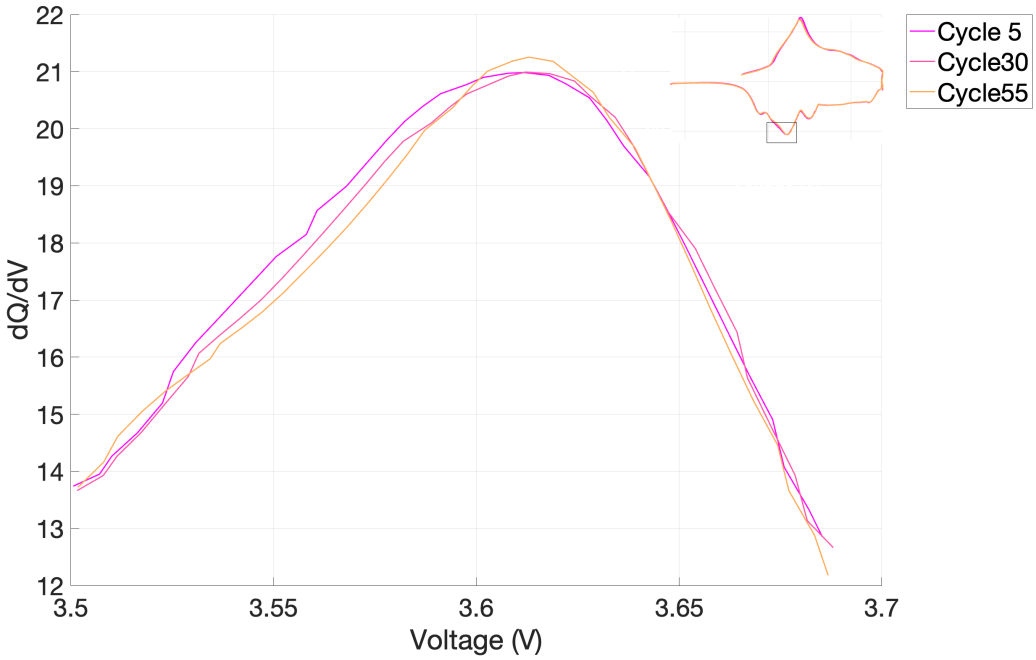

Figure 4.29: Close-up of dQ/dV discharge peak for Grepow, 45 °C

Figure 4.30 illustrates the evolution of the maximum values of the dQ/dV peaks. As previously mentioned, with only three cycles available for comparison, it is not possible to discern any clear trend. Additionally, the y-axis values indicate very minor changes, which again could be due to the short testing period for the battery. Extending the testing duration might reveal more notable changes and clearer trends. By solely examining this segment of the cycling process, it appears that the peaks are increasing rather than decreasing, but by comparing this with the graph for the Grepow at 35 °C and the Melasta at 45 °C, where the peaks initially rises before declining, it is reasonable to assume that the trend will eventually show a decrease for this battery as well.

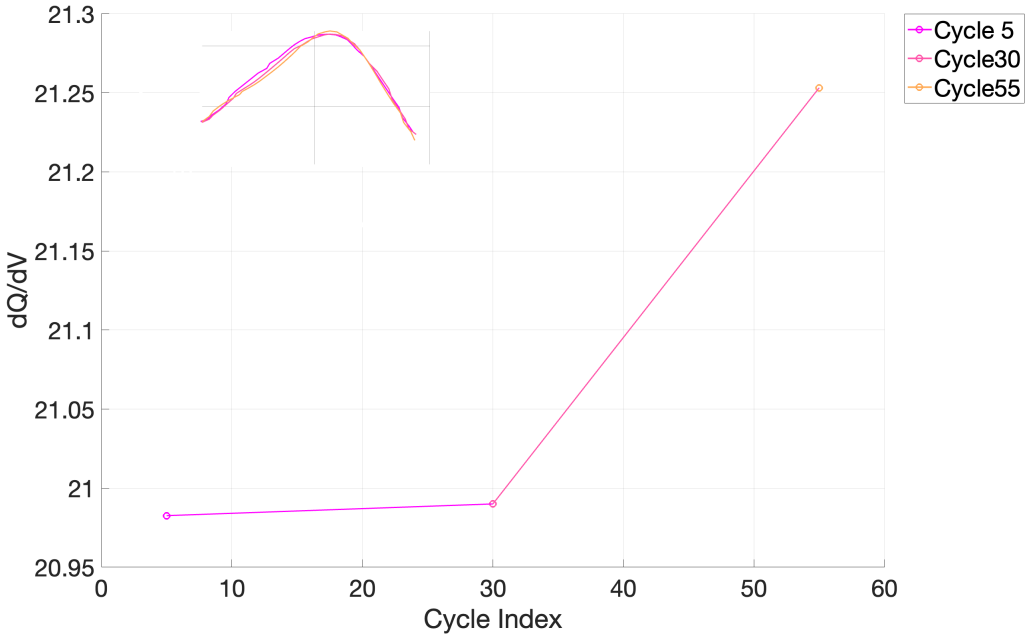

Figure 4.30: Development of the maximum dQ/dV vaules for Grepow, 45 °C

4.5 Comparison Between the Melasta and Grepow Batteries

To determine the optimal battery choice for Revolve NTNU, this chapter will undertake a comparative analysis of the two tested batteries based on the evaluated factors.

4.5.1 State of Health

When it comes to SOH, Melasta displays a more typical battery degradation pattern, where the degradation increases with the temperature. However, the results for Grepow are somewhat different than expected. The battery at 25 °C has degraded the most, but as previously discussed, this may be due to an error. The batteries at 35 and 45 °C for Grepow show almost no change in SOH. Based on these findings, Grepow appears to perform better in terms of the unchanged SOH values, but Melasta may still be preferable because it demonstrates the expected degradation pattern. Nonetheless, since the batteries were not tested for a enough length of time, there is partially limited basis for settling on this choice.

4.5.2 Internal Resistance

It is somewhat challenging to determine the best battery choice based solely on internal resistance, as it does not provide a comprehensive insight into degradation, but rather assists in understanding its correlation with changes in SOH. From the data, Melasta stands out with the lowest overall internal resistance, particularly the Melasta tested at 45 °C, which maintained an

internal resistance of around 2 milliohms throughout the testing. The battery with the poorest performance in this analysis is the Grepow at 25 °C, exhibiting the highest recorded internal resistance at almost 10 milliohms, but as previously mentioned, there are likely issues with this battery.

However, comparing internal resistance solely for degradation purposes seems somewhat pointless, given the minimal changes observed over the short testing period for most batteries, coupled with suboptimal data measurements in many instances and the absence of relation to the graphs for SOH.

4.5.3 Incremental Capacity Analysis

In the analysis of the batteries based on IC, the results mostly reflect the SOH results. Specifically, the battery that exhibit the most change in SOH, such as Grepow at 25 °C, also show the most notable changes in the dQ/dV graphs. The changes observed in all the graphs are relatively minor, as the batteries were not tested over many cycles. Particularly, the batteries tested at 45 °C underwent very few cycles, resulting in further minimal alterations in the graphs. Extending the testing duration would have been optimal for obtaining more pronounced results.

As discussed in Chapter 3.3.4, each battery chemistry typically presents a unique IC curve, characterized by distinctive patterns of peaks and valleys. It is evident that there is a difference between the peaks of the battery types, with Melasta's peaks being sharper and Grepow's more rounded. Variations in cell design, such as size of the cell, electrode thickness, or the type of separator used, can significantly contribute to differences in the sharpness of the dQ/dV curve peaks. Due to cell variations, the SOC can vary locally because different parts of the cell reach the peak at different times. This variation in SOC distribution can result in non-uniform current distributions, leading to less sharp and precise peaks.

4.6 Visual Inspection

The results indicated minimal degradation overall across all temperatures. To reinforce this finding, one battery from Melasta and one from Grepow were selected for visual inspection, both cycled at 35 °C. To look at the cells visually is important because, while numerical data and graphs provide valuable insights into battery degradation, direct visual inspection can offer further insights and confirmation of any degradation signs not necessarily reflected entirely in the numerical data. This may include physical changes such as cracks, delamination, or other visible signs of degradation. Therefore, a combination of numerical data and visual inspection provides a more comprehensive understanding of the battery's condition and degradation patterns.

4.6.1 Melasta

After opening and separating all the electrode layers inside the Melasta cell, it was observed that the battery contained 44 anode layers and 43 cathode layers. The uneven ammount of electrodes is normal, as stated in Chapter 2.1.6. Figure 4.31 illustrates the anode and cathode layers from this cell. The anode layers are recognizable by their copper tabs, while the cathode layers have aluminum tabs.

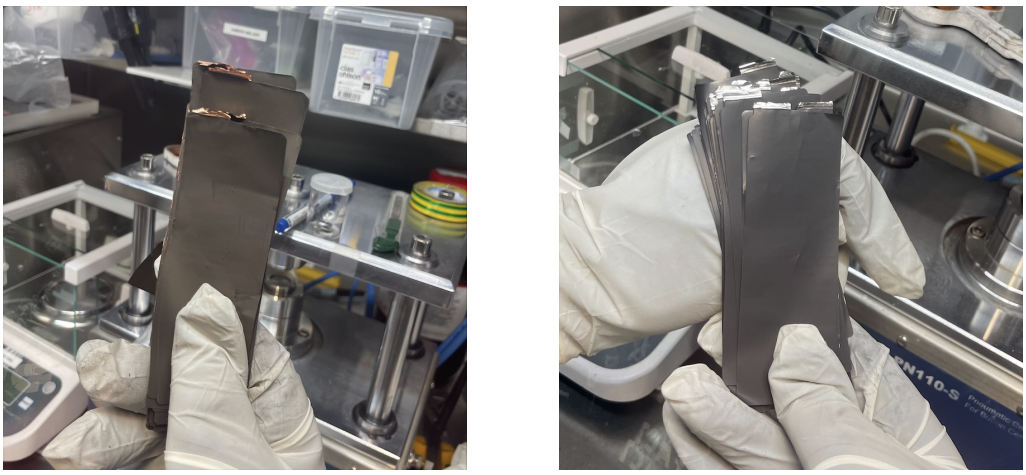

Figure 4.31: The anode layers (left) and cathode layers (right) for a Melasta cell

There are no significant signs of degradation on the inner electrodes, neither on the anodes nor the cathodes. This aligns very well with the numerical data and graphs presented earlier. Apart from some minor color changes, the electrodes appear almost as good as new.

However, a clear indication of the cycling effects is observable on the outermost anode layer, as shown in Figure 4.32. It is possible to see some shifts in the color, a few cracks in the slurry mix coated on the electrode, including an overall more worn surface than on the inside layers.

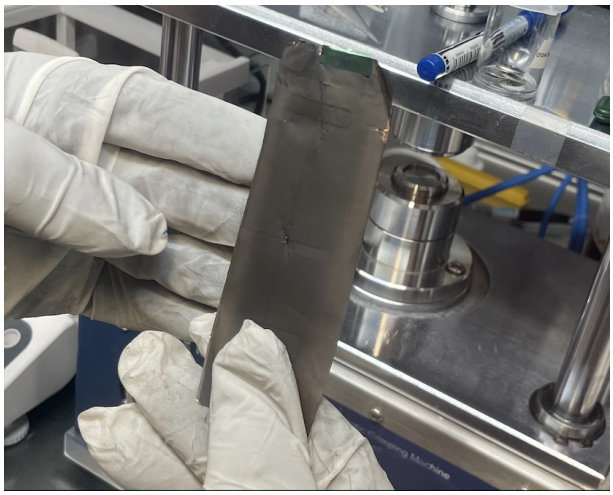

Figure 4.32: A few visual signs of degradation on the outer anode layer of the Melasta cell

4.6.2 Grepow

Figure 4.33 illustrates the anode and cathode layers of one of the Grepow cells. This battery contains 50 anode layers and 48 cathode layers.

Figure 4.33: The anode layers (left) and cathode layers (right) for a Grepow cell

Here, very similar trends to those of the Melasta cell can be observed. The internal electrode layers have held up well throughout the cycling process, and it is challenging to identify any significant signs of degradation, apart from minor changes in coloration. This observation further supports the previous findings, indicating minimal degradation for this battery.

Figure 4.34 shows the external anode of the battery, and like for Melasta, this layer of the Grepow battery has degraded the most. As the figure indicates, there are several signs of degradation. Compared to the inside layers, the external anode shows variations in shade, which may indicate oxidation or other chemical reactions, like dendrite growth, which are small metallic formations, that can form during charging and discharging. There are also signs of coating buildup, a few cracks in the slurry mix here as well, and the surface has become slightly rougher overall.

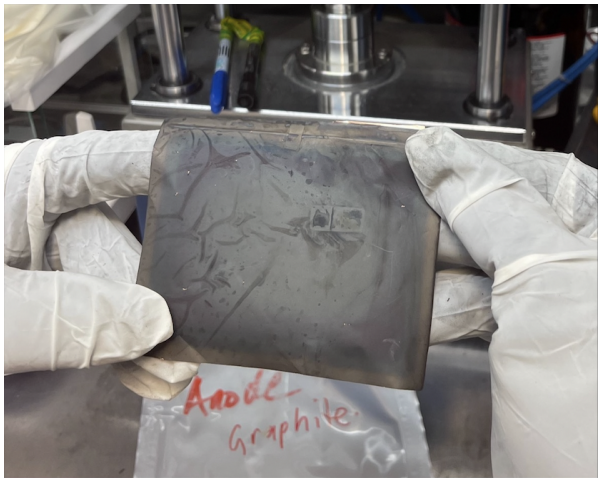

Figure 4.34: More visual signs of degradation on the outer anode layer of the Grepow cell

The anode seems to degrade faster than the cathode for both batteries. This can be due to the anode being the electrode where oxidation occurs, which involves a chemical reaction that leads to the loss of electrons. The anode is also made of materials that are more reactive than the cathode material, contributing to a faster degradation happening at the anode.

4.7 Error Analysis and Validity Considerations

This period was certainly not devoid of mistakes, and sources of error were identified both before, during, and after testing. Constraints, such as limited time and resources, including a shortage of chambers, also led to a reduction in data availability and accuracy. Consequently, there was a big focus on making the most of the available data.

4.7.1 Prior to Testing

A significant initial source of error, occurring even before the testing process commenced, was that the batteries had been stored in a container outside for several years. The Melasta batteries had been stored since 2020, and the Grepow batteries had been stored since 2023. As noted, this suggests that calendar aging may have contributed to the degradation. Long-term storage under unfavorable conditions can cause the battery's capacity to decrease. The batteries have likely decreased in capacity by a couple of percent while being in the container. This is likely the case for Grepow tested at 25 °C, as it has a low initial SOH value, and declines at a faster rate compared to the other batteries.

Additionally, they may have been exposed to various environmental factors such as temperature fluctuations, humidity, and sunlight exposure. These conditions can also lead to degradation of the batteries in several ways. All batteries experience some degree of self-discharge over time, but this can accelerate under poor storage conditions. Self-discharge can result in reduced battery capacity, affecting the performance.

4.7.2 During Testing

Throughout the testing phase, constraints were encountered due to limited time and resources, including a shortage of chambers. This resulted in a lack of data and less accuracy in the data. The plan to test multiple temperatures and C-rates was, as mentioned, most affected by this. The absence of diversity is detrimental for several reasons. Firstly, a narrow range of temperatures and C-rates fails to capture the full spectrum of real-world operating conditions, potentially leading to incomplete conclusions about the battery's performance and degradation behavior. Additionally, excluding certain temperatures and C-rates regimes may overlook critical insights

into temperature-dependent and C-rate-dependent degradation mechanisms. Furthermore, without sufficient variation, it becomes challenging to extrapolate model predictions accurately to different environmental conditions, limiting the model's practical applicability. As a result, there was a huge focus on maximizing the utility of the available data, emphasizing "quality over quantity".

Numerous batteries of the same type were tested at the same temperature to ensure the collection of good data, with one being selected for analysis due to its optimal data quality. For Grepow at 25 °C, the testing was limited to a single test cell, so all the results had to rely on the available data from this battery. Consequently, it is possible that this specific battery was defective, leading to uncharacteristic results and exhibiting unusually fast degradation compared to the other batteries.

The temperature sensor must be securely taped to prevent it from detaching, especially at high temperatures where it is easily exposed to detachment. During the initial testing phase, the temperature sensor for some batteries detached, which subsequently impacted the accuracy of the test results. When applying the Arrhenius equation and plotting the graphs, the calculations relied on accurate battery temperature readings. Therefore, data from batteries where the temperature sensors had detached could not be used for these calculations.

4.7.3 Calculations

When calculating the SOH values of a battery in MATLAB, the actual capacity is divided by the initial capacity. Since an 80% SOC window is used, the initial capacity should be adjusted by multiplying it by this SOC window to reflect the accurate initial capacity. However, including the SOC window in the calculation distorts the SOH values on the y-axis. Multiplying the initial capacity by an 80% SOC window leads to the SOH values significantly exceeding 100%, which may not be accurate. If the SOH values exceed 100%, it could be due to an error in the calculation or measurement method. This might occur if the initial capacity is underestimated, the actual capacity is overestimated, or if the methods used to measure or calculate capacity are incorrect. Therefore, it has been decided not to apply the SOC window to the initial capacity data for the SOH graphs in order to make them more valuable.

When testing the batteries, both the Melasta and Grepow at 35 °C, experienced an error in the data collection. To get enough data from the testing, the program was initially set to sample data every fifth milliseconds during the HPPC pulses. However, for these batteries, the testing program was set to sample data every fifth seconds by a mistake. Due to the lack of frequent data collected to accurately capture the full pulse, the HPPC pulses were affected to appear

as triangles instead of squares. An example of two utilized pulses used to find the internal resistance, are shown in Figure 4.35 and 4.36. This issue also occurred at the start of testing the batteries at 45 °C, but it was corrected once the error was discovered.

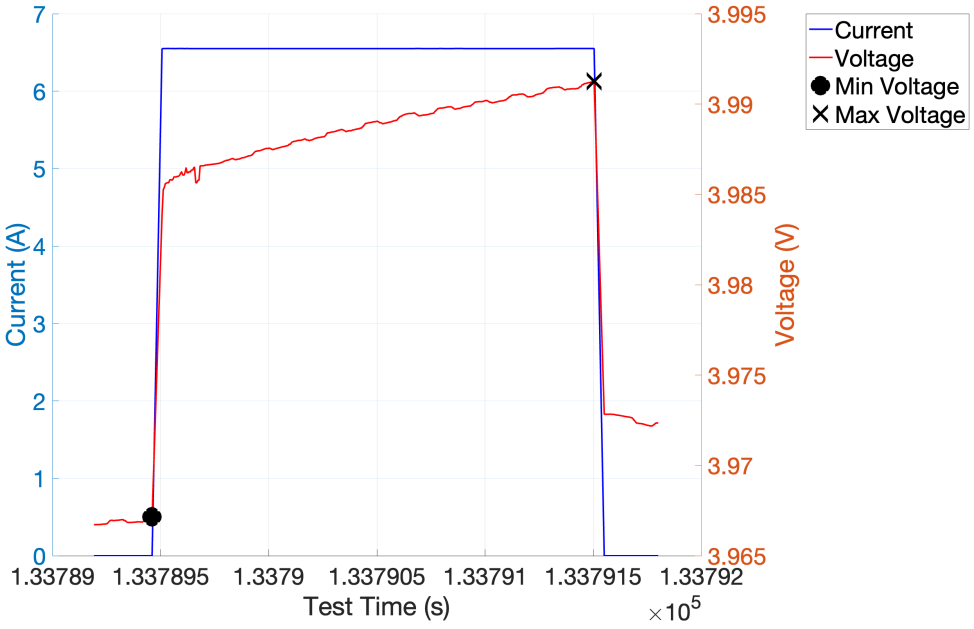

Figure 4.35: A normal square shaped charge current pulse

To calculate the internal resistance for the correct square shaped current pulses in Figure 4.35, Equation 3.1 from Chapter 3.3.3 was utilized. This is accomplished by dividing the voltage difference, as indicated by the black cross and circle in the figure, by the current difference. In this case, the current difference is the highest value, approximately 6.5 A subtracted from 0.

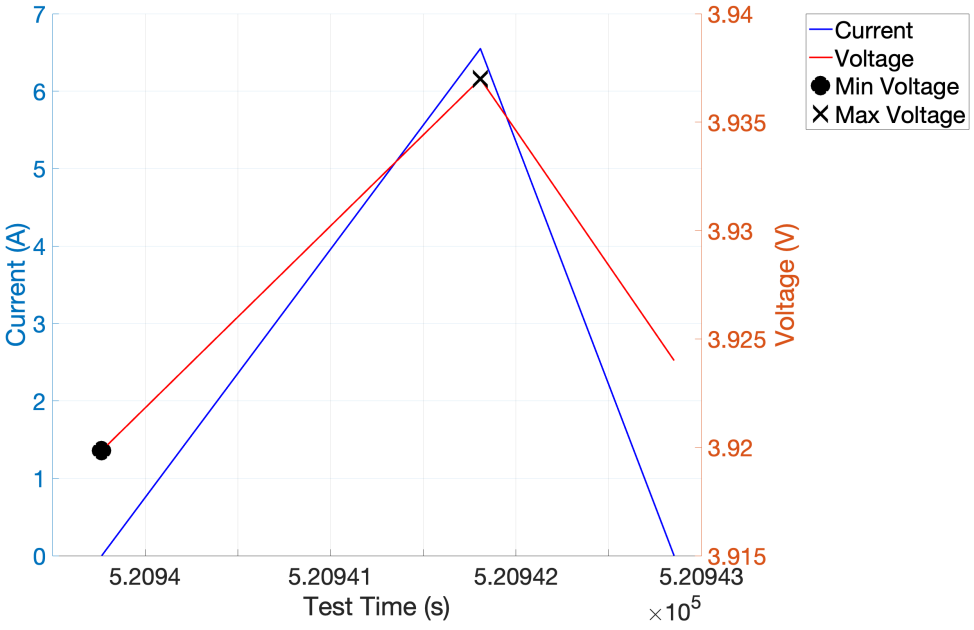

Figure 4.36: Triangle shaped charge current pulse

The procedure for finding the internal resistance is the same for the triangular pulse in Figure 4.36, by taking the max voltage minus the min voltage and dividing this by the current difference. The issue for this pulse occurs as the point representing the maximum voltage is an uncertain peak. Analysing the square pulse, it is evident that the voltage rises throughout. However, since data points were only sampled every fifth seconds, it is uncertain whether the triangular pulse has hit the true peak or a lower voltage value along the line within the pulse. Therefore, using Equation 3.1 will not find the true internal resistance, but rather an approximate value. The difference between internal resistance and the approximate value is not significant, but consequently, when calculating internal resistance based on the triangular pulses, the results were less accurate compared to using data that captures the full squared pulses.

This could explain the increase in internal resistance observed when correcting the pulse shape for the Melasta battery tested at 45°C, as shown in Figure 4.9. The first cycles had triangular pulses, while the later ones had square shaped pulses, leading to a possible lower voltage value found for the triangular pulse. This could result in the calculation of a lower internal resistance for the triangular pulses, which reflects what is observed in the plot.

The irregularities in data collection of the pulses also affected the correlation in SOC window between the different batteries when internal resistance was plotted. It is notable that the batteries at different temperatures have various SOC windows, with some extending from 10% to 80% and others from 20% to 90%, not aligning with the predicted SOC window presented in Table 3.6. This issue likely occurred when the pulse error was corrected, leading to the aberration in values.

4.8 Environmental and Economic Analysis

Evaluating the environmental and economic impacts is essential when assessing a battery's performance and sustainability. The two battery types presented in this study, LCO and NMC, are both environmentally and economically viable, as LIBs in general are sustainable. However, the production of batteries is not completely free from emissions.

NMC batteries offer advantages such as lower GHGs emissions under the material production, as mentioned in Chapter 2.4, and extended lifespan compared to cobalt-based counterparts. LCO batteries are constrained by their shorter longevity and the relatively high cost of cobalt. High-cost batteries with limited durability tend to lack economic efficiency. However, LCO batteries excel in specific energy and energy density, enabling sustained power delivery over prolonged periods, particularly in low-load scenarios.

Throughout the results section, it has also been observed that temperature influences the lifespan of the batteries. Therefore, by cycling the batteries at a lower temperature resulting in extending its lifespan, one can have a positive impact on both the environmental and economic aspects.

A battery with a longer operational lifespan represents the most advantageous option, both from an environmental and economic perspective. Longer-lasting batteries mean fewer replacements over time, which not only conserves resources, but also minimizes waste and pollution associated with battery production, distribution, and disposal. When selecting a battery for optimal performance in a race car, particularly under high-load scenarios, Grepow may emerge as the top choice. This is supported by the theory outlined in Chapter 2.4, indicating that NMC batteries are both safer and offer longer lifespans overall. Furthermore, the results, found in Chapter 4.1.2, suggest minimal degradation of the battery under two out of three temperature conditions. Economically, this longevity reduces the total cost of ownership by spreading the initial investment over a more extended period and decreasing the frequency of replacement purchases. Therefore, it would be economically advantageous to choose the battery that has the longest lifespan and degrades the least.

However, for both batteries, the environmental and economic impact extend beyond manufacturing and usage. It is essential to also ensure the proper disposal and recycling of LIBs to minimize environmental damage.

The factors discussed suggest that the NMC battery, Grepow, is the better option compared to the LCO battery, Melasta, but it is essential to strike a balance between performance demand and environmental impact when selecting the optimal battery alternative for the car.

5 Conclusion

Throughout this thesis, simplifications have been made, and it is important to emphasize that degradation is a very complex process influenced by many factors. In conclusion, the batteries analyzed in this thesis have not displayed significant degradation. This study specifically investigated the impact of temperature on degradation by testing the batteries at 25, 35, and 45 °C.

The problem formulation indicated that this thesis would explore how various factors contribute to degradation, but as mentioned in both the test methodology and discussion sections, in Chapter 3 and Chapter 4, there was insufficient time and resources to investigate how C-rates affect degradation, which was the original plan. The task given was somewhat unrealistic considering the time and resources available to complete it. Therefore, it would be optimal to conduct longer-term testing as discussed in further work, in Chapter 6.

When comparing the two batteries there are, as discussed, advantages and disadvantages to each. Melasta shows results that follow a more typical degradation pattern, with the degradation increasing with the increase of the temperature, making it a more predictable choice, whereas Grepow at 35 and 45 °C demonstrates almost no change in SOH values. This also correlates with the ICA, displaying an increase in degradation at higher temperatures. Based solely on this, Grepow would be the better choice regarding the lifespan of these batteries.

The internal resistance has changed only slightly, decreasing marginally, which could also be due to the fact that the testing period too short. Since the internal resistance hardly provides any significant data to analyze, it does not show a correlation with the batteries' degradation.

Choosing the battery that offers the longest lifespan and minimal degradation would be most sustainable. This selection could positively influence the identification of the option that provides optimal performance, durability, and environmental sustainability for Revolve NTNU, particularly in relation to UN Sustainable Development Goal number 9. All testing conducted in this thesis contributes to advancing sustainability by investigating how temperature affects battery degradation.

6 Further Work

This thesis demonstrated that temperature is a primary factor influencing battery degradation. Conversely, the exact impact of temperature on performance remained somewhat unclear due to limited resources. To explore this further, it is recommended to conduct additional cycles on more cells, starting at multiple different temperatures. This approach could help analyze how the batteries will degrade over a much wider range of temperatures and for a longer period, aiming for at least 1000 cycles. By doing this, a much larger difference between the various temperatures is expected to be observed, compared to what has been observed so far.

For future studies, it is also recommended to examine the impact of various C-rates on battery degradation. Given that C-rates are a crucial factor in degradation, further exploration is compelling if there had been more time. Extending the research to include more cycles would enhance the understanding of the progressive changes in the battery over time. Conducting such extensive testing could provide crucial insights, facilitating the optimization of battery longevity and efficiency.

If the battery testing period were extended, there would also be an opportunity to conduct a more thorough investigation of internal resistance. Currently, the changes in internal resistance are minimal, and in most cases, it has even slightly decreased. However, with prolonged testing, it is likely that the internal resistance would increase as the battery degrades more. Extending the duration of the tests could provide more conclusive data on how internal resistance evolves over time.

When it comes to the IC curves, it would also have been optimal to examine the dV/dQ curves, as well as dQ/dV curves, for all batteries in order to investigate LAM and LLI more comprehensively. As mentioned in Chapter 2.3.6 in the theory, it is more typical to observe LLI in the changes within a dV/dQ curve.

It would also be possible to investigate and analyse more noticeable visual changes within the battery for a more detailed examination of how the physical changes correlate with battery performance and degradation. Over a longer duration, one could closely observe and measure alterations such as increased thickness and more extensive damage on the electrodes, not just the external anode. This can provide deeper insights into the long-term effects of operational stress and environmental conditions on battery health.

References

[1] Ashraf Said Ahmad AlMadhoun. "Ohm's Law". In: *Circuit Design and Simulation Quick Start Guide: Create Schematics and Layout Electronic Components*. Springer, 2023, pp. 91–95.

[2] Seong Jin An et al. "The state of understanding of the lithium-ion-battery graphite solid electrolyte interphase (SEI) and its relationship to formation cycling". In: *Carbon* 105 (2016), pp. 52–76. ISSN: 0008-6223. URL: https://www.sciencedirect.com/science/article/pii/S0008622316302676.

[3] Arbin. *Auxiliary Modules*. URL: https://www.arbin.com/auxiliary-modules/#measurement-auxiliaries.

[4] Arbin. *Laboratory Battery Testing System For Cell Applications*. URL: https://www.arbin.com/wp-content/uploads/2022/06/LBT_Cell-Testing_rev04.pdf.

[5] Pankaj Arora and Zhengming Zhang. "Battery separators". In: *Chemical reviews* 104.10 (2004), pp. 4419–4462.

[6] Faiza Arshad et al. "Life cycle assessment of lithium-ion batteries: a critical review". In: *Resources, Conservation and Recycling* 180 (2022), p. 106164.

[7] Anup Barai et al. "A study of the influence of measurement timescale on internal resistance characterisation methodologies for lithium-ion cells". In: *Scientific reports* 8.1 (2018), p. 21.

[8] Anthony Barré et al. "A review on lithium-ion battery ageing mechanisms and estimations for automotive applications". In: *Journal of Power Sources* 241 (2013), pp. 680–689.

[9] Anand Bhatt, Guoxiu Wang, and Ray Withers. *Lithium-ion batteries*. 2016. URL: https://www.science.org.au/curious/technology-future/lithium-ion-batteries (visited on 04/03/2024).

[10] Tadeusz Białoń et al. "HPPC Test Methodology Using LFP Battery Cell Identification Tests as an Example". In: *Energies* 16.17 (2023), p. 6239.

[11] Christoph Birkl et al. "Degradation diagnostics for lithium ion cells". In: *Journal of Power Sources* 341 (Feb. 2017), pp. 373–386.

[12] George E Blomgren. "The development and future of lithium ion batteries". In: *Journal of The Electrochemical Society* 164.1 (2016), A5019.

[13] Wen-Yeau Chang. "The state of charge estimating methods for battery: A review". In: *International Scholarly Research Notices* 2013 (2013).

[14] Xin-Bing Cheng et al. "A perspective on sustainable energy materials for lithium batteries". In: *SusMat* 1.1 (2021), pp. 38–50.

[15] Soo Seok Choi and Hong S Lim. "Factors that affect cycle-life and possible degradation mechanisms of a Li-ion cell based on LiCoO2". In: *Journal of Power Sources* 111.1 (2002), pp. 130–136. URL: https://www.sciencedirect.com/science/article/pii/S0378775302003051.

[16] Ryan Collin et al. "Advanced Electric Vehicle Fast-Charging Technologies". In: *Energies* 12 (May 2019), p. 1839.

[17] Claus Daniel et al. "Cathode materials review". In: *AIP Conference Proceedings*. Vol. 1597. 1. American Institute of Physics. 2014, pp. 26–43.

[18] Statista Research Department. *Projected global battery demand from 2020 to 2030, by application*. 2023. URL: https://www.statista.com/statistics/1103218/global-battery-demand-forecast/ (visited on 04/03/2024).

[19] Susanne Dörfler et al. "Challenges and key parameters of lithium-sulfur batteries on pouch cell level". In: *Joule* 4.3 (2020), pp. 539–554.

[20] Robert L Fares and Michael E Webber. "What are the tradeoffs between battery energy storage cycle life and calendar life in the energy arbitrage application?" In: *Journal of Energy Storage* 16 (2018), pp. 37–45.

[21] Yang Gao et al. "Lithium-ion battery aging mechanisms and life model under different charging stresses". In: *Journal of Power Sources* 356 (2017), pp. 103–114. ISSN: 0378-7753. URL: https://www.sciencedirect.com/science/article/pii/S0378775317305876.

[22] Xuebing Han et al. "A review on the key issues of the lithium ion battery degradation among the whole life cycle". In: *ETransportation* 1 (2019), p. 100005.

[23] Mohammad A Hannan et al. "A review of lithium-ion battery state of charge estimation and management system in electric vehicle applications: Challenges and recommendations". In: *Renewable and Sustainable Energy Reviews* 78 (2017), pp. 834–854.

[24] *Inertgas Technology*. M. Braun. Jan. 2023.

[25] T Richard Jow et al. "Factors limiting Li+ charge transfer kinetics in Li-ion batteries". In: *Journal of the electrochemical society* 165.2 (2018), A361.

[26] Reiner Korthauer. *Lithium-Ion Batteries: Basics and Applications*. Springer, 2018, p. 17.

[27] L. Krause et al. "Surface Area Increase of Silicon Alloys in Li-Ion Full Cells Measured by Isothermal Heat Flow Calorimetry". In: *Journal of The Electrochemical Society* 164 (Aug. 2017), A2277–A2282.

[28] Amelie Krupp et al. "Incremental capacity analysis as a state of health estimation method for lithium-ion battery modules with series-connected cells". In: *Batteries* 7.1 (2020), p. 2.

[29] Abhishek Kumar and Nirmal Kumar Roy. "Study and modeling of internal resistance of Li-Ion battery with change in temperature & SoC". In: *2022 International Conference on Smart and Sustainable Technologies in Energy and Power Sectors (SSTEPS)*. IEEE. 2022, pp. 43–46.

[30] Soon-Jong Kwon et al. "Performance and life degradation characteristics analysis of NCM LIB for BESS". In: *Electronics* 7.12 (2018), p. 406.

[31] Feng Leng, Cher Ming Tan, and Michael Pecht. "Effect of temperature on the aging rate of Li ion battery operating above room temperature". In: *Scientific reports* 5.1 (2015), p. 12967.

[32] Guoxing Li. "Regulating mass transport behavior for high-performance lithium metal batteries and fast-charging lithium-ion batteries". In: *Advanced Energy Materials* 11.7 (2021), p. 2002891.

[33] Christian Helledal MacDonald Colin Ringdalen; Trandem. "Impact of Cooling Methods on Ageing in Lithium-Ion Battery Cells". In: (2021), p. 157.

[34] Witold Maranda. "Capacity Degradation of Lead-acid Batteries Under Variable-depth Cycling Operation in Photovoltaic System". In: June 2015.

[35] Rotem Marom et al. "A review of advanced and practical lithium battery materials". In: *J. Mater. Chem.* 21 (27 2011), pp. 9938–9954. URL: http://dx.doi.org/10.1039/C0JM04225K.

[36] Lívia Salles Martins et al. "Electric car battery: An overview on global demand, recycling and future approaches towards sustainability". In: *Journal of environmental management* 295 (2021), p. 113091.

[37] Fazel Mohammadi and Mehrdad Saif. "A comprehensive overview of electric vehicle batteries market". In: *e-Prime-Advances in Electrical Engineering, Electronics and Energy* 3 (2023), p. 100127.

[38] Kirill Murashko, Juha Pyrhönen, and Lasse Laurila. "Three-dimensional thermal model of a lithium ion battery for hybrid mobile working machines: Determination of the model parameters in a pouch cell". In: *IEEE Transactions on Energy Conversion* 28.2 (2013), pp. 335–343.

[39] Abdilbari Shifa Mussa et al. "Fast-charging to a partial state of charge in lithium-ion batteries: A comparative ageing study". In: *Journal of Energy Storage* 13 (2017), pp. 325–333.

[40] United Nations. *What are the Sustainable Development Goals?* 2024. URL: https://www.undp.org/sustainable-development-goals (visited on 02/01/2024).

[41] Mengyun Nie and Brett L Lucht. “Role of lithium salt on solid electrolyte interface (SEI) formation and structure in lithium ion batteries”. In: *Journal of the Electrochemical Society* 161.6 (2014), A1001.

[42] Naoki Nitta et al. “Li-ion battery materials: present and future”. In: *Materials today* 18.5 (2015), pp. 252–264.

[43] B Pattipati et al. “Open circuit voltage characterization of lithium-ion batteries”. In: *Journal of Power Sources* 269 (2014), pp. 317–333.

[44] E. Peled et al. “Effect of carbon substrate on SEI composition and morphology”. In: *Electrochimica Acta* 50.2 (2004). Polymer Batteries and Fuel Cells:Selection of Papers from First International Conference, pp. 391–395. ISSN: 0013-4686. URL: https://www.sciencedirect.com/science/article/pii/S0013468604006498.

[45] Mathias Petzl, Michael Kasper, and Michael A Danzer. “Lithium plating in a commercial lithium-ion battery–A low-temperature aging study”. In: *Journal of power sources* 275 (2015), pp. 799–807.

[46] Andreas Podias et al. “Sustainability assessment of second use applications of automotive batteries: Ageing of Li-ion battery cells in automotive and grid-scale applications”. In: *World electric vehicle journal* 9.2 (2018), p. 24.

[47] Veerapandian Ponnuchamy, Stefano Mossa, and Ioannis Skarmoutsos. “Solvent and salt effect on lithium ion solvation and contact ion pair formation in organic carbonates: a quantum chemical perspective”. In: *The Journal of Physical Chemistry C* 122.45 (2018), pp. 25930–25939.

[48] ACS publications. “Nonaqueous Liquid Electrolytes for Lithium-Based Rechargeable Batteries”. In: (2004). URL: https://pubs.acs.org/doi/10.1021/cr030203g.

[49] Ataur Rahman, Rafia Afroz, and Mohd Safrin. “Recycling and disposal of lithium battery: Economic and environmental approach”. In: *IIUM Engineering Journal* 18.2 (2017), pp. 238–252.

[50] Revolve. *Revolve: About us*. URL: https://www.revolve.no/about-us (visited on 01/02/2024).

[51] Dirk U Sauer et al. “State of Charge–What do we really speak about”. In: *The 21st international telecommunications energy conference*. 1999, pp. 6–9.

[52] Bruno Scrosati and Jürgen Garche. “Lithium batteries: Status, prospects and future”. In: *Journal of power sources* 195.9 (2010), pp. 2419–2430.

[53] Gyuwon Seo et al. “Rapid determination of lithium-ion battery degradation: High C-rate LAM and calculated limiting LLI”. In: *Journal of Energy Chemistry* 67 (2022), pp. 663–

671. ISSN: 2095-4956. URL: https://www.sciencedirect.com/science/article/pii/S2095495621006136.

[54] Madhav Singh, Jörg Kaiser, and Horst Hahn. "Thick electrodes for high energy lithium ion batteries". In: *Journal of The Electrochemical Society* 162.7 (2015), A1196.

[55] Chelsea Snyder. *The effects of charge/discharge rate on capacity fade of lithium ion batteries*. Rensselaer Polytechnic Institute, 2016.

[56] Lena Spitthoff, Paul Shearing, and Odne Burheim. "Temperature, Ageing and Thermal Management of Lithium-Ion Batteries". In: *Energies* 14 (Feb. 2021), p. 1248.

[57] Lena Spitthoff, Paul R Shearing, and Odne Stokke Burheim. "Temperature, ageing and thermal management of lithium-ion batteries". In: *Energies* 14.5 (2021), p. 1248.

[58] MSE Supplies. *Source of Detrimental Dendrite Growth in Lithium Batteries Discovered*. 2019. URL: https://www.msesupplies.com/blogs/news/source-of-detrimental-dendrite-growth-in-lithium-batteries-discovered.

[59] Norio Takenaka et al. "Frontiers in Theoretical Analysis of Solid Electrolyte Interphase Formation Mechanism". In: *Advanced Materials* 33 (Aug. 2021), p. 2100574.

[60] MIT Electric Vehicle Team. "A Guide to Understanding Battery Specifications". In: (2008), pp. 1–3. URL: https://web.mit.edu/evt/summary_battery_specifications.pdf.

[61] Stephen E Trask et al. "From coin cells to 400 mAh pouch cells: Enhancing performance of high-capacity lithium-ion cells via modifications in electrode constitution and fabrication". In: *Journal of Power Sources* 259 (2014), pp. 233–244.

[62] Kuo-Hsin Tseng et al. "Regression models using fully discharged voltage and internal resistance for state of health estimation of lithium-ion batteries". In: *Energies* 8.4 (2015), pp. 2889–2907.

[63] Wiljan Vermeer, Gautham Ram Chandra Mouli, and Pavol Bauer. "A Comprehensive Review on the Characteristics and Modeling of Lithium-Ion Battery Aging". In: *IEEE Transactions on Transportation Electrification* 8.2 (2022), pp. 2205–2232.

[64] Jens Vetter et al. "Ageing mechanisms in lithium-ion batteries". In: *Journal of power sources* 147.1-2 (2005), pp. 269–281.

[65] Xuezhe Wei, Bing Zhu, and Wei Xu. "Internal Resistance Identification in Vehicle Power Lithium-Ion Battery and Application in Lifetime Evaluation". In: *2009 International Conference on Measuring Technology and Mechatronics Automation*. Vol. 3. 2009, pp. 388–392.

[66] Rui Xiong et al. “Critical review on the battery state of charge estimation methods for electric vehicles”. In: *Ieee Access* 6 (2017), pp. 1832–1843.

[67] Dongping Xu, Lifang Wang, and Jian Yang. “Research on li-ion battery management system”. In: *2010 International conference on electrical and control engineering*. IEEE. 2010, pp. 4106–4109.

[68] Akira Yoshino. “Brief history and future of the lithium-ion battery”. In: *The Nobel Prizes 2019* (2022), pp. 207–218.

[69] Sheng S Zhang. “Challenges and strategies for fast charge of Li-ion batteries”. In: *ChemElectroChem* 7.17 (2020), pp. 3569–3577.

[70] Linfeng Zheng et al. “Incremental capacity analysis and differential voltage analysis based state of charge and capacity estimation for lithium-ion batteries”. In: *Energy* 150 (2018), pp. 759–769.

[71] Pengcheng Zhu et al. “A review of current collectors for lithium-ion batteries”. In: *Journal of Power Sources* 485 (2021), p. 229321. ISSN: 0378-7753. URL: `https://www.sciencedirect.com/science/article/pii/S0378775320316098`.

A All cells tested

Batteri	Number	dis/charge C-rate	Comment	Location	Channel	Cycles	Temp	Start	Est time[hours]	Est time[days]	Est end	
M	5	1C/2C		T3	8	200	35	14-Mar	673.48	28	11-Apr	100%
M	4	1C/2C		T3	10	200	35	14-Mar	673.48	28	11-Apr	100%
G	7	1C/2C		T3	9	200	35	12-Mar	673.48	28	9-Apr	100%
G	6	1C/2C		T3	11	200	35	12-Mar	673.48	28	9-Apr	100%
M	7	1C/2C	stopped early	T1	25	200	25	22-Mar	673.48	28	19-Apr	100%
M	3	1C/2C		T1	26	200	25	12-Mar	673.48	28	9-Apr	100%
G	9	1C/2C	error	T1	27	200	25	22-Mar	673.48	28	19-Apr	100%
G	8	0,5C/2C	stopped early	T3	12	200	35	14-Mar	873.48	36	19-Apr	100%
M	6	0,5C/2C	stopped early	T3	7	200	35	14-Mar	873.48	36	19-Apr	100%
M	9	0,5C/2C		T3	7	200	45	15-Apr	873.48	36	21-May	94%
M	8	1C/2C		T3	8	200	45	15-Apr	673.48	28	13-May	100%
M	10	1C/2C		T3	9	200	45	15-Apr	673.48	28	13-May	100%
G	10	1C/2C		T3	10	200	45	15-Apr	673.48	28	13-May	100%
G	11	0,5C/2C		T3	12	200	45	15-Apr	673.48	28	13-May	100%
G	12	1C/2C		T3	11	200	45	15-Apr	873.48	36	21-May	94%
G	13	1C/2C		T1	25	200	25	15-Apr	673.48	28	13-May	100%
EP	1	1C/1C	Discarded	T1		100	25	21-Feb	303.42	13	5-Mar	100%
EP	2	1C/0,5C	Discarded	T1		100	25	22-Feb	303.42	13	6-Mar	100%
G	2	1C/1C	Discarded	T3	9	100	35	22-Feb	303.42	13	6-Mar	100%
G	3	1C/0,5C	Discarded	T3	11	100	35	22-Feb	303.42	13	6-Mar	100%
G	4	1C/1C	Discarded	T3	12	100	35	22-Feb	303.42	13	6-Mar	100%
G	1	1C/0,5C	Discarded	T1		100	25	22-Feb	303.42	13	6-Mar	100%
M	1	1C/0,5C	Discarded	T3	8	100	35	22-Feb	303.42	13	6-Mar	100%
M	2	1C/1C	Discarded	T3	10	100	35	22-Feb	303.42	13	6-Mar	100%

B Datasheet from Melasta

Product Specification

Polymer Li-Ion Cell

3.7V 6550mAh 10C

(Model No.: SLPBB042126HN)

Shenzhen Melasta Battery Co.,Ltd

Tongfuyu Industrial Zone,Dalang,BaoAn District,Shenzhen,518109,China

Tel:+86-755-83693563

Fax:+86-755-28120114

E-mail:sales@melasta.com

Http://www.melasta.com

MELASTA **锂聚合物电池 LIPO BATTERIES** **Apr 11th,2019**

All 8 sheets

1. 序言 PREFACE

此规格书适用于深圳市风云电池有限公司的锂聚合物可充电电池产品

The specification is suitable for the performance of Lithium-Polymer (LIP) rechargeable battery produced by the SHENZHEN MELASTA BATTERY CO., LTD.

2. 型号 MODEL

SLPBB042126HN 6550mAh 10C 3.7V

3. 产品规格 SPECIFICATION

单颗电池规格 Specifications of single cell

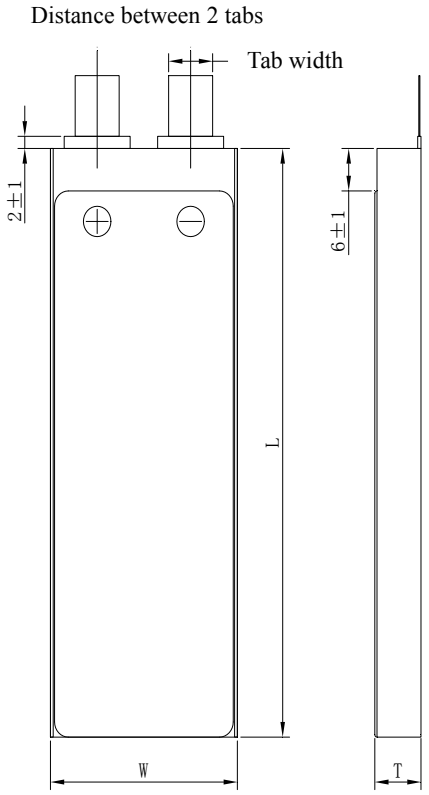

◆电芯正极材料 Cell Cathode Material		LiCoO2
◆标称容量 Typical Capacity①		6550mAh
◆标称电压 Nominal Voltage		3.7V
◆ 充电条件 Charge Condition	最大电流 Max. Continuous charge Current	13.1A
	峰值充电 Peak charge current	64A(≤0.5sec) 54A(≤1sec)
	电压 Voltage	4.2V±0.03V
◆ 放电条件 Discharge Condition	Max Continuous Discharge Current	65.5A
	Peak Discharge Current	98.25A(≤3sec)
	Cut-off Voltage	3.0V
◆交流内阻 AC Impedance(mOHM)		<3.0
◆循环寿命【充电:1C,放电:10C】 Cycle Life【CHA:1C,DCH:10C】		>100cycles
◆使用温度 Operating Temp.	充电 Charge	0℃~60℃
	放电 Discharge	-20℃~70℃
◆ 电芯尺寸 Cell Dimensions	厚度 Thickness(T)	10.7±0.3mm
	宽度 Width(W)	42±0.5mm
	长度 Length(L)	127.5±0.5mm
	极耳间距 Distance between 2 tabs	21±1mm
◆ 极耳尺寸 Dimensions of Cell tabs	极耳材料 Tab Material	Nickel-plated Copper
	极耳宽度 Tab Width	12mm
	极耳厚度 Tab Thickness	0.2mm
	极耳长度 Tab Length	30±1.5mm
◆重量 Weight(g)		128.5±3.0g
①标称容量：0.2C,4.2V~3.0V@23℃±2℃ Typical Capacity:0.2C,4.2V~3.0V@23℃±2℃		

4.电芯性能检查及测试 BATTERY CELL PERFORMANCE CRITERIA

在进行下例各项测试前每颗电池应用 0.5C 放至 3.0V。如果没有特别规定，测试应在电池交付 1 个月内按以下各项条件进行：

Before proceed the following tests, the cells should be discharged at 0.5C to 3.0V cut off. Unless otherwise stated, tests should be done within one month of delivery under the following conditions:

环境温度 Ambient temperature: 20℃±5℃

相对湿度 Relative Humidity: 65±20%RH

注意标准充放电为 Note Standard Charge/Discharge Conditions:

充电 Charge: 以 0.5C 电流恒流充电至限制电压 4.2V 时,改为恒压充电,直到截止电流为 0.05C 时停止充电;The battery will be charged to 4.2V with 0.5C from constant current to constant voltage, when the current is 0.05C, stop to charge.;

放电 Discharge: 0.5C to 3.0V/cell

测试项目 Test	单 位 Unit	规格 Specification	条 件 Condition	备 注 Remarks
容量 Capacity	mAh	≥6550	标准充放电 Standard Charge / Discharge	允许循环 3 次 Up to 3 cycles are allowed
开路电压 Open Circuit Voltage (OCV)	V	≥4.15	标准充电后 1 个小时内 Within 1 hr after standard charge	单位颗 Unit cell
内阻 Internal Impedance (IR)	mΩ	≤3.0	充满电后用 1kHz 测试 Upon fully charge at 1kHz	*
高倍率放电 High Rate Discharge (10C)	min	≥5.4	标准充电/休息 5 分钟 用 10C 放电至 3.0V Standard Charge/rest 5min discharge at10C to 3.0V	允许循环 3 次 Up to 3 cycles are allowed
低温放电 Low Temperature Discharge	min	≥210	标准充电后贮藏在-20±2℃环境中 2 小时 然后用 0.2C 放电 Standard Charge, Storage:2hrs at-2 0±2℃ 0.2C discharge at 0±2℃	3.0V/cell Cut-off
自放电 Charge Reserve	min	≥90% （初始容量 First Capacity）	标准充满电后 20 度贮藏 30 天， 标准 0.5C 放电 Standard charge Storage at 20 degree: 30days Standard discharge (0.5C)	3.0V/cell Cut-off
寿命测试 Cycle Life Test	Cycle times	≥100	充电：0.5C 充电至 4.2V，放电，10C 放电至 3.0V，当放电容量降至初始容量的 80%时，所完成的循环次数定义为该电芯的循环寿命 Charge:0.5C to 4.2V ,Discharge: 10C to 3.0V, 80% or more of 1st cycle capacity at 10C discharge of Operation	Retention capacity 容量保持 ≥80% of initial capacity

短路测试 External Short Circuit	N/A	不着火不爆炸 No Fire and No Explosion	标准充电后，在 20℃±5 环境中用超过 0.75mm² 金属丝将单颗电池短路至电池恢复到常温。 After standard charge, short-circuit the cell at 20℃±5℃ until the cell temperature returns to ambient temperature.(cross section of the wire or connector should be more than 0.75mm²)	*
自由跌落测试 Free Falling(drop)	N/A	不着火不爆炸 No Fire and No Explosion	跌标准充电后，搁置 2 小时。从 1.2M 高任意方向自由跌落 30MM 厚木板 3 次 Standard Charge,and then leave for 2hrs,check battery before / after drop Height: 1.2m Thickness of wooden board: 30mm Direction is not specified Test for 3 times	*

5. 贮存及其它事项 STORAGE AND OTHERS

5.1 环境温度 Ambient temperature: 20℃±5℃

相对湿度 Relative Humidity: 65±20%RH

5.2 请每隔 3 个月按下面方法激活电池一次:

Please activate the battery once every 3 months according to the following method:

0.2C 充电至 4.2V，休息 5 分钟，然后用 0.2C 放电至每颗电池 3.0V，休息 5 分钟，0.2C 充电 3.9V。

Charge at 0.2C to 4.2V, rest 5 min, then discharge with 0.2C to 3.0V/cell,rest 5 min, then charge at 0.2C to 3.9V.

6. 聚合物锂离子充电电芯操作指示及注意事项 HANDLING PRECAUTIONS AND GUIDLINE

声明一：

客户若需要将电芯用于超出文件规定以外的设备，或在文件规定以外的使用条件下使用电芯，应事先联系风云公司，因为需要进行特定的实验测试以核实电芯在该使用条件下的性能及安全性。

Note(1):

The customer is requested to contact MELASTA in advance, if and when the customer needs other applications or operating conditions than those described in this document. Additional experimentation may be required to verify performance and safety under such conditions.

声明二：

对于在超出文件规定以外的条件下使用电芯而造成的任何意外事故，风云公司概不负责

Note (2):

MELASTA will take no responsibility for any accident when the cell is used under other conditions than those described in this Document.

声明三：

如有必要，风云公司会以书面形式告之客户有关正确操作使用电芯的改进措施。

MELASTA will inform, in a written form, the customer of improvement(s) regarding proper use and handing of the cell, if it is deemed necessary.

6.1. 充电 Charging

6.1.1 充电电流 Charging current:

充电电流不得超过本标准书中规定的最大充电电流。使用高于推荐值电流充电将可能引起电芯的充放电性能、机械性能和安全性能的问题，并可能会导致发热或泄漏。

Charging current should be less than maximum charge current specified in the Product Specification. Charging with higher current than recommended value may cause damage to cell electrical, mechanical and safety performance and could lead to heat generation or leakage.

C Datasheet from Grepow

深圳市格瑞普电池有限公司 SHENZHEN GREPOW BATTERY CO., LTD	DOC NO.: 001 REV. : A Page 1 of 16

QR-YF-QP-030-17

Specification Approval Sheet

产品规格书

Battery Type:GRP93A6105-3.8V 10500mAh

电池型号:GRP93A6105-3.8V 10500mAh

Supplier 供应商	Prepared By 编制	赵海伶	2023-03-01
	Checked By（RD） 审核（研发）	黄芳	2023-03-01
	Checked By (QC) 审核（品质）	陈武	2023-03-01
	Approved By 批准	皮利苹	2023-03-01

Customer Approval (客户批准)	Company Name(公司名称)
	Signature/Date(签名/日期)
	Company Stamp(公司印章)

制造商保留在没有预先通知的情况下改变和修正设计及规格说明书的权利
Manufacturer reserve the right to alter or amend the design, model and specification without prior notice

深圳市格瑞普电池有限公司
SHENZHEN GREPOW BATTERY CO., LTD

DOC NO.: 001
REV. : A
Page 5 of 16

QR-YF-QP-030-17

1. 序言 Preface

此规格书适用于深圳市格瑞普电池有限公司的锂聚合物可充电电池产品

The specification is suitable for the performance of Lithium-Polymer (LIP) rechargeable battery produced by the SHENZHENSHI GREPOW BATTERY CO., LTD.

2. 产品规格 Specification

单颗电池规格 Specifications of single cell

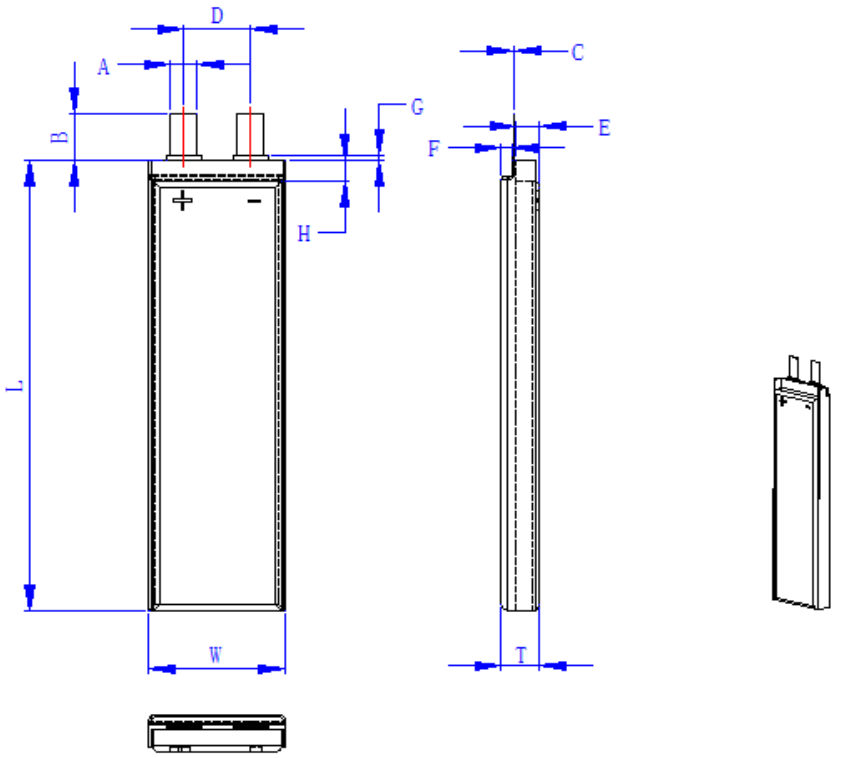

尺寸	厚度 Thickness(T)	≤9.3mm
	宽度 Width(W)	≤106.5mm
	长度 Length(L)	≤106.5mm
	极耳中心距(D) Distance between 2 tabs	55.0±1.5mm
	极耳宽度 Tab Width(A)	30±0.2mm
	极耳厚度 Tab Thickness(C)	0.2mm
	极耳外露长 Tab Length(B)	20.0±1.5mm(含极耳胶，不转镍)
	极耳胶外露长 Sealant Length(G)	0.2-3.0mm
	正封宽 Sealing Width（H）	14.0±1.0mm
	槽 1 Deep groove （E）	5.60mm
	槽 2 Deep groove (F)	2.60mm
重量 Weight		≤195.0g

制造商保留在没有预先通知的情况下改变和修正设计及规格说明书的权利
Manufacturer reserve the right to alter or amend the design, model and specification without prior notice

4. 电池常规性能检查及测试 Routine Inspection And Testing Of Battery Performance

4.1 电池常规性能 Routine Inspection of Battery Performance

标称容量 Typical Capacity①			10500mAh
最小容量 Minimum capacity			10150mAh
标称电压 Nominal Voltage			3.8V
出货电压 Voltage of shipment			3.75V-3.85V
交流内阻 AC Impedance			≤1.4mΩ
充电条件 Charge Condition	标准充电电流 Standard Charge current		2100mA
	快速充电电流 Rapid Charge current		10500mA
充电时间 Charging time	标准充电： 7.5 小时（参考值） Standard Charging：7.5 hours(Ref.) 快速充电：3.0 小时（参考值） Rapid charge：3.0 hours(Ref.)		
放电条件 Discharge Condition	标准放电电流 Standard Discharge current		2100mA
	最大持续放电电流 Max. Constant discharge current		240000mA
	瞬间放电电流 Peak discharge current		315000mA （≤3S）
工作温度范围 Range of work temperature	充电温度 Charge Temperature	5~10℃	(0.2C)
		10~20℃	（0.5C）
		20~30℃	（2C）
		30~60℃	（5C）
		60~65℃	（1C）
	放电温度 Discharge Temperature	-20~0℃	（0.2C）
		0~10℃	（0.5C）
		10~45℃	（240A）
		45-60℃	（ 0.5C）
标称容量：0.2C,4.35V~3.0V@25℃±3℃ Typical Capacity:0.2C,4.35V~3.0V@25℃±3℃			

深圳市格瑞普电池有限公司
SHENZHEN GREPOW BATTERY CO., LTD

DOC NO.: 001
REV. : A
Page 8 of 16

QR-YF-QP-030-17

测试项目 Items	单位 Unit	规格 Specification	条 件 Condition	备 注 Remarks
高倍率放电 High Rate Discharge(240A)	min	≥2.36	标准充电/休息 5 分钟 用 240A 放电至 3.0V Standard Charge/rest 5min discharge at 240A to 3.0V	
寿命测试 Cycle Life Test	Cycle	≥300	测试条件： 1)恒流恒压充电:0.5C 充电至 4.35V，限流 0.02C 2）静置：10min 3）恒流放电：6.5C 放电至 3.0V 4)静置：10min 5）循环 1）至 4）工步 当以放电容量连续两次小于初始容量 80%时， 所完成的循环次数定义为该电芯的循环寿命 Test condition： Step1：Charge: 0.5C to 4.35V , end current 0.02C Step2：Rest :10min Step3：Discharge: 6.5C to 3.0V Step4：Rest：10min Step5：cycle from step1 to step 4 Less than 80% of first capacity two times, the number of cycles completed is defined as the cycle life of the cell	25℃ ±3℃
不同温度下放电特性 Discharge Performance at different temperature	min	≥110	高温：标准充电后储存在 60±2℃的环境中，2 小时后用 0.5C 放电 High Temperature： Storage 2hrs at 60±2℃ after standard charge,0.5C discharge at 60±2℃	3.0V/cell Cut-off
	min	≥210	低温：标准充电后储存在-20±2℃的环境中，4 小时后用 0.2C 放电 Low Temperature：Storage 4hrs at -20±2℃ after standard charge,0.2C discharge at -20±2℃	

自放电 Charge Reserve	N/A	≥90% （初始容量 First Capacity）	标准充满电后常温贮藏 28 天， 标准 0.5C 放电 Standard charge, Storage 28days at room temperature Standard discharge (0.5C)	
		恢复容量≥95%初始容量 Recovery Capacity ≥95%（First Capacity）	按标准充放电制式循环 2 次，取最大值为恢复容量 Standard charge/discharge for 2 cycles，to test recovery capacity	
高温储存特性 High Temperature storage	N/A	恢复容量≥95%初始容量 Recovery Capacity ≥95%（First Capacity）	标准充满电后 60℃储存 4 小时， 标准 0.5C 放电 Standard charge Storage at 60 degree: 4h Standard discharge (0.5C)	3.0V/cell Cut-off

4.2 安全性能测试 Safety Test

测试项目 Items	单位 Unit	规格 Specification	条　　件 Condition	备　　注 Remarks
短路测试 External Short Circuit	N/A	不着火不爆炸 No Fire and No Explosion	常温：标准充电后，在 20℃±5℃环境中用电阻为 80±20 mΩ 的回路连接电池的正负极，直至电池恢复到常温。 Normal Temperature: After standard charge, the cell is to be short-circuit by connecting the positive and negative terminals of the cell with a circuit load having a resistance load of 80 ±20 mΩ at 20℃±5℃ until the cell temperature returns to ambient temperature.	*
过充电 Overcharge	N/A	不着火不爆炸 No fire and no explosion	标准测试环境下将电池以0.2C放电至终止电压，然后接热电偶并置于通风的试验设备中，室温下以3 C充电至4. 8V截止，电池持续充电时间≥7h或电池表面温度下降到比峰值低20% Under a standard test environment,dischargethe battery at 0.2C to the termination voltage,then connect a thermocouple and place it in a ventilated experimental device Charge the battery at 3C at room temperature to 4.8V and cut it off The battery continues to charge for ≥7h or the surface temperature of the battery drops to 20% below the peak value	

强制放电 Forced discharge	N/A	不着火不爆炸 No fire and no explosion	标准测试环境下将电池以0.2C放电至终止电压，然后接热电偶并置于通风的试验设备中，室温下以1C的电流对电池进行反向充电，充电时间不低于90min。 Under a standard test environment,discharge the battery to a termination voltage of 0.2C,then connect a thermocouple and place it in a ventilated experimental device Reverse charge the battery at a current of 1C at room temperature,with a charging time of not less than 90 minutes	
挤压 Crush test	N/A	不着火不爆炸 No fire and no explosion	垂直于电池最大面施压. 压力为13 kN，一旦这个最大压力达到马上卸压。电池在最大面上承受一次挤压，然后搁置4h以上. The pressure is perpendicular to the max surface of cell. the pressure is 13 kN, stop pressing when pressure reaches max . rest more than 4h.	

4.3 环境及机械性能测试 Ambient And Mechanical Character

测试项目 Items	单位 Unit	规格 Specification	条 件 Condition	备 注 Remarks
恒定湿热 Constant temperature and humidity	N/A	不爆炸、不起火、不漏液；No fire, no explosion and no leakage	完全充电后，将电芯放入 40±2℃，相对湿度为 90%~95%的恒温恒湿箱中搁置 2 天 Fully charged, the cell is to be placed in a chamber with a constant 40±2℃, 90%~95% relative humidity for 2 days.	
高空模拟 Altitude simulation Test		不爆炸、不起火、不漏液 No fire, no explosion and no leakage	完全充满电后，电池在绝对压力为11.6Kpa、室温条件下放置 6 小时 Fully charged, the cells are to be stored for 6 hours at an absolute pressure of 11.6 kPa and a room temperature	
温度循环 Temperature cycling test	N/A	不爆炸、不起火、不漏液 No fire, no explosion and no leakage	完全充电后，将电池放置在温控箱内进行如下步骤： 1）温度 75±2℃，保温 6 h； 2）降温至 - 40±2℃，保温 6 h； 3）温度转换时间≤30min； 4）重复步骤 1)----2)，共循环 10 次。Fully	

			charged, the cells are to be placed in a test chamber and subjected to the following cycles: 1. 75±2℃, maintaining this temperature for 6h 2. Raising the chamber temperature to －40 ±2℃ , and maintaining this temperature for 6h 3. Time of temperature transformation within 30 min 4. 10 cycles	
振动 Vibration Test	N/A	不爆炸、不起火、不漏液 No fire, no explosion and no leakage	将标准充电后的电芯固定在振动台上，沿X、Y、Z 三个方向各振动 30 分钟，振幅 1.6 mm，振动频率为 10Hz~55Hz，每分钟变化为 1Hz。After standard charge, fixed the cell to vibration table and subjected to vibration cycling that the frequency is to be varied at the rate of 1Hz per minute between 10Hz~ 55Hz, the excursion of the vibration is 1.6mm.The cell shall be vibrated for 30 minutes per axis of XYZ axes.	*
自由跌落测试 Free Falling(drop)	N/A	不爆炸、不起火、不漏液 No fire, no explosion and no leakage	标准充电后，搁置 2 小时。从 1.2M 高任意方向自由跌落 30MM 厚木板 3 次 Standard Charge ,and then leave for 2hrs,check battery before / after drop Height: 1.2m Thickness of wooden board: 30mm Direction is not specified Test for 3 times	

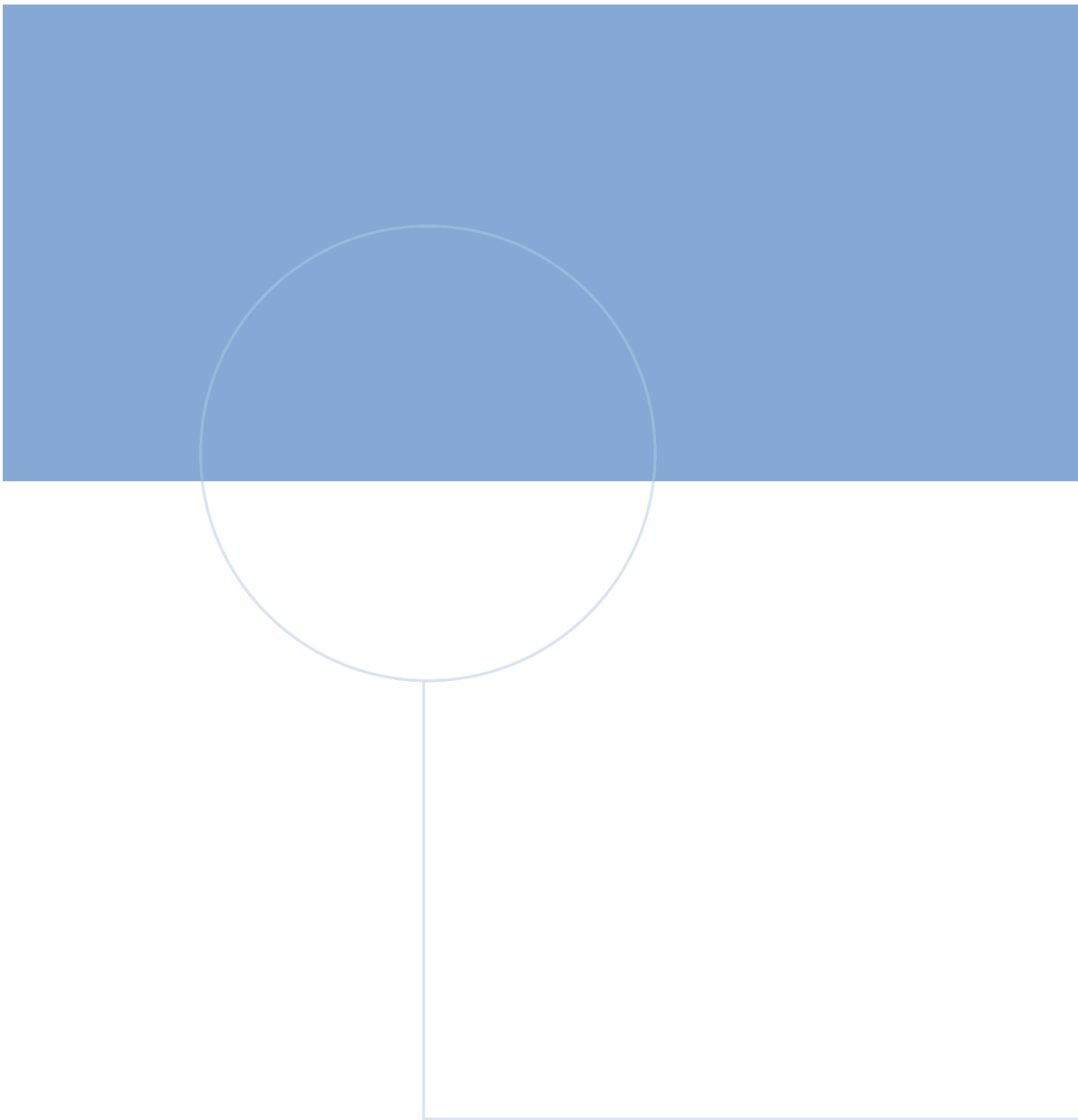

NTNU

Norwegian University of
Science and Technology